Geochronology, Geochemistry and Petrogenesis of Mafic Magmatism in the Coompana Province

Thesis submitted in accordance with requirement of the University of Adelaide for an Honours Degree in Geology

Daniel Christopher Travers

November 2015

ABSTRACT

The Coompana Province between the Gawler Craton in South Australia and the Yilgarn Craton in Western Australia is one of the least understood geological regions in Australia. Recent work by Spaggiari and Smithies (2015) suggests that the known crustal precursors in the Coompana Province originated in a new crustal generation event at ca. 1900 Ma. This new juvenile crustal element then evolved through three distinct reworking and magmatic events at ca. 1610 Ma, ca. 1500 Ma, and between ca. 1192 – 1150 Ma (Wade et al., 2007; Spaggiari and Smithies, 2015). Dating of mafic volcanics underlying the Bight Basin in the south-eastern Coompana Province using the Sm-Nd mineral isochron method has revealed a fourth distinctive episode of mafic magmatism at ca. 860 Ma. The geochemical and Nd-isotopic signatures of ca. 860 ma mafic magmatism, including Nb and Ti anomalies, LREE enrichment, K-anomalies, and highly evolved $\varepsilon Nd_{(860Ma)}$ values between -9.9 and -12.7 provide evidence for assimilation and reworking of subduction/arc related Coompana Province crust. Magmatism at ca. 860 Ma in the Coompana Province was most likely coeval with widespread magmatism that occurred over Central and Southern Australia between ca. 800 – 830 Ma. Magmatism during this period was associated with the NE-SW directed intracratonic extension that resulted in the Centralian Superbasin, and produced various suites of mafic volcanics and intrusives referred to collectively as the Willouran Basic Province. We suggest that the Willouran Basic Province now be extended to include the ca. 860 Ma mafic volcanics and intrusives in the south-eastern Coompana Province.

KEYWORDS

Neoproterozoic; Coompana Province; Mafic magmatism; Sm-Nd geochronology; Willouran Basic Province

Contents

LIST OF FIGURES AND TABLES

1. INTRODUCTION

The geological record for central and southern Australia during the early Neoproterozoic is marked by significant periods of extension, basin development and voluminous igneous activity, linked with the formation of the regionally extensive Centralian Superbasin, which has been related to the fragmentation of the supercontinent Rodinia (e.g. de Vries et al., 2008; Wang et al., 2010). The Centralian Superbasin comprised the Amadeus, Ngalia, southern Georgina, Murraba and Officer Basins, and was contiguous with the Adelaide Rift Complex in southern South Australia (Munson et al., 2013). The basin covered much of the Australian continent, prior to being dismembered during the Petermann and Alice Springs orogenies (Munson et al., 2013). Significant magmatic activity occurred across central and southern Australia prior to and during the initial stage of basin development. This is preserved today in the extensive NW-trending mafic dykes of the Gairdner Dyke Swarm (GDS) that extend across the Gawler Craton and Stuart Shelf, NW-trending mafic dykes of the Amata Suite in the Musgrave Province, mafic intrusive bodies in the Willyama Inlier, and a number of suites of volcanic rocks at the base of the Adelaide Rift Complex and in the Amadeus basin (e.g. Crawford and Hilyard, 1990; Zhao et al., 1994; Wingate et al., 1998a). Early geochemical, stratigraphic, and geochronological work indicated that these suites of mafic rocks were co-magmatic between ca. 800 – 830 Ma and make up a regionally extensive igneous province, later termed the Willouran Basic Province (Figure 1; Crawford and Hilyard, 1990; Zhao et al., 1994; Wingate et al., 1998a). However, the absolute extent of ca. 800 – 830 Ma magmatism across south and central Australia is not known.

In the early 1970's, the South Australian Bureau of Mineral Resources completed an aeromagnetic survey over the Coompana Province in south-western South Australia (Lambourn, 1972). This revealed a northwest-trending mafic dyke swarm near the Western Australian border and mafic intrusive plugs (Lambourn, 1972; Flint and Daly, 1993). Ground was subsequently acquired by Shell Australia, C.R.A Exploration and BHP Minerals, who drill tested a number of these anomalies for base metal mineralisation and shale oil . Although none of the drillholes returned economic intervals, they intersected a series of mafic intrusives and basaltic lava flows stratigraphically overlain and interlayered with the Phanerozoic and Neoproterozoic sediments of

the Bight basin (Carpentaria Exploration Co. Pty. Ltd., 1982; Carpentaria Exploration Co. Pty. Ltd. and BHP Minerals Pty. Ltd., 1982; The Shell Co. of Australia Ltd, 1983). These mafic intrusives and basic volcanics have been correlated with other suites of rocks in the Willouran Basic Province due to their geochemical and stratigraphic similarities (e.g. Scott and Spear, 1969; Thomson, 1970; Flint and Daly, 1993). However, their ages are not known.

The Coompana Province is currently a focus of the Western Craton margins project of the Geological Survey of South Australia (GSSA). This project aims to produce a geological and geodynamic framework for this largely unknown region. This study forms a part of this initiative, and aims to constrain the timing, as well as the geochemical and Nd isotopic characteristics of the mafic magmatism that overlies the Mesoproterozoic or older basement of the Coompana Province and to investigate whether these mafic rocks are part of the basement sequence or could represent a southwestern extension of the Willouran Basic Province. This study presents the first age data from the Coompana Province mafic volcanics determined through the Sm-Nd mineral isochron method, together with new Nd isotopic data, and major and trace element data. This data is compared with published data from other mafic volcanics and intrusives throughout the Willouran Basic Province, allowing correlations to be made.

Pioneering work by Wade et al. (2007b) and more recent work by the Geological Survey of Western Australia (GSWA; Spaggiari and Smithies, 2015) have revealed three distinct episodes of mafic and felsic magmatism in the Coompana Province between ca. 1610 Ma and ca. 1140 Ma. The results from this study suggest that a fourth episode of mafic magmatism occurred in the Coompana Province during the early Neoproterozoic which is most likely coeval with the other magmatic suites in the Willouran Basic Province. The results from this study have important implications for our understanding of the development of the Coompana Province, and also provide new constraints on the extent of the Willouran Basic Province.

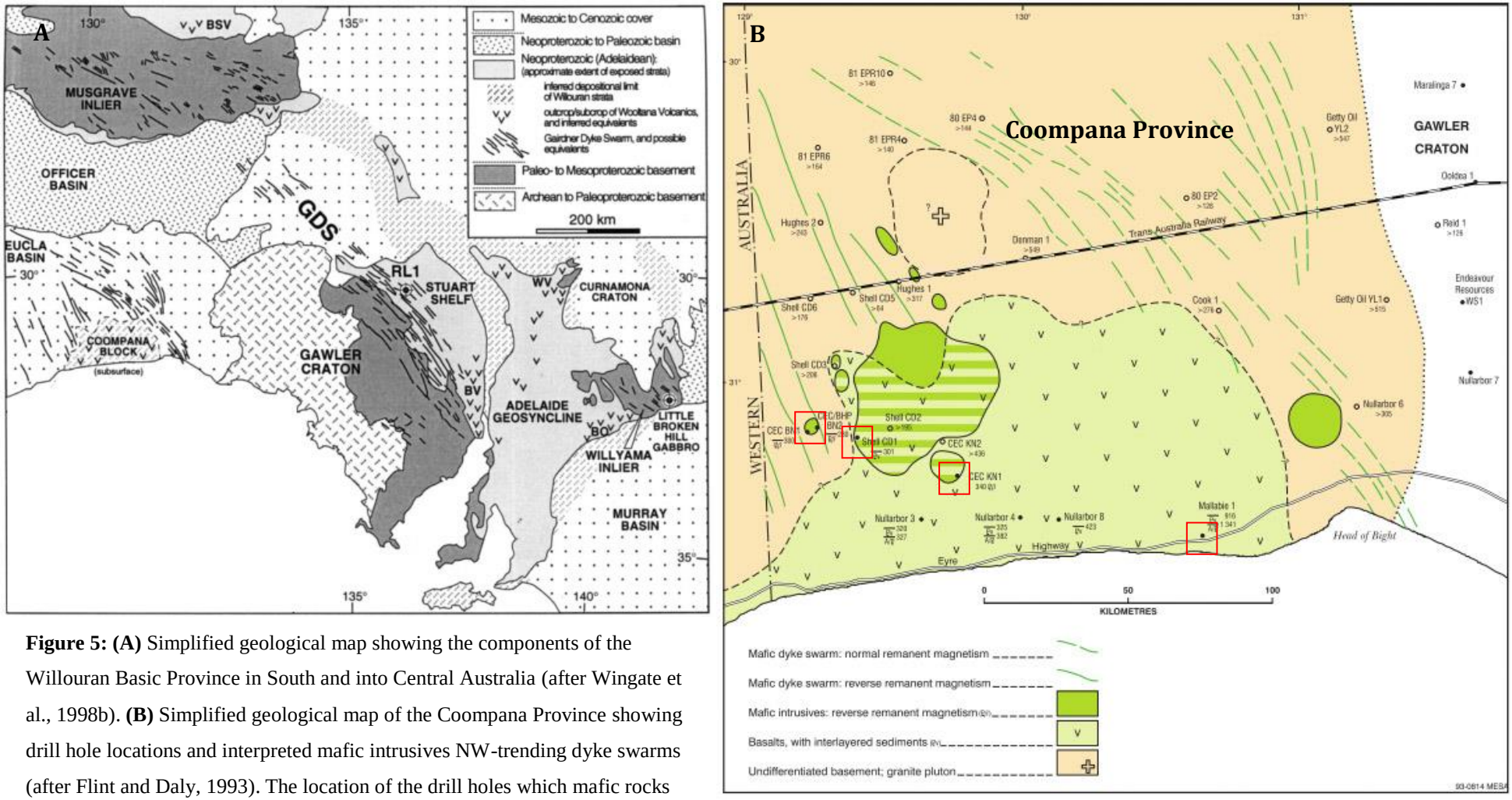

Figure 5: (A) Simplified geological map showing the components of the Willouran Basic Province in South and into Central Australia (after Wingate et al., 1998b). **(B)** Simplified geological map of the Coompana Province showing drill hole locations and interpreted mafic intrusives NW-trending dyke swarms (after Flint and Daly, 1993). The location of the drill holes which mafic rocks were taken from for this study are highlighted in red.

2. GEOLOGICAL BACKGROUND

2.1. Geology and mafic magmatism of the Coompana Province

The Coompana Province is situated between the Gawler Craton and Yilgarn Craton in western South Australia (Figure 5), and represents one of the least known geological regions in Australia due to extensive cover in addition to limited drilling, geophysical work, and geological appraisal. Recent work by Spaggiari and Smithies (2015) suggest that the known crustal precursors in the Coompana Province originated in a new crustal generation event at ca. 1900 Ma analogous to the Madura and Musgrave Province's (Kirkland et al., 2014; Smithies et al., 2015). This new juvenile crustal element then evolved through three distinct reworking and magmatic events (Figure 2; Wade et al., 2007; Spaggiari and Smithies, 2015). These include ca. 1610 Ma Toolgana Supersuite magmatism, ca. 1500 Unadwidgi Supersuite magmatism, and a later magmatic event between ca. 1192 – 1150 Ma which produced a diverse range of magmatic rocks referred to collectively as the Moondini Supersuite (Spaggiari and Smithies, 2015). Basement is relatively shallow in the western Coompana Province (Forrest Zone) in Western Australia, with recent drill holes intersecting basement between approximately 285 m and 395 m, but deepens significantly to the east in South Australia.

Early aeromagnetic work across the Coompana Province in South Australia by the South Australian Bureau of Mineral Resources defined a NW-trending mafic dyke swarm near the Western Australian border and mafic intrusive plugs (Lambourn, 1972; Flint and Daly, 1993). In 1981, the Shell Australia diamond drill hole CD1 intersected basaltic lava flows at ~300 m (Figure 5; The Shell Co. of Australia Ltd, 1983). During the same year, Carpentaria Exploration drilled the rotary percussion holes BN1 and BN2 near CD1 which intersected basalt and dolerite at ~ 300m respectively (**Error! Not a valid bookmark self-reference.** (Carptentaria Exploration Co. Pty Ltd and BHP Minerals Pty Ltd, 1982). BN2 was later extended to a depth of ~423 m via. diamond drilling to further assess the source of a negative magnetic anomaly, however, the rock type remained unchanged (Aldous, 1982). This led Aldous (1982) to suggest that the dolerite was therefore most likely represented one of the mafic intrusive bodies defined in the aeromagnetic patterns. Carpentaria Exploration also drilled the rotary percussion hole KN1, which intersected gabbro at 340 m (Figure 1;

Carpentaria Exploration Co. Pty. Ltd., 1982). In all of the drill holes, mafic volcanics and intrusives were variably overlain by the sedimentary units of the Bight basin**,** and none of the drillholes intersected the crustal units of the Coompana Province. Volcanics were also intersected further to east in the Outback Oil Company NL drill hole Mallabie 1. This intersected basalt between approximately 915 m and 1205 m overlain by various sedimentary units of the Denmam Basin (Scott and Spear, 1969). The basalt interval in Mallabie 1 was underlain by sandstone which overlies granitic basement (Scott and Spear, 1969). This was dated at ca. 1505 Ma, indicating it forms part of the Unadwidgi Supersuite (Wade et al., 2007).

The ages of the mafic volcanics and intrusives in the south-eastern Coompana Province are unknown, and it is possible they could represent a fourth episode of magmatism in this poorly understood region. Correlations have been proposed between these mafic volcanics and intrusives with the Gairdner Dyke Swarm and Beda Volcanics of the eastern Gawler Craton, and also with the basic volcanics of the Adelaide Geosycnline (Scott and Spear, 1969; Flint and Daly, 1993) which together form part of the Willouran Basic Province.

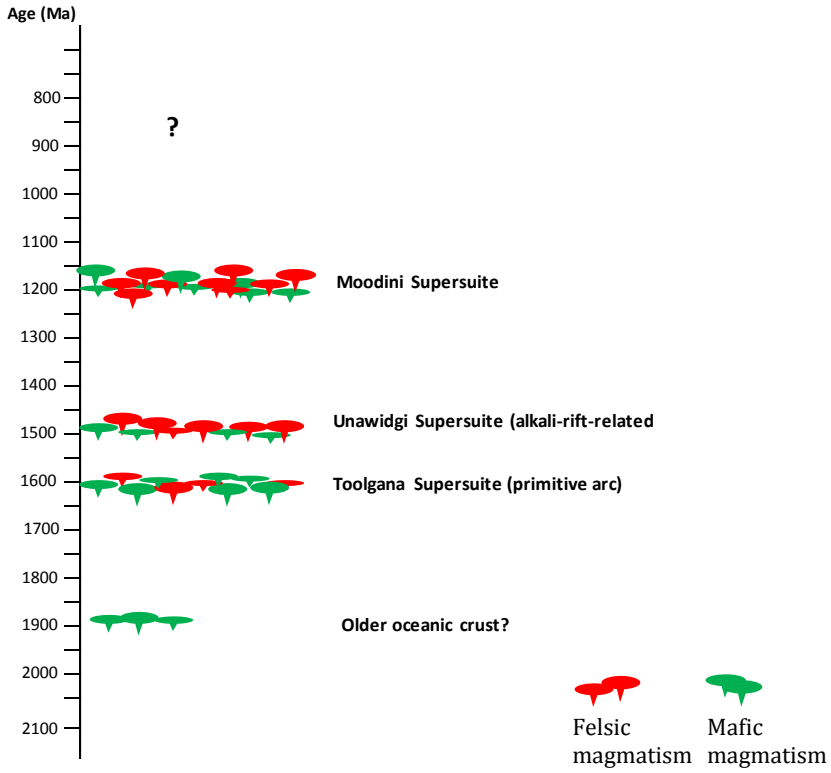

Figure 6: Time-space diagram showing the known magmatic events in the Coompana Province (after Spaggiari and Smithies, 2015).

2.2. The Willouran Basic Province

The Willouran Basic Province in South and Central Australia comprises extrusive and intrusive mafic and felsic igneous rocks that spread across the Adelaide Geosycnline, Gawler Craton, Musgrave Province, and Amadeus Basin (Figure 1; Crawford and Hilyard, 1990; Zhao et al., 1994; Wang et al., 2010). Intrusive rocks include the NW-trending mafic dykes of the Gairdner Dyke Swarm (GDS) that extend across the Gawler Craton and Stuart Shelf, the NW-trending mafic dykes of the Amata Suite across the Musgrave Province, and the Little Broken Hill gabbro and associated dykes in the Willyama Inlier on the north-eastern margin of the Adelaide Geosyncline (Figure 3; Crawford and Hilyard, 1990; Zhao and McCulloch, 1993; Zhao et al., 1994; Wingate et al., 1998). The extrusive components largely comprise continental flood basalts preserved near the base of the Adelaide Geosyncline (Figure 7Wooltana Volcanics, Cadlareena Volcanics, Noranda Volcanics, Depot Creek Volcanics and other minor units) and their stratigraphic equivalents in the Gawler Craton (Beda Volcanics of the Stuart Shelf), Curnamona Province (Wilangee Basalt), and near the base of the Amadeus Basin (Bitter Springs Volcanics) (Figure 2; Crawford and Hilyard, 1990; Zhao et al., 1994; Wingate et al., 1998; Wade et al., 2014a).

Collectively, the various intrusive and extrusive components are likely to have formed between ca. 830 and 800 Ma (Fanning et al., 1986; Zhao and McCulloch, 1993; Zhao et al., 1994; Sun et al., 1996; Wingate et al., 1998b; Wang et al., 2010). The various suites have almost uniform major element compositions: ~50% SiO2, ~14% Al2O3, ~10% Fe2O3, ~8% MgO, ~ 1.6% TiO2 (Wooltana Volcanics: Crawford and Hilyard, 1990; Zhao et al., 1994; Foden et al., 2002; Wang et al., 2010; Bitter Springs Volcanics: Zhao et al., 1994; Gairdner Dyke Swarm; Zhao et al., 1994; Foden et al., 2002; Beda Volcanics: Foden et al., 2002; Wang et al., 2010). Similarities are also observed in the trace element compositions of the suites, which are typical of tholeiitic, continental flood basalt magmatism(Crawford and Hilyard, 1990; Zhao et al., 1994; Wang et al., 2010). Nd-isotopic signatures for the various suites are relatively uniform, with $\varepsilon Nd_{(825Ma)}$ peaks at +1.6 and +3.9 (Wang et al., 2010). This is consistent with depleted and enriched end member melts, respectively (Zhao et al., 1994; Wang et al., 2010). It also suggests that crustal contamination was minimal amongst the various suites, as the

varying crustal evolution histories across the Gawler Craton and Musgrave Province would impact the Nd-isotopic signatures of the rocks (Zhao et al., 1994).

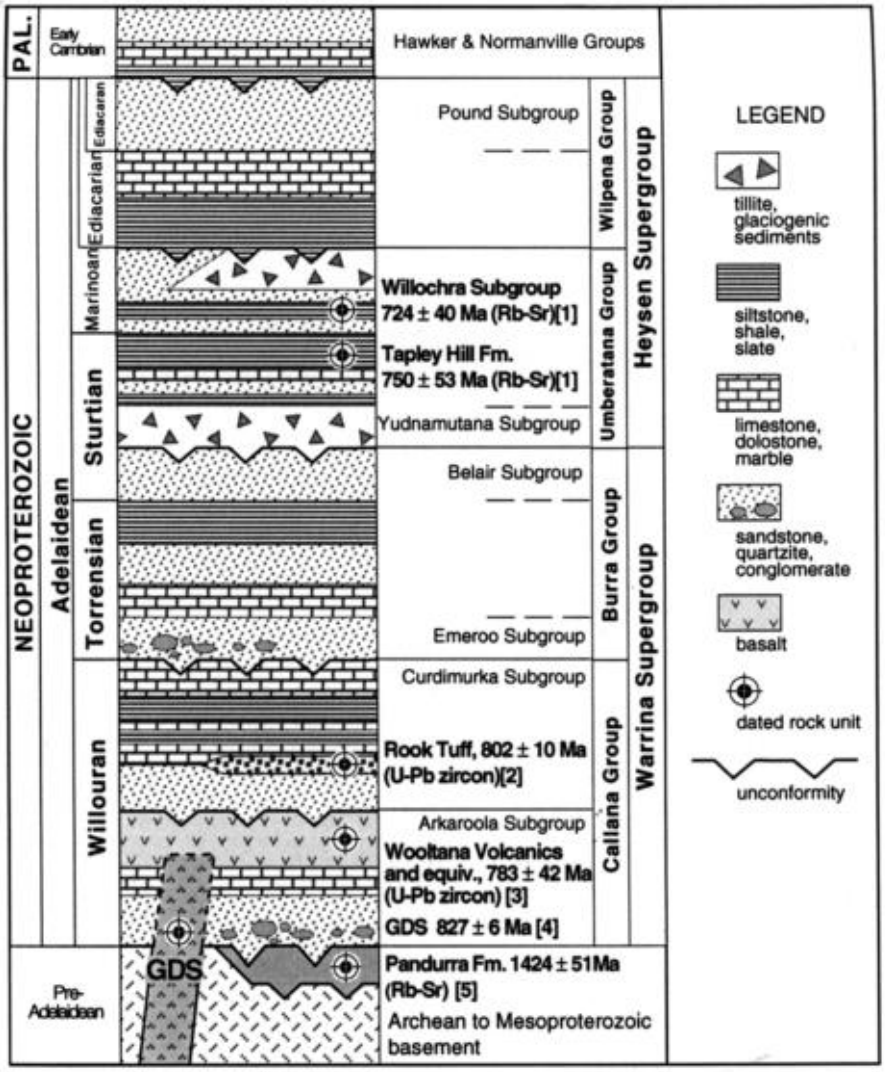

Figure 7: Schematic simplified cross-section for the Neoproterozoic rocks in the Adelaide Geosycnline and stratigraphic equivalents on adjacent platforms, including the Gairdner Dyke Swarm (after Wingate et al., 1998a). No thickness is implied for any of the units in the diagram, and the entire sequence is not present at any single location (Wingate et al., 1998a). Ages in the diagram are from: [1] Kendall et al. (2006); [2] Fanning, M. unpublished data in Preiss (2000); [3] Fanning et al., (1986); [4] Fabris et al. (2005); [5] Preiss et al. (2008); [6] Wingate et al. (1998a).

3. SAMPLES AND ANALYTICAL METHODS

3.1. Samples

Twelve samples of the dolerite intersected during the extension of drill hole BN2, nine samples of the basalt intersected in CD1, together with samples of basalt intersected in Mallabie 1 and BN1, and a gabbro intersected in KN1 were selected for this study. Care was taken to select samples that appeared the least effected by weathering or alteration. Thin sections of each of the samples were prepared by Adelaide Petrographics using blocks cut at the University of Adelaide or Minerex Peterographics in Kalgoorlie using blocks cut at the GSSA. Five samples of the basalt intersected in CD1 were selected for Sm-Nd geochronology (Figure 8). Samples of the basalt in CD1 were selected as they appeared relatively coarser grained and less affected by weathering and alteration than the other samples.

3.2. Whole rock geochemistry and mineral chemistry

Twenty-two samples were analysed for major, trace and rare earth elements (REE) at ALS in Adelaide and in Perth, Western Australia. Details of sample preparation and analysis procedures are provided in Appendix E. Full analytical procedures can be found in ALS Minerals (2009) and ALS Geochemistry (2015). Polished thin sections of the five basalt samples from drillhole CD1 selected for Sm-Nd geochronology were analysed by Electron Probe Micro Analysis (EPMA) to determine major element compositions of clinopyroxene and plagioclase. Multiple analyses were completed on grains in each thin section to ensure the resulting major element compositions of plagioclase and clinopyroxene were representative of the entire sample. Analyses were carried out at Adelaide Microscopy using a Camera SXFive electron microprobe (4 WDS spectrometers). Trace element analysis of plagioclase and clinopyroxene grains analysed by EPMA were undertaken via Laser Ablation Inductively Coupled Plasma Mass Spectrometry (LA-ICP-MS) using an ESI NWR-213 laser attached to an Agilent 7500cs ICP-MS at Adelaide Microscopy. Full details of analytical methods and operating conditions used for EPMA and LA-ICP-MS analysis are provided in Appendix D.

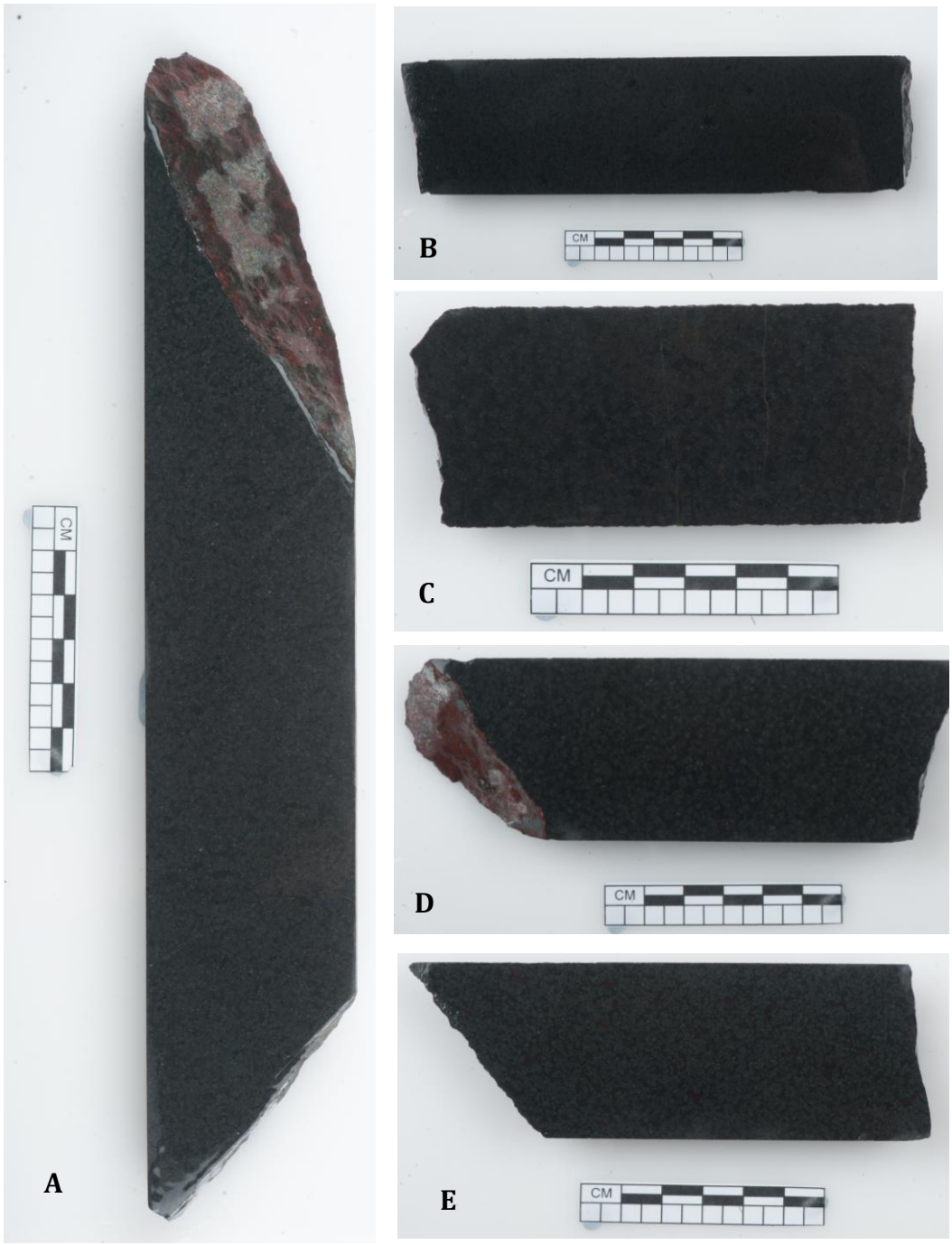

Figure 8: Photographs of basalt samples used for Sm-Nd geochronology of plagioclase and clinopyroxene from the Shell Australia drillhole CD1 (The Shell Co. of Australia Ltd, 1983). Basalt in CD1 is typically medium – coarse grained, amygdaloidal, and does not appear to be significantly affected by weathering or alteration. **(A)**: Sample 2129331 (335.1m-335.38m); **(B)** Sample 2129330 (331.7m – 332.4m); **(C)** Sample 2129333 (358.02m – 358.45m) **(D)** Sample 2129329 (328.5m – 327.75m); **(E)** Sample 2129327 (320.7m – 320.88m).

3.3. Whole rock Sm-Nd isotopic analysis

The five basalt samples from CD1 selected for Sm-Nd geochronology, as well as the basalt sample from BN1, a dolerite sample from BN2, and the gabbro sample from KN1 were selected for whole rock Sm-Nd isotopic analysis. All five basalt samples from CD1 were chosen to provide the option of constructing three point isochrons with the plagioclase and clinopyroxene mineral separates. Samples from the other drill holes were selected to provide regional constraints on the Nd isotopic signature of magmatism in the Coompana Province. Where possible, care was taken to select samples that appeared the least effected by weathering or alteration.

Analyses were undertaken at the University of Adelaide following the analytical techniques of (Payne et al., 2006). Samples were weighed and then spiked with a $^{150}Nd/^{147}Sm$ solution. HNO_3 and HF was added to the samples in Teflon vials. The Teflon vials were heated on a hot plate at 140°C for 2 days. The HF and HNO3 was then evaporated, and HNO3 were added shortly before the samples were completely dry. HF was added and the samples were heated on a hot plate at 140°C for a further 2 days. The samples were then evaporated to dryness. 6M HCL was then added and the samples were heated overnight at 140◦C. Rare Earth Elements (REEs) were separated in 2mL AG 50W X8 200-400 mesh resin in Polyprep columns. Sm-Nd was then isolated in Eichrom Ln resin in quartz glass columns. Sm and Nd isotopic measurements were carried out on an Isotopx Phoenix thermal ionization mass spectrometer (TIMS). The procedural blank used during this study yielded 14pg Nd. The running average for the JNdi-1 standard is 0.512107±0.000003 (1σ, n=48). Analysis of the BNHO2 standard yielded an $^{143}Nd/^{144}Nd$ ratio of $0.512970\pm2x10^{-6}$ (2s.e.).

3.4. Sm-Nd Geochronology

The five basalt samples from drill hole CD1 selected for Sm-Nd geochronology were sent to Curtin University for mineral liberation using an in-house selFrag Lab machine. A detailed overview of the selFrag process is available in Giese et al. (2007). Clinopyroxene and plagioclase were then separated at the University of Adelaide using a refined separation process developed for this study involving sieving, electromagnetic separation, heavy liquid density separation, and handpicking under a binocular microscope. This produced portions of plagioclase and clinopyroxene which were more than 99% pure. A detailed overview of this procedure is provided in Appendix D.

Sm and Nd from the plagioclase and clinopyroxene mineral separates were then isolated following the same procedure used for isolating Sm and Nd from the whole rock samples detailed in section 3.3. Samples were spiked with a mixed ^{150}Nd and ^{147}Sm spike with sample to spike ratio optimised using trace element data from in-situ LA-ICP-MS analysis of the corresponding thin sections for each sample. Samples were agitated in an ultrasonic bath between dissolutions in HNO_3 and HF, and prior to evaporating HNO_3 and HF from the second dissolution in order to aid the dissolution process. Sm and Nd isotopic measurements for the mineral separates were completed during the same analytical sessions as the whole rock measurements.

4. RESULTS

4.1. Petrography

Detailed petrographic observations highlighting mineralogical and textural properties of the basalt samples from CD1 selected for Sm-Nd geochronology, samples of the dolerite from BN2, and the basalt sample from Mallabie 1 are provided in Figures 5,6, and 7, respectively. The basalt in CD1 typically comprises fine and medium grained plagioclase laths and more angular grains in a matrix with clinopyroxene. Different types of clinopyroxene are present, including augite and also altered brown-red coloured grains interpreted to represent more Fe-rich end-members such as hedenbergite. Fine-coarse grained K-feldspar phenocrysts are common throughout the samples. Amygdales comprising chlorite with occasional epidote and quartz occur within grain boundaries, and are also observed overprinting primary mineral phases and in the groundmass. Chlorite veins and veinlets occur throughout the samples. Fine grained disseminated hematite and also occasional magnetite with ilmenite lamellae occur throughout the samples. These occur within grain boundaries and overprint earlier mineral phases. The primary igneous textures remain relatively well intact in most samples.

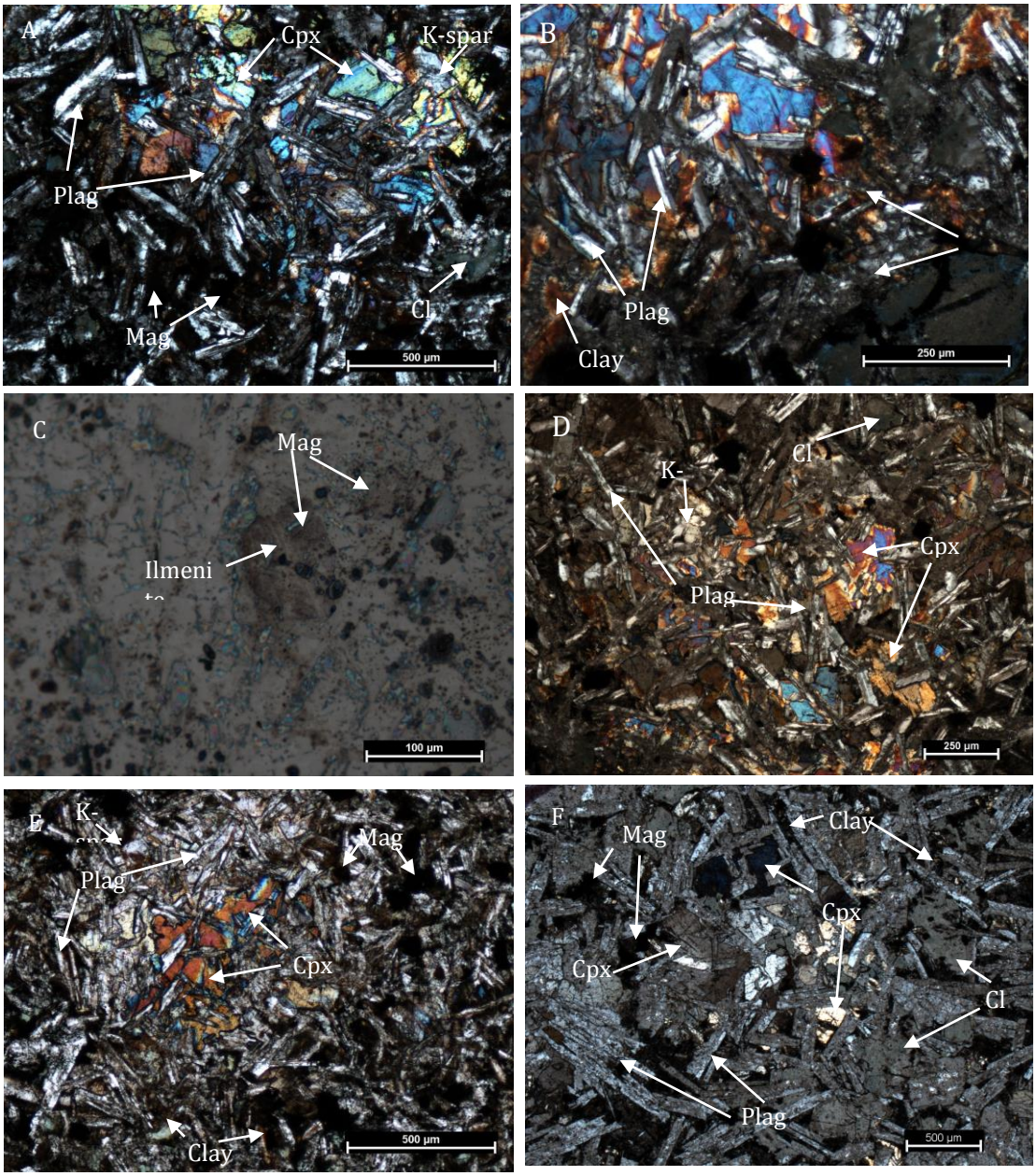

Figure 9: Photomicrographs taken under cross polarised and reflected light highlighting mineralogical and textural features of basalt samples selected from drillhole CD1 for Sm-Nd geochronology. **(A)** Photomicrograph taken under cross polarised light of sample **2129327** (320.7m – 320.88). Clinopyroxene (augite) with fine-medium grained laths of plagioclase and k-feldspar phenocrysts. Minor fine grained euhedral chlorite masses occur throughout the sample. Minor chlorite veinlets overprinting earlier mineral phases are also observed. Primary igneous textures remain well intact. **(B)** Photomicrograph taken under cross polarised light of sample **2129329** (328.5m – 329.08m). Plagioclase and clinopyroxene (augite) occur with chlorite euhedral masses with a clay matrix. Altered brown-red coloured varities of clinopyroxene occur through the sample. Euhedral chlorite masses are common, and are observed overprinting and overprinted by clinopyroxene and plagioclase. Quartz is observed within the euhedral masses. Minor chlorite veinlets occur throughout the sample and also overprint earlier mineral phases. The primary igneous texture of the rock remains relatively well intact. In reflected light **(C)**, disseminated magnetite with ilmenite lamellae are observed throughout the sample.

Figure 5 continued: (**D)** Photomicrograph taken under cross polarised light of sample **<u>2129330</u>** (331.7m – 332.4m). Fine and medium grained plagioclase occurs with clinopyroxene (augite). Other alkali feldspar phenocrysts are present. Chlorite is present in the groundmass (overprinted by plagioclase) and also overprints earlier mineral phases. Oxides are present throughout the sample. **(E)** Photomicrograph taken under cross polarised light of sample **<u>2129331</u>** (335.1m – 335.38m). Fine grained plagioclase and clinopyroxene together with k-spar, scattered chlorite amygdales and occasional veining, and murky clay. Primary igneous textures appear notably disturbed with respect to the other samples from CD1. Plagioclase and clinopyroxene are also typically finer grained. Fine-grained disseminated magnetite occurs throughout the sample. **(F)** Photomicrograph taken under cross polarised light of sample **<u>2129333</u>** (358.02m – 358.45m). Abundant fine- coarse grained plagioclase laths define a groundmass with fine-medium grained clinopyroxene. Altered clinopyroxene (brown-red colour) also occurs throughout the sample. Fine-medium grained euhderal masses of chlorite are common, however, chlorite veinlets are rare. Euhedral masses are present in the groundmass and are also observed overprint clinopyroxene and plagioclase. Disseminated magnetite occurs throughout. Minor clay also occurs in the groundmass. The sample appears relatively fresh, and primary igneous textures are largely intact.

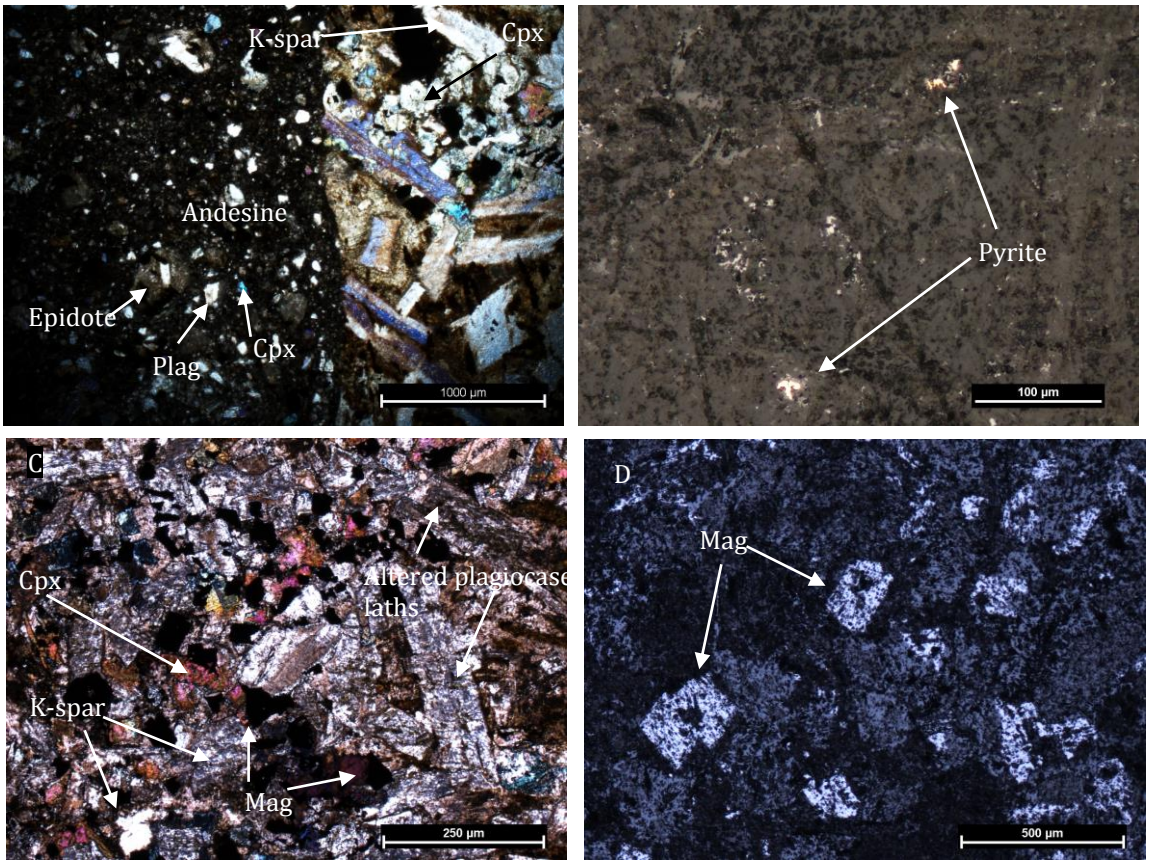

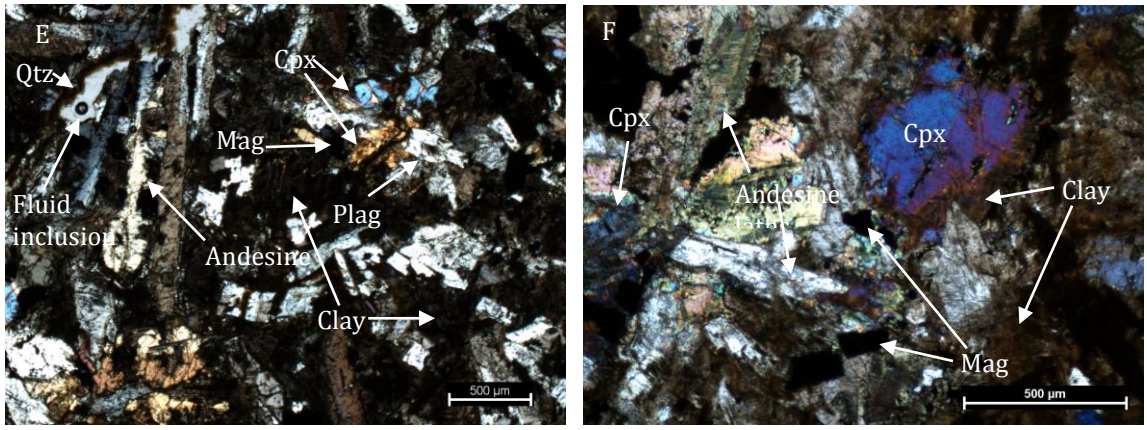

Figure 10: Photomicrographs taken under cross polarised and reflected light highlighting mineralogical and textural features of dolerite samples taken from drillhole BN2. The dolerite typically comprises small-large heavily altered plagioclase / andesine laths and clinopyroxene in a groundmass of plagioclase, K-feldpar, and clay. Primary igneous textures are significantly disturbed. Chlorite and epdotite are common throughout the samples. Both occur in either amygdales which overprint earlier mineral phases, or as veins which cross-cut earlier minerals and at grain boundaries. Disseminated magnetite is abundant throughout the samples. Ileminte lamellae are common in magnetite. Quartz veining is also observed throughout the samples. Detailed petrographic observations are provided below. **(A)** Photomicrograph taken under cross polarised light showing the contact between the brecciated and non-brecciated region of sample **2129338** (422.59 – 423m). The non-brecciated region sample shows similar textural and mineralogical properties to the other samples. The brecciated region comprises fine grained plagioclase and clinopyroxene, together with alkal-feldspar and widespread epidote amygdales. **(B)** Photomicrograph taken in reflected light showing minor disseminated pyrite in sample **2129338**. **(C)** Photomicrograph taken under cross polarised light of sample **2129342** (462.8 – 463.47m) at 2.5x magnification. Heavily altered andesine and plagioclase laths occur with clinopyroxene and alkali-feldspar. Clay is abundant throughout the sample. Primary igneous textures are significantly disturbed. **(D)** Reflected light photograph showing opaque minerals in **2129342**. Disseminated magnetite occurs throughout the sample, overprinting primary mineral phases. **(E)** Photomicrograph taken under cross polarised light of sample **2078886** (467.7m – 468.1). Altered glagioclase and andesine laths occur with clinopyroxene in a murky clay matrix. Disseminated magnetite occurs throughout the sample, and quartz veins are also observed. Fluid inclusions occur in some quartz veins. The sample is heavily altered and primary igneous textures appear largely destroyed. **(F)** Photomicrograph taken under cross polarised light of sample **2129344** (481.55m – 482.24m). Heavily altered andesine laths occur with clinopyroxene in a murky clay matrix. Disseminate magnetic occurs throughout the sample. Fine-medium grained euhedral chlorite masses are also common. The sample is heavily altered and primary igneous textures appear largely destroyed.

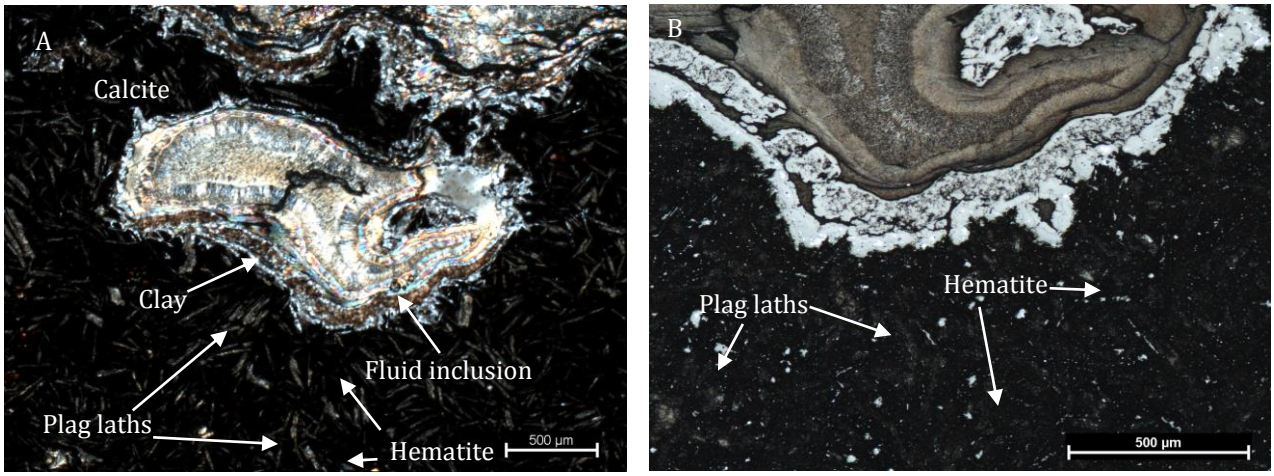

Figure 11: Photomicrographs taken in cross polarised light **(A)** and reflected light **(B)** show typical mineralogical and textural properties of the Mallabie 1 sample **2078890** (921.1m -921.5m). Medium-coarse grained amygdales comprising fine grained, fibrous clay 'boundary' with cores infilled with carbonate and minor quartz occur in a dark groundmass comprising hematite and small plagioclase laths. Amygdales range from fine to coarse grained. Spherical and elongate varieties are both observed. Fluid inclusions are present in quartz. The plagioclase laths in the groundmass do not appear to have a distinct orientation. This rock is heavily altered, with primary igneous textures significantly disturbed.

4.2. Geochemistry and mineral chemistry

4.2.1. Major-elements

Results from major and trace element analyses of whole rock samples are provided in Appendix B. All major elements are presented as wt% oxides. Harker diagrams of MgO vs. major element oxides show a distinct chemical separation between the CD1 basalt samples and the BN2 dolerite samples (Figure 12). The CD1 basalt samples have uniform SiO2 (48 – 50%), TiO2 (0.9 – 1.1%), Al2O3 (15-16%), Fe2O3 (11-12%),MgO (7.4 – 9.4%), K2O(0.5 – 1.8%) and Na2O (2.0 – 3.3%), and variable CaO (3.1 – 9.5%). The dolerite samples from BN2 also show uniform major element compositions: SiO2 (53 – 58%), TiO2 (1.6 – 1.7%), Al2O3 (11-12 %), Fe2O3 (15 - 17%), MgO (1.4 – 2.1 %), K2O (1.4 – 3.3 %), Na2O (3.0 – 5.1 %), and CaO (4.8 – 5.5%). The BN2 dolerite samples are notably enriched in $F_{e2}O_3$, and depleted in MgO with respect to the CD1 basalt samples. The major element composition of the basalt sample from BN1 is almost identical to the BN2 samples, while the basalt sample from Mallabie 1 and the gabbro sample from KN1 have similar major element compositions to the CD1 samples.

Major element classification diagrams are presented in Figure 14. Most of the samples from CD1 are classified as basalt or trachy-basalt on a total alkali vs. silica (TAS) diagram for volcanic rocks (Le Maitre et al., 1989), while the BN2 samples are typically classified as basaltic-trachyandesite. The Mallabie 1 sample is classified as a tephrite / basanite, while the BN1 sample is classified as as a basaltic-trachyandesite. The BN2 samples are classified as syeno-diorite on a TAS classification diagram for plutonic rocks (Cox et al., 1979), and the KN1 sample is classified as a gabbro. The samples show calc-alkaline to shoshonitic affinities on an SiO_2 (%) vs. K_2O (%) diagram, with the BN2 and BN1 samples plotting in the higher-K area of the diagram. In comparison, almost all of the samples show tholeiitic affinities on an AFM diagram.

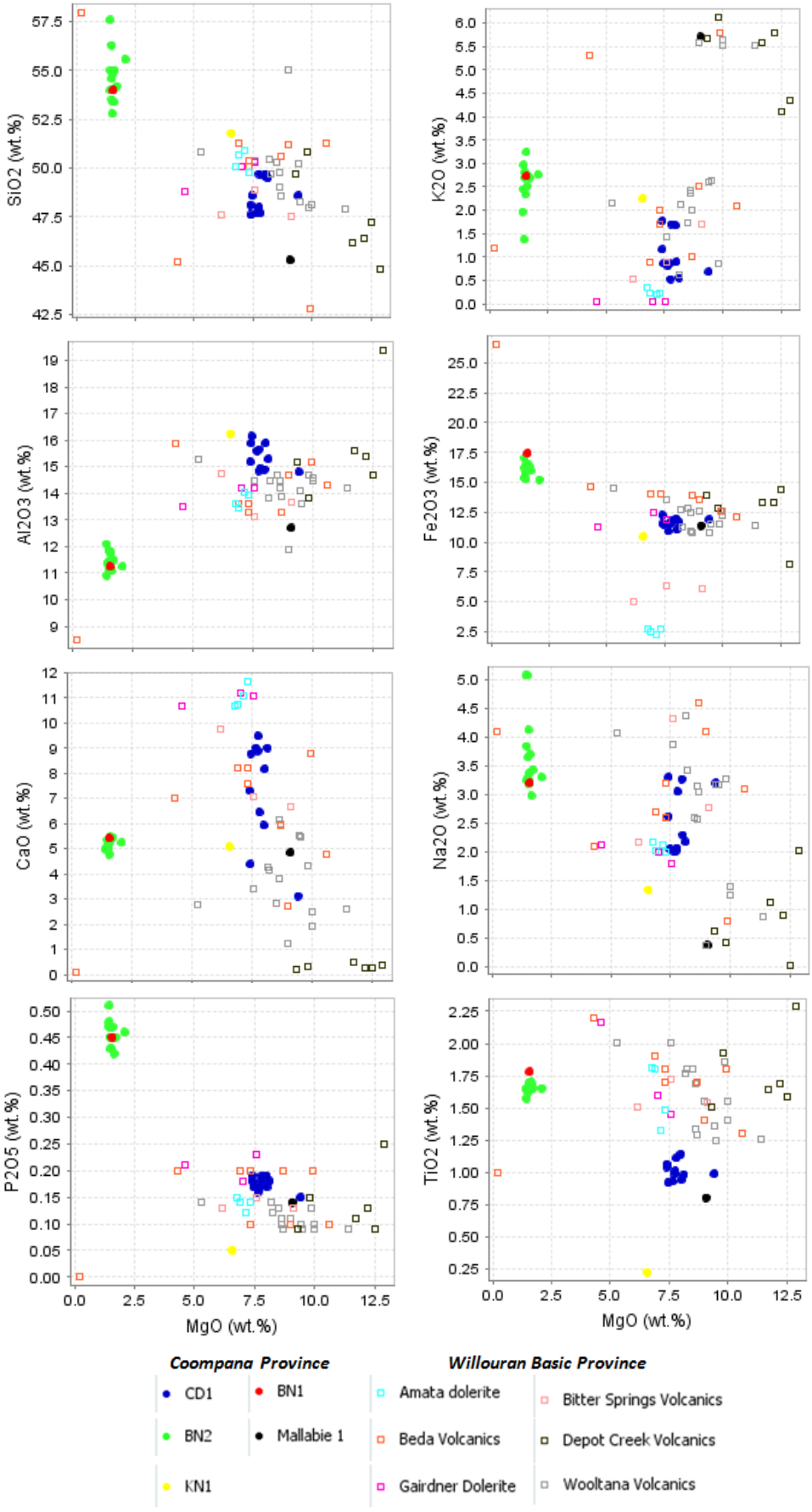

Figure 12. Bivariate plots of major element oxides (wt. %) vs. MgO (wt. %) for mafic rocks from the Coompana Provnce taken for this study. Major element compositions for samples from other suites of volcanic and intrusive rocks in the Willouran Basic Province are plotted for reference (Wooltana Volcanics: Crawford and Hilyard., 1990; Wang et al., 2010; Bitter Springs Volcanics: Zhao et al., 1994; Depot Creek Volcanics: Wang et al., 2010; Gairdner Dolerite: Zhao et al., 1994; Beda Volcanics: Wade et al., 2014; Amata Dolerite: Zhao et al., 1994).

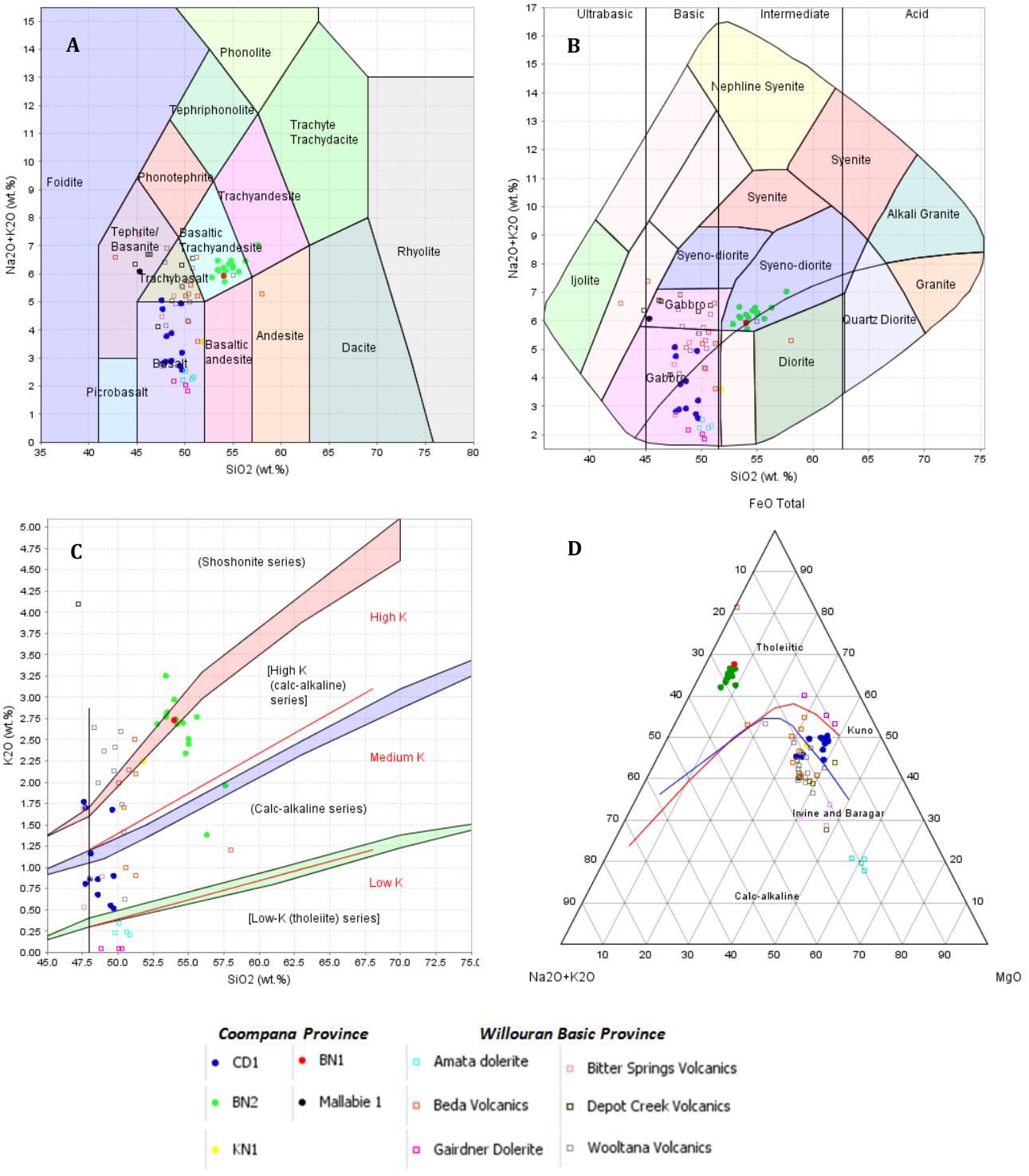

Figure 13(A) TAS classification diagram for volcanic igneous rocks (after Le Maitre et al., 1989). (B) TAS classification diagram for plutonic igneous rocks (after Cox et al., 1979). (C) SiO_2 vs. K_2O diagram for the subdivision of subalkalic rocks (after Le Maitre et al., 1989; Rickwood, 1989). (D) AFM diagram for the subdivision of calc-alkaline and tholeiitics igneous rocks (after Kuno, 1968; Irvine and Baragar, 1971). In all diagrams, samples from various suites in the Willouran Basic Province are plotted for reference (Wooltana Volcanics: Crawford and Hilyard., 1990; Wang et al., 2010; Bitter Springs Volcanics: Zhao et al., 1994; Depot Creek Volcanics: Wang et a., 2010; Gairdner Dolerite: Zhao et al., 1994; Beda Volcanics: Wade et al., 2014; Amata Dolerite: Zhao et al., 1994).

4.2.2. Trace and rare earth element variation

Tectonic setting discrimination diagrams are presented in Figure 15. On an Nb/Y vs. Zr/Ti diagram, almost all of the samples are classified as sub-alkaline and plot in or on the boundary of the andesite basaltic – andesite region (Pearce, 1996). On a Ti/V diagram (Shervais, 1982), the CD1 basalt samples plot across the boundary between calc-alkaline basalts, continental flood basalts and arc tholeiite, within the Ti/V ratio range of 20 and 50. The basalt sample from Mallabie 1 plots in the MORB region of the diagram, while the gabbro sample from KN1 has a Ti/V ratio between 10 and 20, and plots in the arc tholeiite region of the diagram. The dolerite sample from BN2 and the basalt sample BN1 are depleted in V with respect to the other samples, and have Ti/V ratios over 100. Almost all of the samples taken for this study are classified as arc calc-alkaline and calc-alkaline basalts on Y-La-Nb and Ti-Zr-Y classification diagrams (Figure 15; Pearce and Cann, 1973; Cabanis, 1989).

Immobile trace element ratio variation diagrams are presented in Figure 16. All diagrams are normalised to the primitive mantle composition of McDonough and Sun (1995). An (Gd/Yb)PM vs. (Nb/La)PM diagram is shown in Figure 16A. Almost all of the samples have (Gd/Yb)PM ratios less than 1.5. (Nb/La)PM ratios for the samples from CD1 and Mallabie 1 are greater than the samples from BN2 and BN1, however, values are broadly similar, ranging between 0.19 to 0.31. The basalt sample from BN1 and the gabbro sample from KN1 plot roughly at the boundary between the BN2 and CD1 samples. An Gd/Yb (PM) vs. (La/Sm)PM diagram is presented in Figure 16B. The dolerite samples from BN2 have higher and more varied (La/Sm)PM ratios than the basalt samples from CD1, ranging between 3.2 and 4.0. The basalt samples from CD1 have (La/Sm)PM ratios between 2.76 and 3.12. The basalt sample from BN1 plots within the range of the BN2 dolerite samples ((La/Sm)PM = 3.32), while the samples from Mallabie 1 and KN1 have similar ratios ((La/Sm)PM = 2.44 and 3.08, respectively) to the CD1 samples. An (Th/Yb)PM vs. (Nb/Yb)PM diagram normalised is shown in Figure 16C. (Nb/Yb)PM ratios for most of the samples are broadly similar, ranging from 0.81 to 1.28, however the dolerite samples from BN2 samples have considerably higher (Th/Yb)PM ratios (BN2 from 1.7 to 2.3; CD1 from 6.9 to 7.6). The basalt sample from Mallabie 1 sample has similar (Th/Yb)PM and (Nb/Yb)PM ratios to the CD1 samples (2.02 and 0.93 respectively), while the basalt sample from BN1 sample has similar ratios to the BN2 samples (7.1 and 1.2 respectively). The sample from KN1 has an anomalously high (Th/Yb)PM ratio (12.9) with respect to the other samples. An (Nb/Th)PM vs. (Th/Yb)PM diagram

is provided in Figure 16D. (Nb/Th)PM ratios for the BN2 dolerite samples (0.15 – 0.17) are lower than the CD1 basalt samples (0.32 to 0.58). The (Nb/Th)PM ratio for the Mallabie 1 basalt sample (0.46) is within the range of the values for the CD1 basalt samples. The gabbro sample from KN1 has a slightly lower (Nb/Th)PM ratio (0.09) than the BN2 dolerite samples.

Primitive mantle normalised trace element variation diagrams are presented in (McDonough and Sun, 1995). Primitive mantle normalised trace element patterns for the samples are fractionated, and show depletions in Nb and Ti, and K-enrichment. The dolerite samples from BN2 are enriched in most of the trace elements with respect to the basalt samples from CD1. However, they are notably depleted in Sr with respect to most of the CD1 basalt samples, which show no notable Sr depletion. Primitive mantle normalised REE variation diagrams are presented in (McDonough and Sun, 1995). All of the samples have enriched LREE/HREE ratios ($(La/Yb)_N$ from 3.5 to 5.8). However, LREE/HREE ratios for the dolerite samples ($(La/Yb)_N$ from 4.9 to 5.5) are more enriched than the CD1 basalt samples ($(La/Yb)_N$ from 3.5 to 4.3). LREE/HREE ratios for the Mallabie 1, KN1, and BN1 samples are similar to the BN2 samples. The samples are moderately depleted in HREE ($(La/Yb)_N$ from 1.0 – 1.3). A moderate degree of LREE fractionation is observed ($(La/Sm)_N$ from 2.8 to 4.0). The BN2 dolerite samples show slightly higher degrees of LREE fractionation ($(La/Sm)_N$ from 2.4 to 4.0) than the CD1 basalt samples ($(La/Sm)_N$ from 2.7 to 3.1). The samples have small negative Eu anomalies ($[Eu/Eu^*]_N = 0.39 – 0.60$), with the BN2 dolerite samples showing more negative Eu anomalies ($[Eu/Eu^*]_N = 0.37 – 0.44$) than the CD1 basalt samples ($[Eu/Eu^*]_N = 0.44 – 0.49$). The dolerite samples from BN2 and the basalt sample from BN1 are significantly depleted in Ni and Cr with respect to the CD1, Mallabie 1, and KN1 samples. In all of the BN2 and BN1 samples, either Ni or Cr (or both) concentrations were below the analytical detection limits. In comparison, Cr/Ni ratios for the CD1, Mallabie 1, and KN1 samples are relatively uniform, ranging between 0.55 and 0.94.

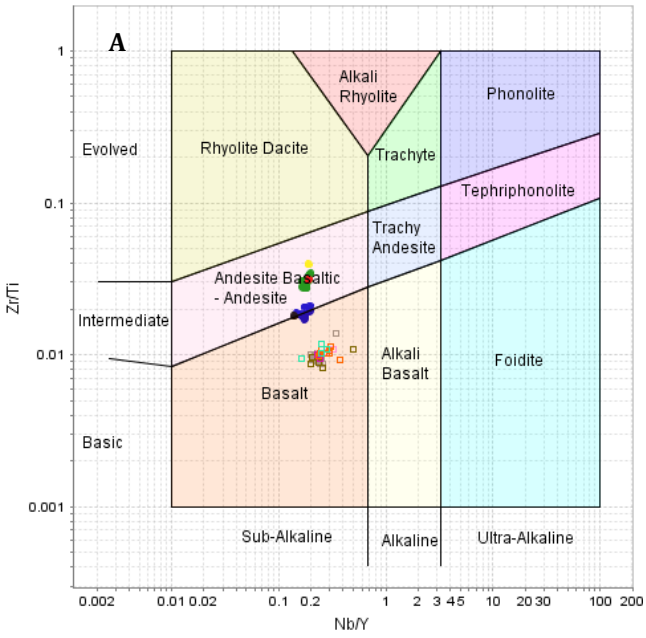

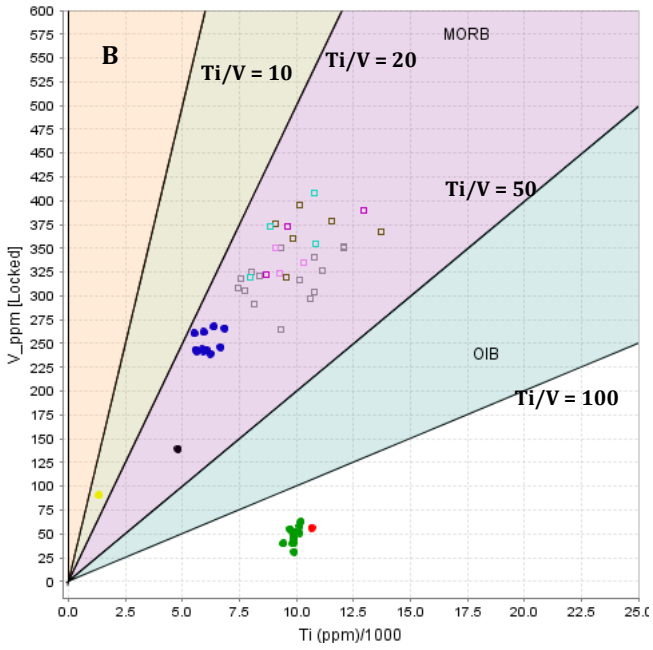

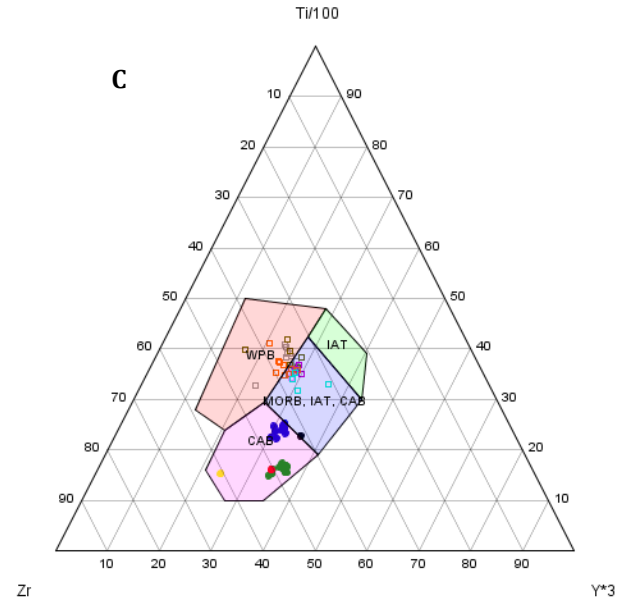

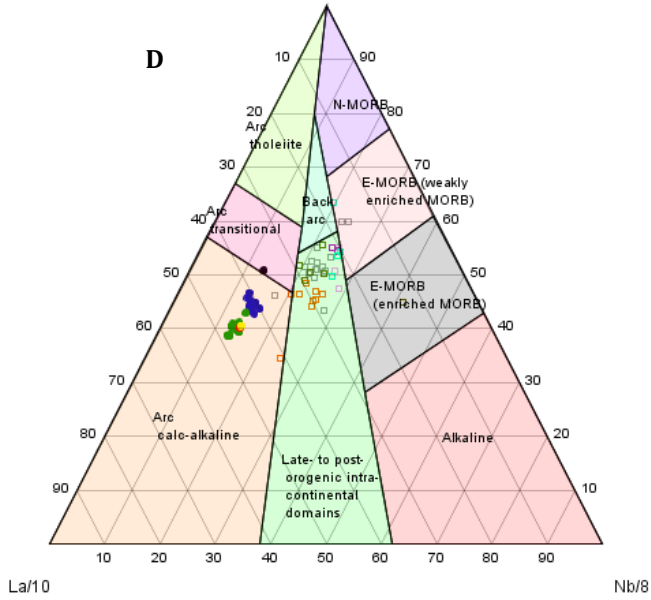

Coompana Province		*Willouran Basic Province*	
CD1	BN1	Amata dolerite	Bitter Springs Volcanics
BN2	Mallabie 1	Beda Volcanics	Depot Creek Volcanics
KN1		Gairdner Dolerite	Wooltana Volcanics

Figure 15: (A) Zr/Ti vs. Nb/Y classification diagram (Pearce, 1996) highlighting variations in the types of basalt present in the south-eastern Coompana Province. **(B)** Ti/V tectonic setting classification diagram (after Shervais, 1982). MORB plots between Ti/V ratios of 20 and 50, however, there is significant overlap between MORB and the fields for continental flood basalt and back-arc basin basalts. Ocean island (OIB) and alkali basalts plot between Ti/V ratios of 50 and 100. Island-arc tholeiites plot within Ti/V ratios of 10 and 20, and overlap onto the MORB field. Calc-alkali basalts have Ti/V ratios between 15 and 50. There is considerable overlap between the Ti/V ranges for calc-alkaline basalts, continental flood basalts and arc tholeiites. **(C)** Ti-Zr-Y discrimination diagram (after Pearce and Cann, 1973). **(D)** La/10-Y/15-Nb/8 discrimination diagram (after Cabanis, 1989). Trace element compositions of volcanic and extrusive mafic rocks from various suites in the Willouran Basic Province are plotted for reference (Wooltana Volcanics: Crawford and Hilyard., 1990; Wang et al., 2010; Bitter Springs Volcanics: Zhao et al., 1994; Depot Creek Volcanics: Wang et a., 2010; Gairdner Dolerite: Zhao et al., 1994; Beda Volcanics: Wade et al., 2014; Amata Dolerite: Zhao et al., 1994).

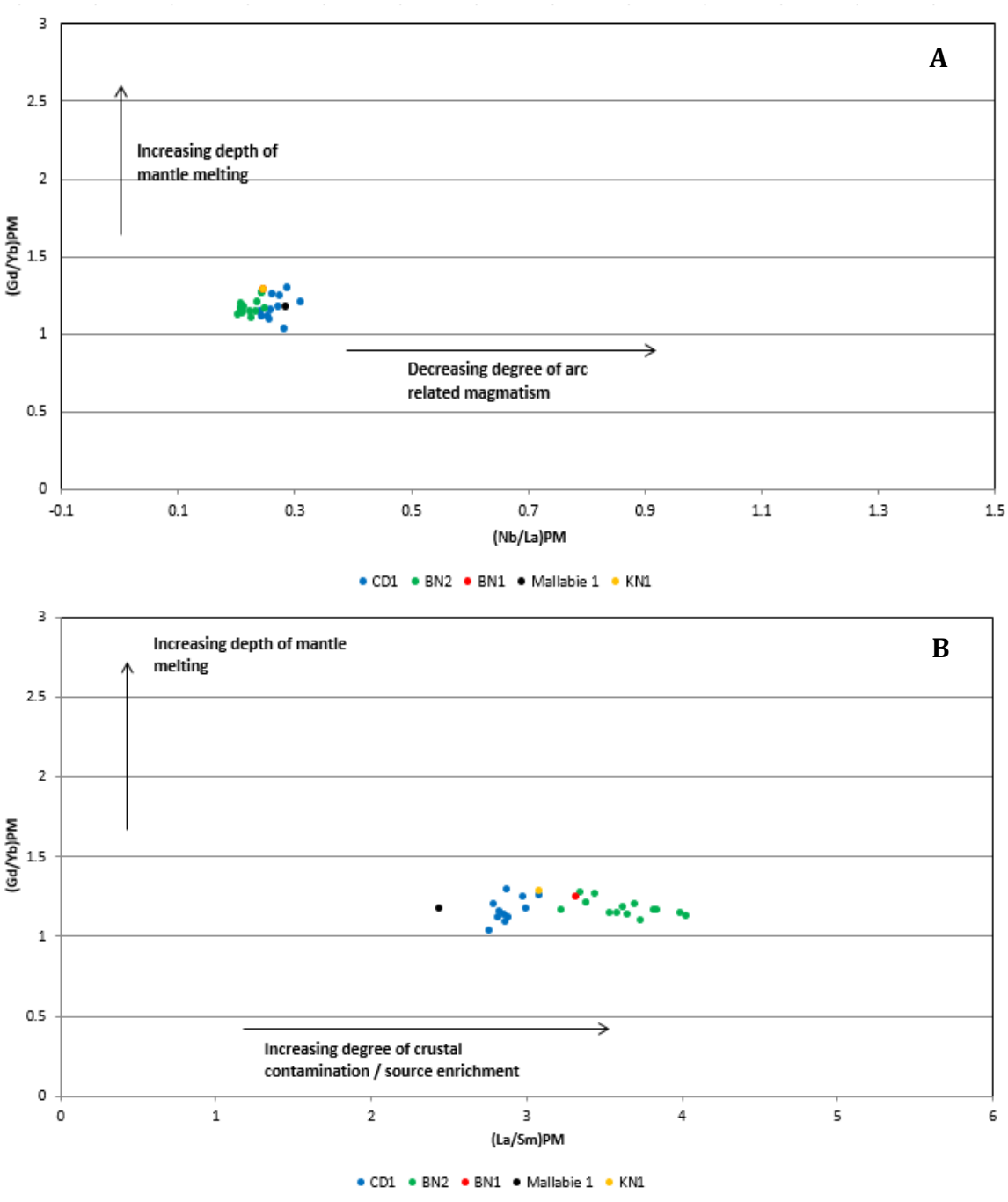

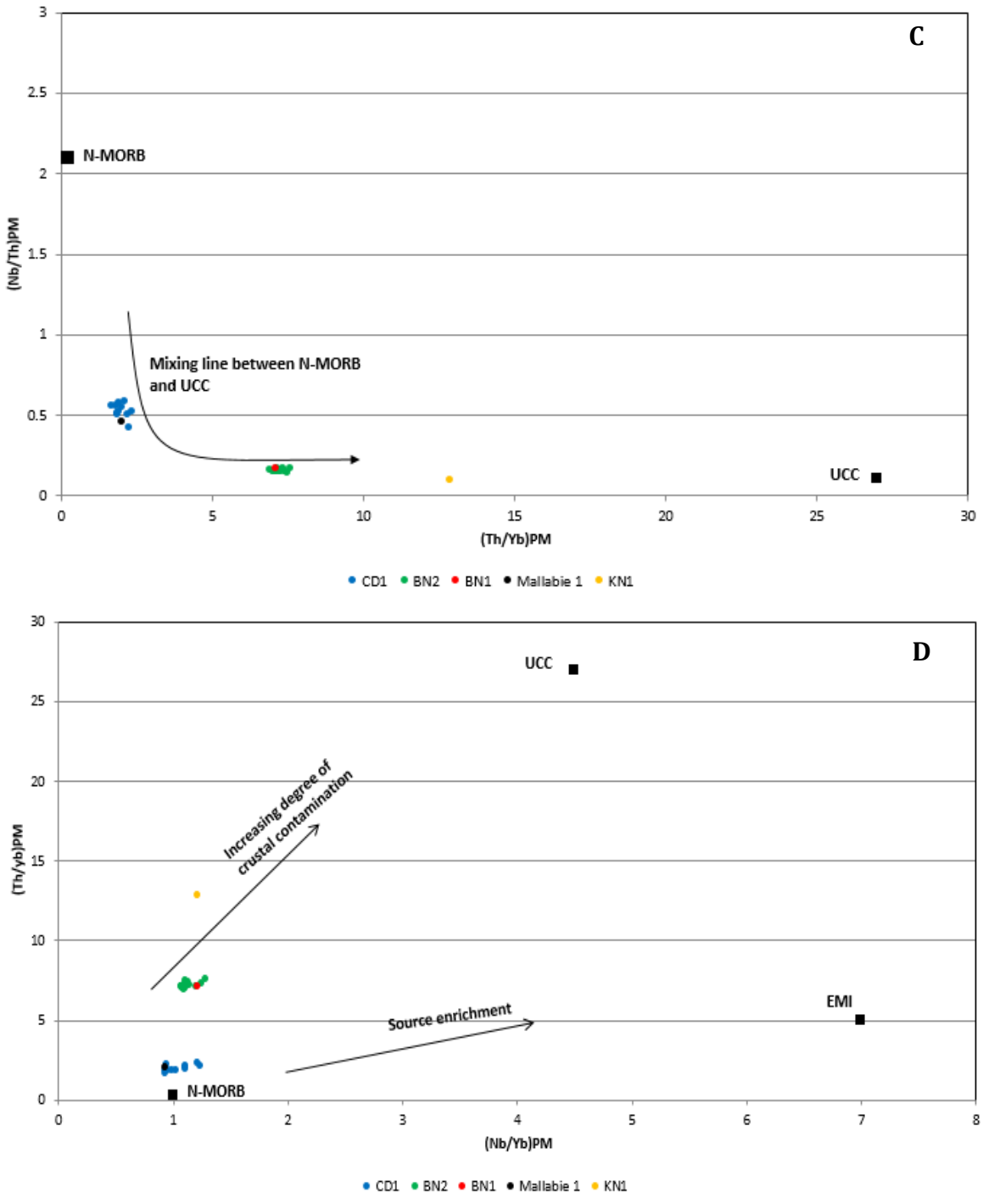

Figure 16: **(A)** Diagram showing variations in (Gd/Yb)PM and (Nb/La)PM ratios. **(B)** Diagram showing variations in (Gd/Yb)PM and (La/Sm)PM ratios. **(C)** Diagram showing variations in (Nb/Th)PM and (Th/Yb)PM ratios. The upper continental crust (UCC) value is from Taylor and McLennan (1985) and the N-MORB composition is from Hofmann (1988). An approximate mixing line between N-MORB and UCC is shown for reference. **(D)** Diagram showing variations in (Th/Yb)PM and (Nb/Yb)PM ratios. The enriched mantle value is from Condie (2001), and the primitive mantle (PM) value is from McDonough and Sun (1995). Lines showing increasing degrees of crustal contamination and source enrichment are shown for reference. In all diagrams ratios are normalised to the primitive mantle (PM) values of McDonough and Sun (1995).

4.2.3. Mineral chemistry of plagioclase and clinopyroxene

Major element and trace element data from in-situ electron probe micro analysis and LA-ICP-MS analysis of clinopyroxene and plagioclase from the basalt samples in CD1 selected for Sm-Nd geochronology is provided in Appendix C**.** Average trace element compositions of clinopyroxene and plagioclase from each of the samples are provided for reference in Table 1. Primitive mantle normalised REE variation diagrams (McDonough and Sun, 1995) showing variations in REE patterns for plagioclase and clinopyroxene, and representative whole rock patterns are presented in Figure 18. In each of the samples, plagioclase is characterized by a significant positive Eu anomaly (average Eu/Eu^{PM} = 1.76 – 5.30; where PM denotes the primitive mantle composition of McDonough and Sun (1995).

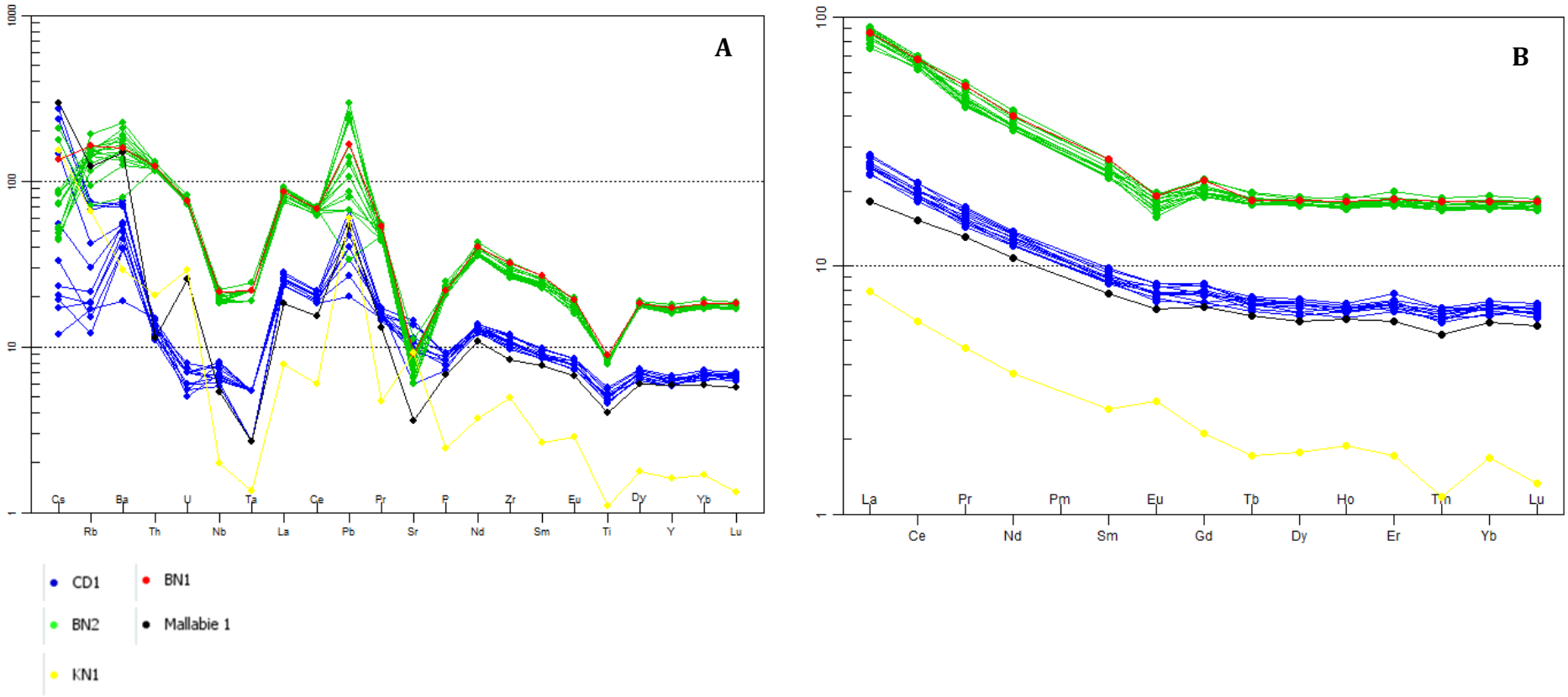

Figure 17: (A) Primitive mantle trace element variation diagram highlighting variations in the trace element compositions amongst the mafic rocks in the south-eastern Coompana Province. **(B)** Primiative mantle normalised REE variation diagram highlighting the LREE enrichment typical of the samples, and the considerable enrichment in both HREE and LREE of the BN2 dolerite and BN1 basalt samples with respect to the other samples. In each diagram values are normalised to the primitive mantle composition of McDonough and Sun (1995).

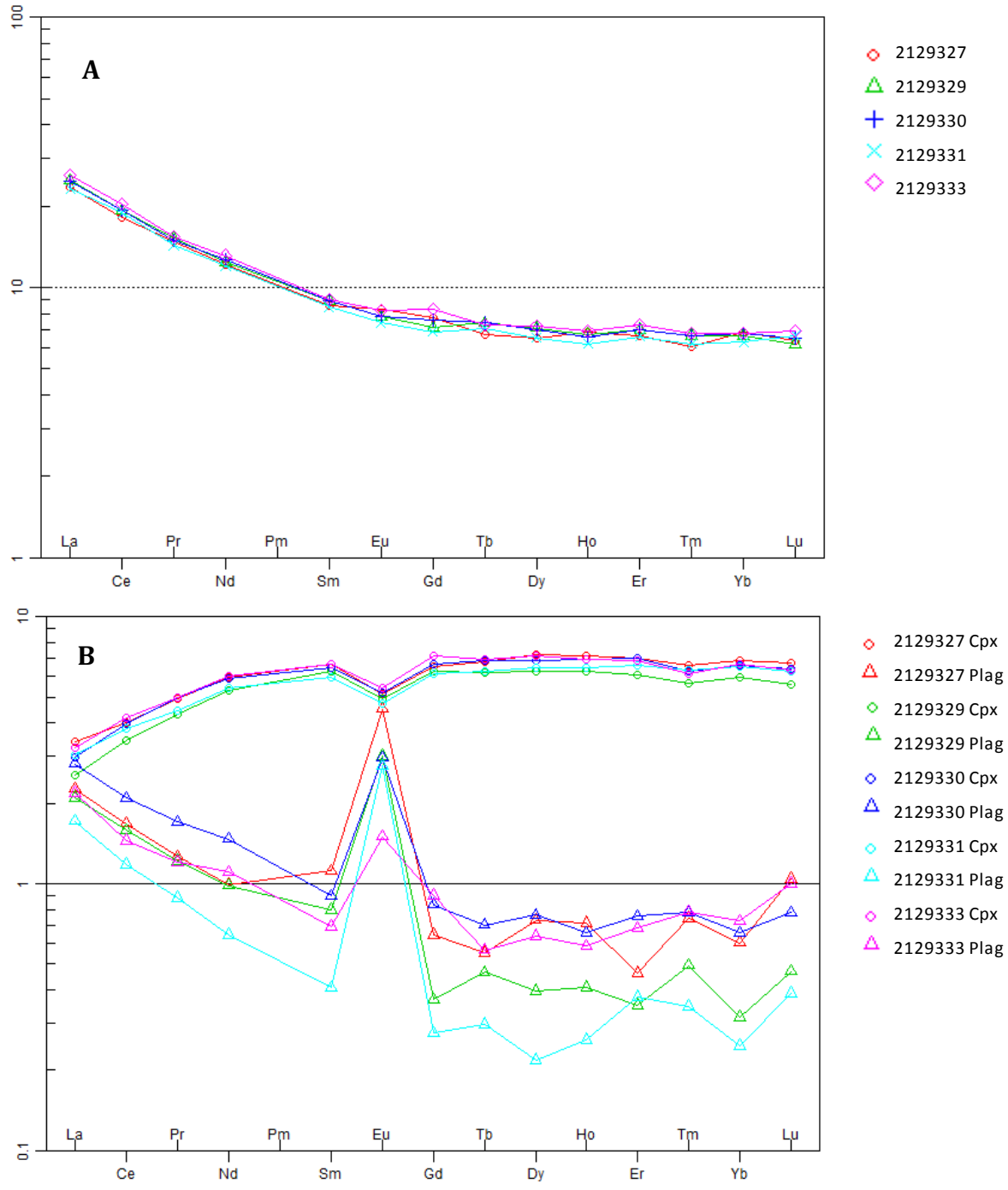

Figure 18: (A) Primitive mantle-normalised REE variation diagram for whole rock samples from CD1 selected for Sm-Nd geochronology. **(B)** Primitive mantle-normalised REE variation diagram for plagioclase and clinopyroxene from the respective CD1 samples analysed in-situ using LA-ICP-MS. Plagioclase displays LREE enrichment and flat to relatively variable HREE patterns. Clinopyroxene is depleted in LREE with respect to plagioclase, and shows relatively flat MREE and HREE patterns. In each diagram REE values are normalised to the primitive mantle values of McDonough and Sun (1995).

Table 1: Representative trace element compositions of plagioclase and clinopyroxene for the basalt samples from drill hole CD1 selected for Sm-Nd geochronology

	2129327		2129329		2129330		2129331		2129333	
	Cpx	**Plag**	**Cpx**	**Plag**	**Cpx**	**Plag**	**Cpx**	**Plag**	**Cpx**	**Plag**
ppm										
La	2.224	1.466	1.626	1.358	1.938	1.820	1.961	1.110	2.090	1.415
Ce	6.699	2.810	5.633	2.655	6.643	3.507	6.347	1.975	6.885	2.430
Pr	1.195	0.321	1.049	0.309	1.264	0.432	1.126	0.224	1.247	0.306
Nd	6.867	1.238	6.424	1.228	7.319	1.833	6.781	0.803	7.372	1.378
Sm	2.443	0.453	2.430	0.324	2.626	0.365	2.416	0.165	2.662	0.281
Eu	0.745	0.694	0.727	0.463	0.800	0.455	0.731	0.425	0.811	0.231
Gd	3.204	0.350	3.261	0.200	3.630	0.453	3.337	0.150	3.838	0.490
Tb	0.594	0.054	0.585	0.046	0.677	0.069	0.617	0.029	0.675	0.056
Dy	4.186	0.491	4.049	0.267	4.635	0.515	4.347	0.147	4.680	0.428
Ho	0.929	0.106	0.904	0.061	1.027	0.097	0.964	0.039	1.018	0.087
Er	2.617	0.202	2.599	0.153	3.068	0.330	2.881	0.165	2.937	0.298
Tm	0.390	0.051	0.369	0.034	0.425	0.053	0.427	0.024	0.414	0.053
Yb	2.640	0.265	2.529	0.139	2.908	0.288	2.854	0.109	2.878	0.319
Lu	0.388	0.071	0.368	0.032	0.433	0.053	0.423	0.026	0.421	0.068

4.3. Whole rock Sm-Nd isotope systematics

Results from Sm-Nd isotopic analyses of whole-rock mafic samples are summarized in Table 2. ε Nd(T) is calculated at 860 Ma for all samples based on results from Sm - Nd geochronology of basalt samples from CD1 (Table 3). Nd isotopic data expressed in epsilon notation (εNd) are plotted against age in Figure 19. Average crustal evolution lines for the Gawler Archaen (Swain et al., 2005) and Toolgana Supersuite in the Coompana Province (Smithies et al., 2015) are plotted for reference. Measured $^{143}Nd/^{144}Nd$ ratios for the samples range from 0.51168 to 0.51184. All of the samples plot in a tight group and show marked negative $\varepsilon Nd_{(860Ma)}$ values between -9.9 and -12.7.

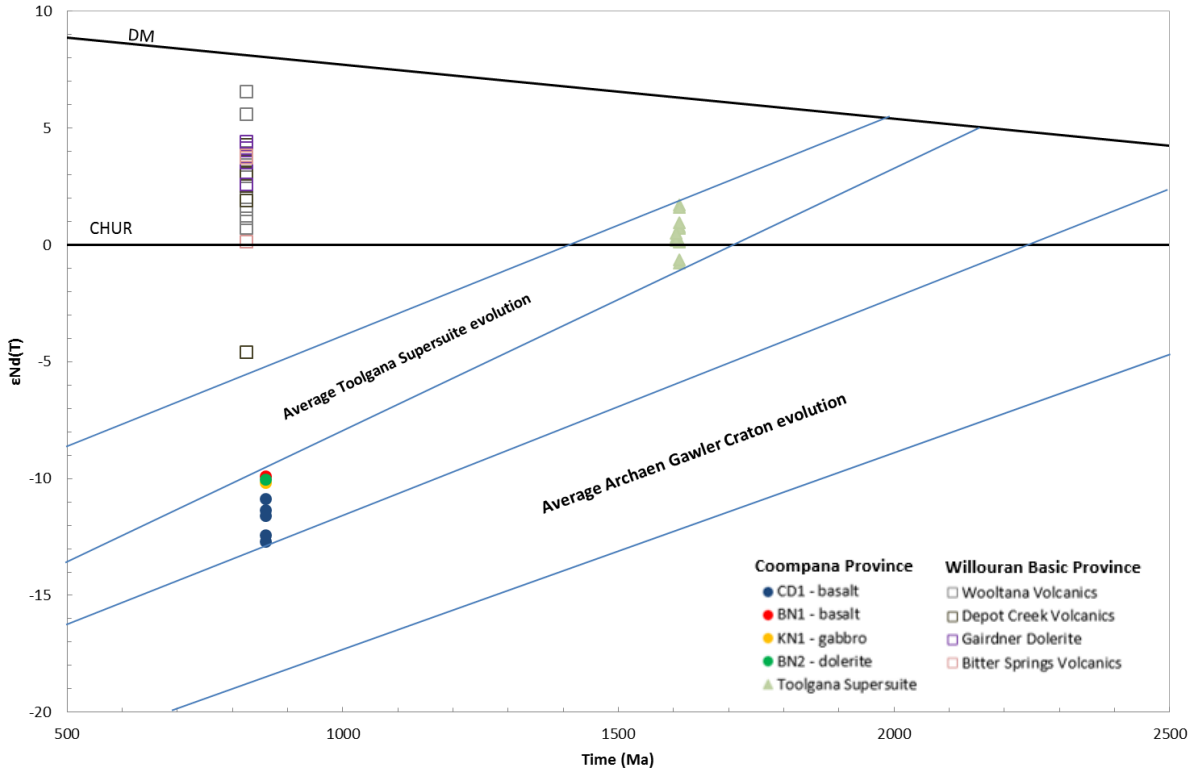

Figure 19: εNd evolution diagram highlighting the evolved εNd(860Ma) values of the mafic rocks in the south-eastern Coompana Province. Average crustal evolution lines for the Toolgana Supersuite in the Coompana Province and Archaen Gawler Craton are plotted using data from Spaggiari and Smithies (2015) and Swain et al. (2005), respectively. εNd(825Ma) values for various intrusive and volcanic suites in the Willouran Basic Province are also plotted for reference (Wooltana Volcanics: Foden et al., 2002; Wang et al., 2010; Depot Creek Volcanics: Wang et al., 2010; Gairdner Dolerite: Zhao et al., 1994; Amata Suite: Zhao et al., 1994; Bitter Springs Volcanics: Zhao et al., 1994).

Table 2: Sm-Nd isotopic data for mafic rocks from the south-eastern Coompana Province

Sample No.	Drillhole	Rock type	Interval (m)	Sm (ppm)	Nd (ppm)	$^{147}Sm/^{144}Nd$	$^{143}Nd/^{144}Nd$ (±2σ)	εNd(0)[a]	eNd(T)	TDM (Ma)[b]	T
2078892	BN1	Basalt	340 - 350	10.1264	48.0856	0.127323	0.511742 ± 2	-17.5	-9.9	2450	860
2129340	BN2	Dolerite	433.8 - 434	9.8556	46.8556	0.127171	0.511733 ± 2	-17.7	-10.0	2461	860
2078893	KN1	Gabbro	370 - 380	1.1808	4.8375	0.147578	0.511842 ± 5	-15.5	-10.2	2961	860
2129327	CD1	Basalt	320.7 - 320.9	3.3647	15.4224	0.131907	0.511681 ± 2	-18.7	-11.6	2696	860
2129329	CD1	Basalt	328.5 - 329.1	3.9204	16.7496	0.141514	0.511678 ± 2	-18.7	-12.7	3053	860
2129330	CD1	Basalt	331.7 - 332.4	3.7613	16.2624	0.139839	0.511683 ± 2	-18.6	-12.4	2975	860
2129331	CD1	Basalt	335.1 - 335.38	3.7061	15.6951	0.142763	0.511780 ± 3	-16.7	-10.8	2894	860
2129333	CD1	Basalt	358 - 358.5	3.8594	16.8669	0.138341	0.511729 ± 2	-17.7	-11.3	2827	860

a $143Nd/144Nd_{CHUR}(0) = 0.512638$, $147Sm/144Nd_{CHUR}(0) = 0.196600$

b Depleted mantle model ages of Goldstein et al. (1984): $^{143}Nd/^{144}Nd = 0.51315$, $^{147}Sm/^{144}Nd = 0.2145$

4.4. Sm-Nd Geochronology

Sm-Nd isotopic compositions of the mineral separates of plagioclase and clinopyroxene from the CD1 basalt samples are provided in Table 3. Sm and Nd concentrations obtained by isotope dilution were generally different to the corresponding in-situ data (Table 2). Variations of up to 30% have previously been recorded by other workers (e.g. Rampone et al., 2014). Calculations were made using Isoplot (Ludwig, 2003), and the resulting isochrons are shown in **Figure 20**. For this study, two-point isochrons were constructed using plagioclase and clinopyroxene mineral separates. In four of the five samples, plagioclase and clinopyroxene show strong fractionation and generate well-constrained isochrons. These samples produce ages that fall within the range 848±11 Ma and 963±26 Ma, and initial εNd values range between -10.5 and -12.4. Within this range, two sets of two ages are indistinguishable within error. Collectively, the four samples yield a weighted mean age of 859±66 Ma. In one sample, plagioclase and clinopyroxene displayed only minor fractionation and produce a less well constrained isochron, yielding an age of 1292±44 Ma.

Table 3: Nd isotopic compositions and Sm, Nd compositions of plagioclase and clinopyroxene fractions separated from the CD1 basalt samples.

Sample	Analysis	Nd (ppm)	Sm (ppm)	$^{143}Nd/^{144}Nd$ (±2σ)	$^{147}Sm/^{144}Nd$[a]	Age (Ma)	ϵ_{Nd}(initial)
2129327	*plag*	0.889	0.181	0.5116522 ± 3	0.123066	848±11	-11.2
	cpx	7.646	2.819	0.5122079 ± 5	0.222922		
2129329	*plag*	0.729	0.181	0.5115598 ± 29	0.130470	908±42	-13.3
	cpx	11.583	4.510	0.5121851 ± 5	0.235393		
2129330	*plag*	1.595	0.328	0.5116399 ± 13	0.124269	963±26	-10.5
	cpx	9.468	3.265	0.5121721 ± 3	0.208498		
2129331	*plag*	1.117	0.230	0.5116234 ± 9	0.124581	1292±44	-12.4
	cpx	9.129	2.478	0.5119588 ± 4	0.164109		
2129333	*plag*	0.921	0.181	0.5115721 ± 9	0.118717	842±14	-12.4
	cpx	11.879	4.527	0.5121887 ± 2	0.230411		

a 3% estimated error

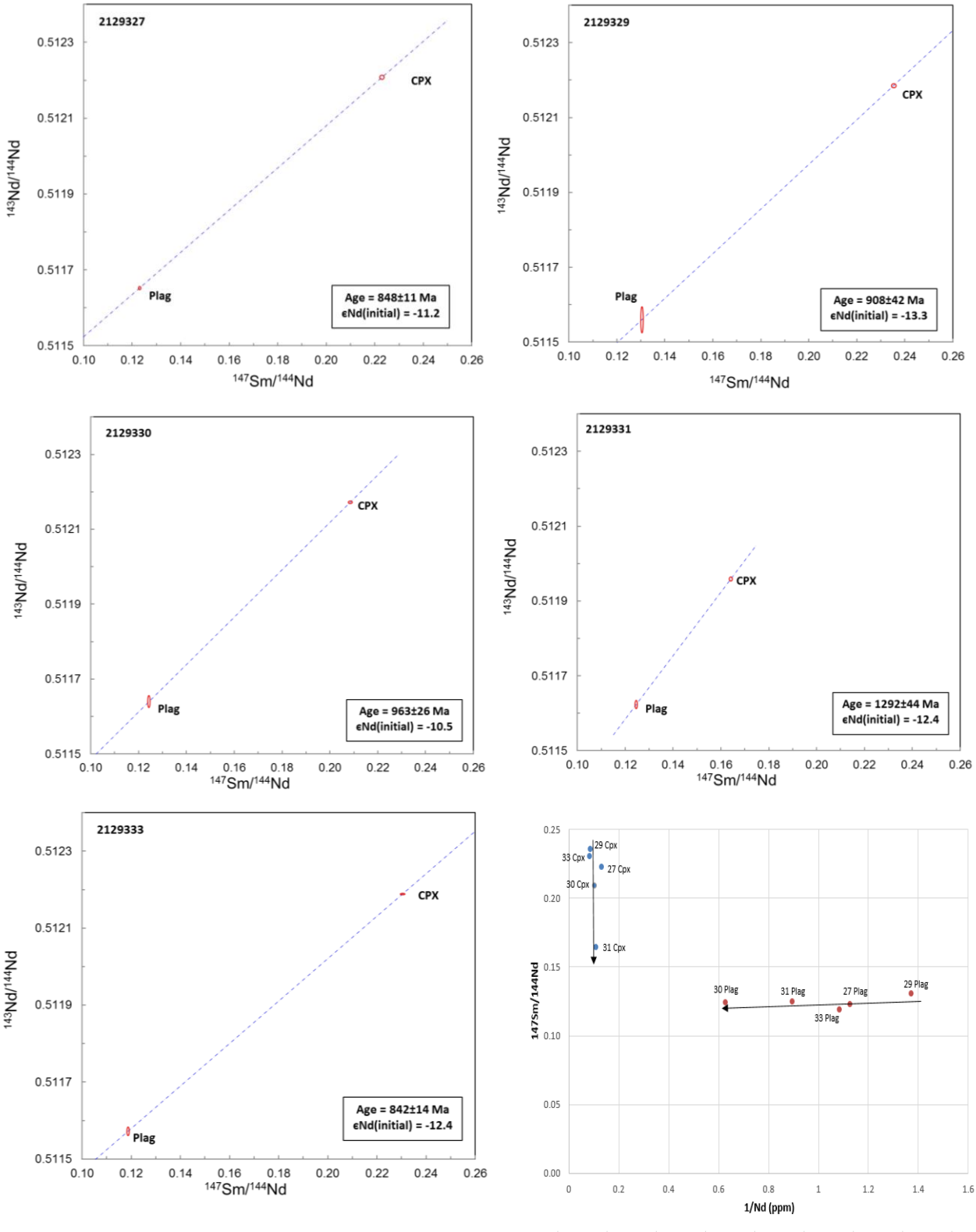

Figure 20: 143Nd/144Nd vs. 147Sm/144Nd internal isochrones of the plagioclase and clinopyroxene separates from the basalt samples taken from drillhole CD1. Isochrons were generated in Isoplot (Ludwig, 2003). An 147Sm/144Nd vs. 1/Nd variation diagram for plagioclase and clinopyroxene mineral separates is also presented.

5. DISCUSSION

5.1. Interpretation of mineral isochron ages and implications for timing of mafic magmatism in the Coompana Province

Significant difficulties have been noted by a number of authors when attempting to date mafic rocks using the Sm-Nd internal isochron method (e.g. Zhao and McCulloch, 1993 and references therein). Zhao and McCulloch (1993) noted that in the absence of U-Pb zircon/baddleyite ages or well-constrained stratigraphic relations, it is difficult to assess whether an Sm-Nd internal isochron age can be treated as a true crystallization age. Zhao and McCulloch (1993) indicated that the ages obtained through the internal isochron can represent a later metamorphic age (e.g. McCulloch and Black, 1984; Windrim et al., 1984), and although the REE's Sm and Nd are considered immobile, mobility and fractionation has been reported under low-temperature hydrothermal conditions (Hellman and Henderson, 1977; McLennan and Taylor, 1979).

During this study, attempts to separate baddleyite and zircon from the basalt samples were unsuccessful. Regardless, we argue that the ages obtained from four of the five mineral isochrons are likely to represent the magmatic age of the rocks for a number of reasons. Firstly, although the basalts intersected in drillhole CD1 have undergone low-temperature hydrothermal alteration, primary igneous textures remain largely intact (see section 4.1 and Figure 5). Hydrothermal alteration also appears to not have significantly modified the composition of Sm and Nd in the rocks (see section 5.2.1). Secondly, the refined mineral separation process used during this study was effective in producing portions of plagioclase and clinopyroxene that were more than 99% pure. The selFrag machine was effective in liberating grains, and considerable time was spent hand-picking grains which appeared effected by alteration. During this study, the more Fe-rich clinopyroxene varities were removed using the Frantz™ separator, and only augite was included in the final clinopyroxene portions. The more Fe-rich varieties of clinopyroxene have higher magnetic susceptibility ranges, while augite has a lower range. Clinopyroxene with lower magnetic susceptibility is suggested to have lower REE abundances and higher Sm/Nd ratios than varieties with higher magnetic susceptibilities (Zhao and McCulloch, 1993). Furthermore, REE abundances and Sm-Nd isotopic ratios vary amongst the sub-splits of clinopyroxene and plagioclase (Table 3; **Error! Reference source not found.**). This is consistent with crystal fractionation during crystallisation and suggests that the phases analysed represent primary magmatic products (Zhao and McCulloch, 1993).

Finally, four of the five samples produced broadly similar ages and two sets of two isochrons produced ages indistinguishable within error (Table 3; **Figure 20**). The reasons behind the considerably older age produced from sample 2129330 are unknown, however, are likely to be due to sample contamination or other human errors. Although isotopic disturbance related to hydrothermal alteration or other geological processes can not be completely ruled out, the evidence provided above suggests that the internal isochron ages of four of the five samples are likely to represent their primary magmatic ages. This reveals a distinctive episode of early-Neoproterozoic mafic magmatism in the Coompana Province at ca. 860 Ma. Therefore, these mafic units are not part of the Mesoproterozoic or older rocks that comprise the Coompana Province basement but are potential correlatives with the mafic units of the Willouran Basic Province

5.2. Geochemistry and Nd-isotopic signature of mafic magmatism

5.2.1. Effects of secondary alteration on the geochemical and isotopic systems

Hydrothermal alteration can modify the major element composition of a host rock and can cause trace element and REE mobility, causing the geochemical signature of a rock to differ from the signature at the time of formation (e.g. Rollinson, 1993). Therefore, it is important to first assess whether the trace and major element concentrations of the samples are undisturbed before determining the petrogenetic and source characteristics of mafic magmatism. The effects of secondary alteration on the major element compositions of mafic rocks can be assessed using CIW diagrams (Harnois, 1988; Wang et al., 2010). A minor negative correlation between CaO and CIW in the CD1 basalt samples suggests that alteration has caused some degree of CaO depletion (e.g. Wang et al., 2010). The positive correlation between K_2O and CIW for the samples from CD1 and BN2 suggests that these mafic rocks may have undergone K-metasomatism (Crawford and Hilyard, 1990; Wang et al., 2010). The BN2 dolerite samples show a stronger correlation between K_2O and CIW than the CD1 basalt samples. All of the other major elements appear to show no significant correlation with CIW. This suggests that their respective compositions have not been significantly effected by secondary alteration. The effects of secondary alteration on the trace element compositions of the mafic samples for the study were assessed using bivariate plots of Zr vs. selected immobile and incompatible trace elements ()**.** Nb, Nd, Sm, and Hf are positively correlated with Zr in both the intrusive and volcanic samples, suggesting they are immobile and not effected by alteration. Lu and Y show a minor positive correlation with Zr. Th, Yb,and Ti do not

appear to correlate with Zr, indicating these elements could have been mobile during alteration or alternatively effected by other secondary processes.

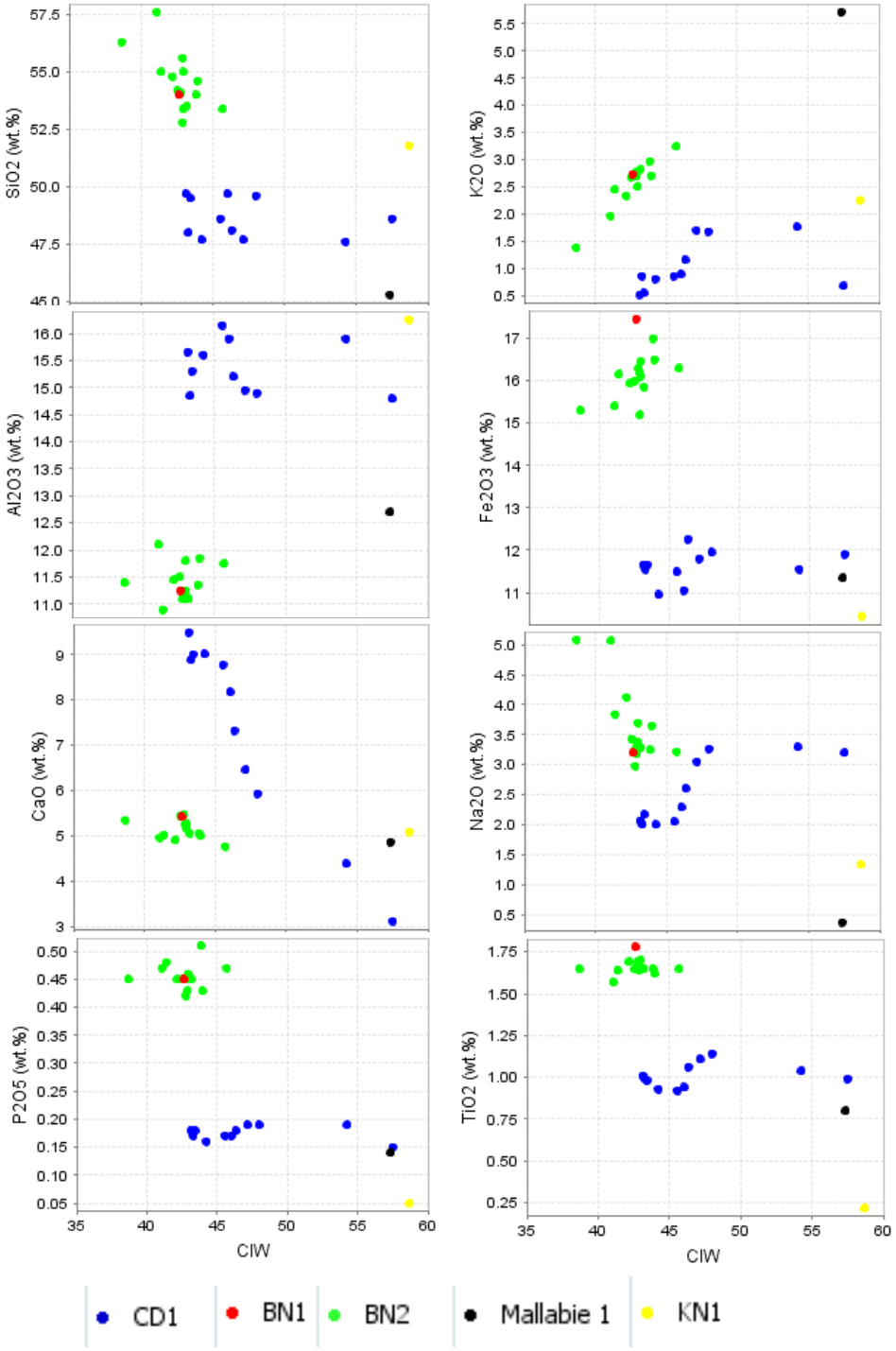

Figure 21: Selected major elements vs. CIW variation diagrams used to assess the effects of hydrothermal alteration on major element compositions of the samples for this study. CIW=Al2O3/(Al2O3+CaO+Na2O), molecular ratio (Harnois, 1988)

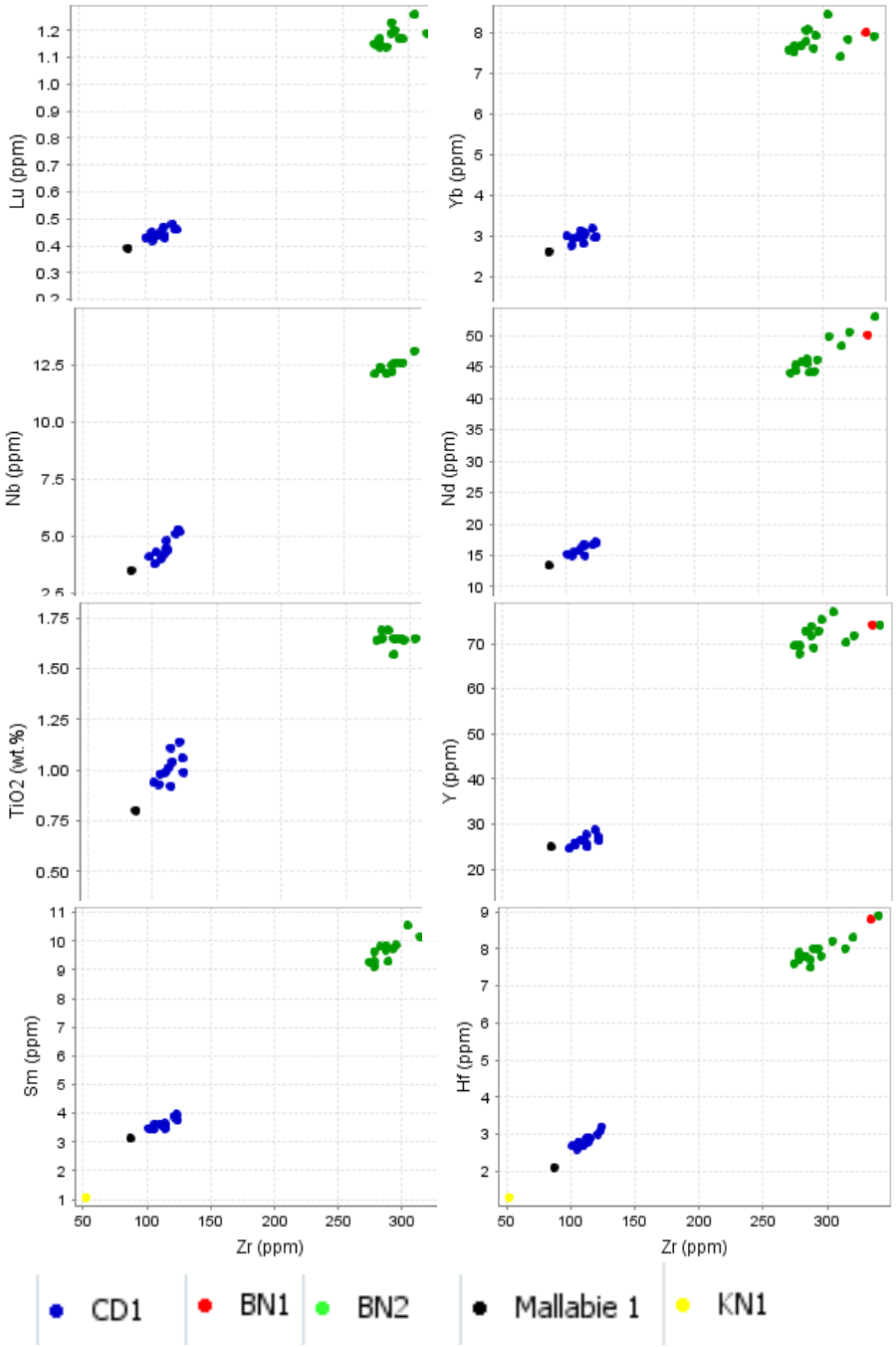

Figure 22: Trace element vs. Zr variation diagrams used to assess element mobility and the effect of secondary alteration on the composition of samples taken for this study.

5.2.2. Petrogenesis, crustal contamination, and source characteristics of mafic magmatism

Despite their close proximity and inferred genetic relationship (e.g. Flint and Daly, 1993), the suites of mafic rocks show significant major and trace element variation. Possible causes for this include varying degrees of partial melting, crystal differentiation, or the assimilation of varying degrees of crustal material (Lindh et al., 2001). The dolerite samples from BN2 and the basalt sample from BN1 are notably enriched in Fe_2O_3, and depleted in MgO with respect to the CD1, Mallabie 1, and KN1 samples. No mantle is able to produce a primary liquid as iron-rich as the samples in this study, indicating that differences in the chemical composition amongst the suites cannot be due to variable degrees of partial melting (Lindh et al., 2001). The BN1 and BN2 samples are significantly depleted in Cr and Ni with respect to the CD1, Mallabie 1, and KN1 samples. Cr/Ni ratios are not affected by crustal contamination, therefore variations must have originated early in the development of these mafic rocks (Lindh et al., 2001). Lindh et al. (2001) suggested that variations in Cr/Ni ratios could be due to crystal fractionation. This is consistent with the elevated Fe_2O_3 and depleted MgO content of the BN2 and BN1 samples with respect to the CD1, Mallabie 1, and KN1 samples. Lindh et al. (2001) also noted that early crystal fractionation can cause Fe-enrichment in mafic rocks.

Major and trace element variation diagrams provide evidence for either tholeiitic or calc-alkaline affinities (**Figure 14** and Figure 15). Ti/V ratios for the samples from CD1 and Mallabie 1 (Ti/V between 20 and 50) are consistent with continental flood basalt or MORB-type magmatism, and indicate that melts were produced by 20 – 30% partial melting under reducing conditions within an extensional environment (Figure 6; Shervais, 1982). However, there is considerable overlap between calc-alkaline basalts, continental flood basalts and arc tholeiites zone on the diagram, and most of the samples plot in this overlapping zone. In comparison, Ti/V ratios for the BN2 and BN1 samples are more consistent with alkaline magmas (Shervais, 1982). Ti-Zr-Y and Y-La-Nb discrimination diagrams also provide evidence for calc-alkaline magmatism, and the samples are all enriched in K (**Error! Reference source not found.** and Figure 14). Higher absolute abundances of K are typical of calc-alkaline magmatism, while lower abundances are more common of tholeiitic magmas (Peccerillo and Taylor, 1976). However, calc-alkaline affinities are also observed by crustal assimilation of subduction modified crust by tholeiitic magams (Grove et al., 1982).

Immobile and incompatible trace-element ratios were used to: (1) constrain the type of the magma source or sources for the mafic rocks in the south-eastern Coompana Province; and (2) assess whether the primary geochemical

signature of these rocks has been affected by assimilation of crustal material or magma mixing with more enriched melts (e.g. Jowitt and Ernst, 2013; Wallace et al., 2015).

(Gd/Yb)PM ratios plotted against (Nb/La)PM ratios were used to determine the depth of the mantle source of the magma from which these rocks were derived, and to assess whether the mafic rocks were formed from arc-related magmas or if more primitive, mantle-derived magmas assimilated arc-lithospheric material (Figure 16). The low (Gd/Yb)PM ratios for the samples (less than 1.5) suggest that magmas were derived from moderate to high-degree partial melting of spinel lherzolite mantle at shallow depths (Wallace et al., 2015). (Gd/Yb)PM ratios amongst the suites of mafic rocks are also tightly grouped, indicating that they could be derived from the same mantle source (Wallace et al., 2015). (Nb/La)PM ratios for the samples are low, indicating either arc related magmatism or alternatively that mantle-derived magmas have assimilated arc-lithospheric material (Wallace et al., 2015). (Nb/La)PM ratios for the samples from BN2 and BN1 are slightly lower than the basalt samples from CD1 and the sample from Mallabie 1, indicating that they may have assimilated more arc-lithospheric material. (La/Sm)PM ratios plotted against (Gd/Yb)PM ratios were used to determine whether the magmas were derived from an enriched or crustal source, or if they were derived from a more juvenile, depleted source (Figure 8; Jowitt and Ernst, 2013). All of the samples have (La/Sm)PM ratios over two, suggesting either crustal contamination or that magmas were derived from a relatively enriched part of the mantle (Wallace et al., 2015). The near uniform (Gd/Yb)PM ratios suggest a common mantle source, therefore, differences in (La/Sm)PM ratios could be a function of varying degrees of crustal contamination amongst the samples. This suggests that the mafic rocks from BN2 and BN1 could have assimilated more crustal material than the mafic rocks intersected in CD1, Mallabie 1, and KN1.

(Th/Yb)PM and (Nb/Yb)PM ratios were used to further assess whether the geochemical signature of the samples reflects crustal contamination or alternatively if magmas were derived from melting of enriched mantle sources (8; Pearce, 2008). (Nb/Yb)PM values for the samples are similar to values expected of unenriched (e.g. MORB-like) mantle material (Wallace et al., 2015). Similarly low (Nb/Yb)PM values amongst the samples suggests that they were derived from the same mantle source. Low (Nb/Yb)PM values coupled with high (Th/Yb)PM values in the BN2 and BN1 samples suggest crustal contamination (Pearce, 2008; Jowitt and Ernst, 2013). The higher (Th/Yb)PM values of the BN2 and BN1 samples with respect to the CD1 and Mallabie 1 samples further suggests they may have assimilated more crustal material. The gabbro sample from KN1 has the highest (Th/Yb)PM value of the samples, indicating it might have assimilated the most crustal material of the rocks taken for this study. The low (Nb/Th)PM

amongst samples with respect to N-MORB provide further evidence for crustal contamination (Figure 8; Lightfoot and Hawkesworth, 1988; Lightfoot et al., 1990; Jowitt and Ernst, 2013).

Almost all of the samples show pronounced depletion in the HFSE's Nb and Ti coupled with LREE enrichment and HREE depletion. Depletions in HFSE (in particular Nb and Ti) with respect to the LILEs, coupled with enriched LREEs and depleted HREEs are distinctive features of subduction-related convergent margin magmatism (e.g. Swain et al 08). However, Nb and Ti depletions coupled with LREE are also widespread geochemical features of the continental crust (Rudnick and Gao, 2003). The sample from KN1 is the most depleted in Nb and Ti of the samples taken for this study, and the BN2 and BN1 samples are considerably more depleted than the Mallabie 1 and CD1 samples. This further suggests that they may have assimilated more crustal material than the other samples. Enrichment in HREE and LREE can also be attributed to crystal fractionation (Lindh et al., 2001). Crystal fractionation is suggested to have caused the variations in Fe_2O_3 and MgO observed amongst the samples. Therefore, it is possible that a combination of crystal fractionation and crustal contamination has caused the variably trace element and REE values observed amongst the samples.

Recent work by the GSWA suggests that the known crustal precursors in the Coompana Province originated in a new crustal generation event at ca. 1900 Ma, and is a correlative for the precursor protoliths from the Musgrave Province and Madura Province basement (Kirkland et al., 2013, 2014; Spaggiari and Smithies, 2015). This new juvenile crustal element then evolved through three distinct reworking and magmatic events. At ca. 1610 Ma, Toolgana Supersuite magmatism included co-genetic suites of granite and monzodioritic rocks that preserve volcanic arc like compositions indicating a subduction-modified source (Spaggiari and Smithies, 2015). These have been correlated with the Saint Peter Suite along the south-western margin of the Gawler Craton (Smithies et al., 2015). At ca. 1500, a second magmatic event involved significant extension and addition of new juvenile asthenopheric derived melts and assimilation of the arc-modified Toolganna Supersuite (Wade et al., 2007; Smithies et al., 2015) The final event recorded in the Coompana basement rocks is the ~ 1192 – 1150 Ma Moondini Supersuite magmatism which produced a diverse range of magmatic rocks and is suggest to represent deep melting of an earlier subduction metasomatised lithosphere (Smithies et al., 2015). The geochemical characteristics of the ca. 860 Ma mafic rocks from the Coompana Province, including Nb and Ti anomalies, LREE enrichment, K-anomalies, and calc-alkaline affinities on trace and major element classification diagrams are consistent with assimilation of subduction/arc related continental crust (e.g. Swain et al., 2008). This indicates that the Toolgana Supersuite is the likely contaminant.

The mafic rocks in the Coompana Province are characterized by highly evolved $\varepsilon Nd_{(860Ma)}$ values (Figure 19 and Table 2). Evolved values are typical of an enriched mantle or crustal source (Rollinson, 1993). The Nd-isotopic data for the crustal units in the Coompana Province indicate that juvenile, depleted mantle material was added over the three time intervals discussed above (Smithies et al., 2015). Smithies et al. (2015) suggest that the compositional evolution of these crustal units does not require the addition or contribution from older, non-radiogenic sources. When re-calculated at 860 Ma, the most isotopically evolved sample from the Coompana Province crust yields an $\varepsilon Nd_{(860Ma)}$ value of -9.6 (Smithies et al., 2015). Therefore, it is possible that the highly evolved Nd isotopic values of the mafic samples taken for this study are entirely due to assimilation of Coompana Province crust, and, like the earlier crustal units do not require addition or contribution from older radiogenic sources. However, the marked negative $\varepsilon Nd_{(850Ma)}$ values for the samples indicate that addition of radiogenic Nd from a more evolved crustal source is possible .

Mixing calculations using the expression of Patchett and Bridgwater (1984) were completed to determine how much Toolgana Supersuite crustal material or Archaen Gawler Craton (Mulgathing Complex) crustal material would need to be added to a mantle-derived melt in order to attain the highly evolved Nd-isotopic values of the mafic rocks (Figure 19). The Nd concentration of potential mantle-derived melts for the Coompana Province mafic rocks are not known. As such, an average N-MORB source with Nd concentration of 11 ppm was used in this study (Hofmann, 1988; Hart et al., 1999). It has been noted previously that the Nd concentration of the source melt do impact the results of the calculations (e.g. Wade et al., 2006), and as such, the results should be treated simply as estimations. The mixing calculations argue for the addition of approximately 105 % Toolgana Supersuite material to an N-MORB source to yield the evolved Nd-isotopic values for the mafic rocks or alternatively 39 % of a more evolved Archaen Gawler craton source (average Mulgathing Complex). It is likely that the mafic rocks in the Coompana Province have assimilated some degree of Toolgana Supersuite crustal material, given their subduction/arc-related geochemical features, however, assimilation of more evolved material can not be conclusively ruled out.

5.3. Regional correlations and new constraints for the Willouran Basic Province

During this study, only samples of the basalt intersected in drill hole CD1 were dated using the Sm-Nd mineral isochron method. The BN2 dolerite, BN1 basalt, KN1 gabbro, and the CD1 basalts have variable major and trace element composition. This is attributed to varying degrees of crustal contamination and crystal fractionation. When accounting for the effects of these secondary processes, it is possible that they have similar primary geochemical signatures, indicating they may be derived from the same mantle source. Mafic rocks intersected these drill holes are overlain by various sedimentary units of the Bight and Dennam bains (Carpentaria Exploration Co. Pty. Ltd., 1982; The Shell Co. of Australia Ltd, 1983). Therefore, even if the mafic rocks intersected in each of the drillholes were derived from different magma sources, the stratigraphic similarities suggest they were coeval. The relationship between the basalt in CD1 and the basalt in Mallabie 1 is unclear. Both have similar major and trace element compositions, however, the Nd-isotopic composition of the basalt in Mallabie 1 is unknown. However, volcanics in CD1 and Mallabie 1 are stratigraphically overlain by Permain sedimentary units of the Bight and Denman Basins, respectively (Outback Oil Company NL, 1969; The Shell Co. of Australia Ltd, 1983). This indicates they are likely to be coeval. Mallabie 1 is located almost 150 km from CD1, suggesting that ca. 860 Ma mafic magmatism could spread over most of the south-eastern Coompana Province. It has been suggested that one of the mafic intrusions defined in the aeromagnetic patterns was intersected in drillhole BN2 (Aldous, 1982; Carpentaria Exploration Co. Pty. Ltd., 1982; Flint and Daly, 1993). Therefore, considering the likely co-genetic nature of these mafic rocks, it is possible that the other negative magnetic anomalies defined in the aeromagnetic patterns could also represent ca. 860 Ma mafic intrusives.

The mean weighted age of the four samples not considered to be disturbed by sample contamination or other human errors (859±66 Ma) is indistinguishable within error of the ca. 800 – 830 Ma age constraints for the various suites of intrusive and extrusive rocks in the Willouran Basic Province (Fanning et al., 1986; Zhao and McCulloch, 1993; Zhao et al., 1994; Sun et al., 1996; Wingate et al., 1998b; Wang et al., 2010). Mafic magmatism occurred across much of central and southern Australia during this period, and was associated with NE-SW-directed intracratonic extension which resulted in the formation of aerially extensive Centralian Superbasin and the development of the Adelaide Geosycnline (de Vries et al., 2008). Considering that no other episodes of mafic magmatism are recognised in central or southern Australia during this period, ca. 860 Ma magmatism in the Coompana Province most likely occurred

during this widespread magmatic event. The geochemical and Nd-isotopic signatures of ca. 860 Ma mafic rocks in the Coompana Province and the suites of mafic rocks in the Willouran Basic Province vary considerably. The various suites of extrusive and intrusive mafic rocks in the Willouran Basic Province have almost uniform geochemical and Nd-isotopic compositions (e.g. Crawford and Hilyard, 1990; Zhao et al., 1994; Wang et al., 2010). This has been suggested to represent a common mantle source, and also imply that crustal contamination was minimal (Zhao et al., 1994). When accounting for the effects of crustal contamination and crystal differentiation on the primary geochemical signature of the mafic rocks in the Coompana Province, it is possible that they were similar to the signatures of the suites in the Willouran Basic Province. This would suggest a common mantle source. However, it is difficult to accurately quantify the extent that these processes have modified the primary geochemical signatures of the mafic rocks.

Crawford and Hilyard (1990) first considered the Willouran Volcanics at the base of the Adelaide Geosyncline and the GDS across the Gawler Craton as a large basic province. The dimensions of the province were later extended by Zhao et al. (1994) to include the mafic dykes of the Amata Suite in the Musgrave Province and the BSV in the Amadeus Basin, and by Wingate et al. (1998) to include a series of mafic intrusives in the Willyama Inlier. Correlations have also been proposed by Claoué-Long and Hoatson (2010) with mafic rocks in the Patterson Province (Maidment et al., 2008) and with a swarm of undated NW-trending dolerite dykes at the southwest margin of the Kimberley Province (Griffin et al., 1993). We suggest that the Willouran Basic Province now be extended to include the ca. 860 Ma mafic volcanics and intrusives in the south-eastern Coompana Province. No age constraints are available for the NW-trending mafic dykes defined in the aeromagnetic patterns of the Coompana Province. However, given their similar orientation with the mafic dykes of the GDS and Amata Suite, and that they are likely to be co-genetic with the mafic volcanics and intrusives, it is possible that they too form part of this regionally extensive igneous province.

6. CONCLUSIONS

The results from this study have important implications for our understanding of the geological evolution of the Coompana Province, and also provide new constraints on the extent of the Willouran Basic Province:

- Three episodes of Paleo- to Mesoproterozoic mafic and felsic magmatism have previously been recognised in the Coompana Province between ca. 1610 Ma and ca. 1140 Ma (Wade et al., 2007; Spaggiari and Smithies, 2015). Dating of basalt intersected in the Shell Australia drill hole CD1 in the south-eastern Coompana Province using the Sm-Nd mineral isochron method reveals a fourth distinctive, Neoproterozoic, episode of mafic magmatism at ca. 860 Ma.

- The geochemical and Nd-isotopic signatures of ca. 860 ma mafic magmatism in Coompana Province, including Nb and Ti anomalies, LREE enrichment, K-anomalies, calc-alkaline affinities, and near uniform highly evolved $\varepsilon Nd_{(860Ma)}$ values between -9.9 and -12.7 are consistent with assimilation of crustal material (e.g. Swain et al., 2008). While the assimilation of minor quantities of evolved, Archaen Gawler Craton crust cannot be completely ruled out, the subduction/arc related Coompana Province crust is suggested to be the likely contaminant.

- Geochemical variations amongst mafic rocks in the south-eastern Coompana Province are attributed to varying degrees of crystal differentiation and crustal contamination of magma derived from the same mantle source. However, different mantle sources can not conclusively be ruled out.

- The results from this study indicate that ca. 860 Ma mafic magmatism in the south-eastern Coompana Province was most likely coeval with the other magmatic suites which make up the Willouran Basic Province. We suggest that the Willouran Basic Province now be expanded to include the ca. 860 Ma mafic volcanics and intrusives in the south-eastern Coompana Province.

7. ACKNOWLEDGEMENTS

Supervisors Professor Martin Hand and Dr. Rian Dutch are thanked for their generous support and guidance throughout the year. The Geological Survey of South Australia is thanked for providing financial support for this project. A very big thanks go to David Bruce for his help and guidance in the isotope lab, and also to Ben Wade and the staff at Adelaide microscopy for all of their help over the year. Justin Payne is thanked for his assistance with Hf-isotopic analysis. Katie Howard is thanked for all of her help and guidance across the year. The AusIMM are also thanked for the opportunity to receive a Sir Frank Espie / Rio Tinto Leadership Award this year.

8. REFERENCES

ACHTERBERGH, E. VAN, RYAN, C., JACKSON, S., AND GRIFFIN, W. 2001. Data reduction software for LA-ICP-MS. *Laser-Ablation-ICPMS in the …*.

ALDOUS, R. 1982. A report on the drilling extension of CEC's drillhole BN2 at the Bundulla E.L. (no. 849) South Australia (Camberwell).

ALS GEOCHEMISTRY 2015. ALS Geochemistry; Schedule of Services & Fees; 2015 AUD.

ALS MINERALS 2009. Geochemical Procedure: ME- MS81.

CABANIS, B., AND LECOLLE, M. 1989. Le diagramme La/10-Y/15-Nb/8: un outil pour la discrimination des séries volcaniques et la mise en évidence des processus de mélange et/ou de contamination crustale. *CR Acad. Sci. Ser. II* **309**, 2023–2029.

CARPENTARIA EXPLORATION CO. PTY. LTD. 1982. Open File Envelope No. 3604: EL503 and EL905; Koonalda; Progress reports for the period 7/8/79 to 18/7/82.

CARPENTARIA EXPLORATION CO. PTY. LTD., AND BHP MINERALS PTY. LTD. 1982. EL 472 and EL 849 Bundulla; Progress reports for the period 24/5/79 TO 19/10/82 Open File Envelope No. 3515; ((unpublished): South Australian Department of Mines and Energy).

CARPTENTARIA EXPLORATION CO. PTY LTD, AND BHP MINERALS PTY LTD 1982. Open File Envelope No. 3515, EL472 and EL 849 Bundulla (Adelaide, South Australia).

CLAOUÉ-LONG, J., AND HOATSON, D. 2010. Australian LIPs and the Australian Precambrian 'barcode' (Canberra).

CONDIE, K. 2001. Mantle Plumes and Their Record in Earth History (Oxford, United Kingdom: Cambridge University Press).

COX, K.G., BELL, J.D., AND PANKHURST, R.. 1979. The interpretation of igneous rocks (London: George, Allen and Unwin).

CRAWFORD, A.J., AND HILYARD, D. 1990. Geochemistry of Late Proterozoic tholeiitic flood basalts, Adelaide Geosyncline, South Australia. In The Evolution of a Late Precambrian-Early Palaeozoic Rift Complex: The Adelaide Geosyncline, pp. 49–67.

FABRIS, A., CONSTABLE, S., CONOR, C., WOODHOUSE, A., HORE, S., AND FANNING, M. 2005. Age, origin, emplacement and mineral potential of the Oodla Wirra Volcanics, Nackara Arc, central Flinders Ranges. *MESA Journal* **37**, 44–52.

FANNING, C.M., LUDWIG, K.R., FORBES, B.G., AND PREISS, W. V 1986. Single and multiple grain U–Pb zircon analyses for the early Adelaidean Rook Tuff, Willouran Ranges, South Australia. In Geological Society of Australia Abstracts, pp. 71–72.

FLINT, R.B., AND DALY, S.J. 1993. Coompana block. *The Geology of South Australia* **1**, 168–169.

GIBSON, G.M., MAIDMENT, D.M., AND HAREN, R. 1996. Re-evaluating the structure of Broken Hill: implication for mineral exploration and the interpretation of airborne magnetic data. *AGSO Research Newsletter* **25**, 1–3.

GIBSON, G.M., MAIDMENT, D.W., AND HAREN, R. 1997. Willyama Supergroup, Broken Hill, Australia: a 1600 Ma granulite terrane situated along the Neoproterozoic margin of Gondwana following continental rifting and break-up of Rodinia. In Terrane Dynamics 97, Abstracts of the International Conference on Terrane Geology. Christchurch, NZ, pp. 71–74.

GIESE, J., SEWARD, D., GNOS, E., AND KURZ, D. 2007. Comparative apatite fission track study of conventionally versus selFrag Lab fragmented samples. *Geochimica et Cosmochimica Acta* **71**, A322.

GRIFFIN, T.J., TYLER, I.M., AND PLAYFORD, P.E. 1993. Lennard River, Western Australia. *Western Australia Geological Survey* **1**, 0.

GROVE, T.L., GERLACH, D.C., AND SANDO, T.W. 1982. Origin of calc-alkaline series lavas at Medicine Lake Volcano by fractionation, assimilation and mixing. *Contributions to Mineralogy and Petrology* **80**, 160–182.

HARNOIS, L. 1988. The CIW index: A new chemical index of weathering. *Sedimentary Geology* **55**, 319–322.

HART, S.R., BLUSZTAJN, J., DICK, H.J.B., MEYER, P.S., AND MUEHLENBACHS, K. 1999. The fingerprint of seawater circulation in a 500-meter section of ocean crust gabbros. *Geochimica et Cosmochimica Acta* **63**, 4059–4080.

HELLMAN, P.L., AND HENDERSON, P. 1977. Are rare earth elements mobile during spilitisation?

HOFMANN, A.W. 1988. Chemical differentiation of the Earth: the relationship between mantle, continental crust, and oceanic crust. *Earth and Planetary Science Letters* **90**, 297–314.

IRVINE, TN., AND BARAGAR, WRA. 1971. A guide to the chemical classification of the common volcanic rocks. *Canadian Journal of Earth Sciences* **8**, 523–548.

JOWITT, S.M., AND ERNST, R.E. 2013. Geochemical assessment of the metallogenic potential of Proterozoic LIPs of Canada. *Lithos* **174**, 291–307.

KENDALL, B., CREASER, R.A., AND SELBY, D. 2006. Re-Os geochronology of postglacial black shales in Australia: Constraints on the timing of 'Sturtian' glaciation. *Geology* **34**, 729–732.

KIRKLAND, C.L., SMITHIES, R.H., AND SPAGGIARI, C. V 2014. Foreign contemporaries–Unravelling disparate isotopic signatures from Mesoproterozoic Central and Western Australia. *Precambrian Research*.

KIRKLAND, C.L., SMITHIES, R.H., WOODHOUSE, A.J., HOWARD, H.M., WINGATE, M.T.D., BELOUSOVA, E.A., CLIFF, J.B., MURPHY, R.C., AND SPAGGIARI, C. V 2013. Constraints and deception in the isotopic record; the crustal evolution of the west Musgrave Province, central Australia. *Gondwana Research* **23**, 759–781.

KUNO, H. 1968. Differentiation of basalt magmas. *Basalts* **2**, 623–688.

LAMBOURN, S.S. 1972. An interpretation of the airborne magnetic and radiometric survey of the Coompana, Nullabor, Fowler, and Nuyts (Onshore) 1:250 000 sheet areas, S.A. 1972/3 (Canberra).

LIGHTFOOT, P.C., AND HAWKESWORTH, C.J. 1988. Origin of Deccan Trap lavas: evidence from combined trace element and Sr-, Nd- and Pb-isotope studies. *Earth and Planetary Science Letters* **91**, 89–104.

LIGHTFOOT, P.C., HAWKESWORTH, C.J., DEVEY, C.W., ROGERS, N.W., AND CALSTEREN, P.W.C. V. 1990. Source and Differentiation of Deccan Trap Lavas: Implications of Geochemical and Mineral Chemical Variations. *Journal of Petrology* **31**, 1165–1200.

LINDH, A., ANDERSSON, U.B., LUNDQVIST, T., AND CLAESSON, S. 2001. Evidence of crustal contamination of mafic rocks associated with rapakivi rocks: an example from the Nordingrå complex, Central Sweden. *Geological Magazine* **138**, 371–386.

LUDWIG, K. 2003. User's manual for Isoplot 3.00: a geochronological toolkit for Microsoft Excel.

MAIDMENT, D., HUSTON, D., MAAS, R., CZARNOTA, K., NEUMANN, N., MCINTYRE, A., AND BAGAS, L. 2008. The Nifty-Kintyre-Duke Cu–U–Pb–Zn mineralizing events: links to the evolution of the Yeneena Basin, northwest Paterson Orogen. *Geological Sur-Vey of Western Australia, Record* **2**, 3.

LE MAITRE, R.W., BATEMAN, P., DUDEK, A., KELLER, J., LAMEYRE, J., LE BAS, M.J., SABINE, P.A., SCHMID, R., SORENSEN, H., AND STRECKEISEN, A. 1989. A classification of igneous rocks and glossary of terms: Recommendations of the International Union of Geological Sciences Subcommission on the Systematics of Igneous Rocks (Blackwell Oxford).

MCCULLOCH, M.T., AND BLACK, L.P. 1984. Sm Nd isotopic systematics of Enderby Land granulites and evidence for the redistribution of Sm and Nd during metamorphism. *Earth and Planetary Science Letters* **71**, 46–58.

MCDONOUGH, W.F., AND SUN, S. -S. 1995. The composition of the Earth. *Chemical Geology* **120**, 223–253.

MCLENNAN, S.M., AND TAYLOR, S.R. 1979. Rare earth element mobility associated with uranium mineralisation. *Nature* **282**, 247–250.

MUNSON, T., KRUSE, P., AND AHMAD, M. 2013. Centralian Superbasin: in Ahmad M and Munson TJ (compilers). Geology and mineral resources of the Northern Territory.

OUTBACK OIL COMPANY NL 1969. Open File Envelope No. 1172: Mallabie 1 Well Completion Report (Adelaide, South Australia).

PATCHETT, P.J., AND BRIDGWATER, D. 1984. Origin of continental crust of 1 . 9-1 . 7 Ga age defined by Nd isotopes in the Ketilidian terrain of South Greenland. *Contributions to Mineralogy and Petrology* **87**, 311–318.

PATCHETT, P.J., KOUVO, O., HEDGE, C.E., AND TATSUMOTO, M. 1982. Evolution of continental crust and mantle heterogeneity: Evidence from Hf isotopes. *Contributions to Mineralogy and Petrology* **78**, 279–297.

PAYNE, J.L., BAROVICH, K.M., AND HAND, M. 2006. Provenance of metasedimentary rocks in the northern Gawler Craton, Australia: Implications for Palaeoproterozoic reconstructions. *Precambrian Research* **148**, 275–291.

PAYNE, J.L., PEARSON, N.J., GRANT, K.J., AND HALVERSON, G.P. 2013. Reassessment of relative oxide formation rates and molecular interferences on in situ lutetium-hafnium analysis with laser ablation MC-ICP-MS. *Journal of Analytical Atomic Spectrometry* **28**, 1068–1079.

PEARCE, J., AND CANN, J. 1973. Tectonic setting of basic volcanic rocks determined using trace element analyses. *Earth and Planetary Science Letters* **19**, 290–300.

PEARCE, J.A. 1996. A User ' s Guide to Basalt Discrimination Diagrams. *Geological Association of Canada, Short Course Notes* **12**, 79–113.

PEARCE, J.A. 2008. Geochemical fingerprinting of oceanic basalts with applications to ophiolite classification and the search for Archean oceanic crust. *Lithos* **100**, 14–48.

PECCERILLO, A., AND TAYLOR, S.R. 1976. Geochemistry of Eocene calc-alkaline volcanic rocks from the Kastamonu area, northern Turkey. *Contributions to Mineralogy and Petrology* **58**, 63–81.

PLAVSA, D., COLLINS, A.S., PAYNE, J.L., FODEN, J.D., CLARK, C., AND SANTOSH, M. 2014. Detrital zircons in basement metasedimentary protoliths unveil the origins of southern India. *Bulletin of the Geological Society of America* **126**, 791–812.

PREISS, W. V 2000. The Adelaide Geosyncline of South Australia and its significance in Neoproterozoic continental reconstruction. *Precambrian Research* **100**, 21–63.

PREISS, W.., FANNING, M.., SZPUNAR, M.., AND BURTT, A. 2008. Age and tectonic significance of the Mount Crawford granite gneiss and a related intrusive in the Oakbank inlier, Mount Lofty Ranges, South Australia. *MESA Journal* **49**, 38–49.

RAMPONE, E., BORGHINI, G., ROMAIRONE, A., AND ABOUCHAMI, W. 2014. Lithos Sm – Nd geochronology of the Erro-Tobbio gabbros (Ligurian Alps , Italy): Insights into the evolution of the Alpine Tethys. **205**, 236–246.

RICKWOOD, P.C. 1989. Boundary lines within petrologic diagrams which use oxides of major and minor elements. *Lithos* **22**, 247–263.

ROLLINSON, H. 1993. Using geochemical data: evaluation, presentation, interpretation.

RUDNICK, R.L., AND GAO, S. 2003. Composition of the continental crust. *Treatise on Geochemistry* **3**, 1–64.

SCOTT, A.F., AND SPEAR, G.W. 1969. Mallabie no. 1 well completion report. *South Australia. Department of Mines and Energy. Open File Envelope* **1172**,.

SEGAL, I., HALICZ, L., AND PLATZNER, I.T. 2003. Accurate isotope ratio measurements of ytterbium by multiple collection inductively coupled plasma mass spectrometry applying erbium and hafnium in an improved double external normalization procedure. *Journal of Analytical Atomic Spectrometry* **18**, 1217.

SHERVAIS, J.W. 1982. Ti-V plots and the petrogenesis of modern and ophiolitic lavas. *Earth and Planetary Science Letters* **59**, 101–118.

SLÁMA, J., KOŠLER, J., CONDON, D., AND CROWLEY, J. 2008. Plešovice zircon—a new natural reference material for U–Pb and Hf isotopic microanalysis. *Chemical* ….

SMITHIES, R., SPAGGIARI, C., KIRKLAND, C., WINGATE, M., AND ENGLAND, R. 2015. Forrest Zone: geochemistry and petrogenesis. In Eucla Basement Stratigraphic Drilling Results Release Workshop: Extended Abstracts, (Perth), pp. 41–51.

SPAGGIARI, C., AND SMITHIES, R. 2015. Eucla Basement Stratigraphic Drilling Results Release Workshop: Extended Abstracts. (Perth, Western Australia: The Geological Survey of Western Australia),.

SUN, S.S., SHERATON, J.W., GLIKSON, A.Y., AND STEWART, A.J. 1996. A major magmatic event during 1050–1080 Ma in central Australia, and an emplacement age for the Giles Complex. *AGSO Research Newsletter 24* 13–15.

SWAIN, G., BAROVICH, K., HAND, M., FERRIS, G., AND SCHWARZ, M. 2008. Petrogenesis of the St Peter Suite, southern Australia: Arc magmatism and Proterozoic crustal growth of the South Australian Craton. *Precambrian Research* **166**, 283–296.

SWAIN, G., WOODHOUSE, A., HAND, M., BAROVICH, K., SCHWARZ, M., AND FANNING, C.M. 2005. Provenance and tectonic development of the late Archaean Gawler Craton, Australia; U-Pb zircon, geochemical and Sm-Nd isotopic implications. *Precambrian Research* **141**, 106–136.

TAYLOR, S., AND MCLENNAN, S. 1985. The Continental Crust: Its Composition and Evolution: An Examination of the Geochemical Record Preserved in Sedimentary Rock. (Oxford, United Kingdom: Blackwell Scientific).

THE SHELL CO. OF AUSTRALIA LTD 1983. Open File Envelope No. 4046: EL 747, EL748 and EL 749 (Adelaide, South Australia).

THOMSON, B.P. 1970. A review of the Precambrian and Lower Palaeozoic tectonics of South Australia. *Trans. R. Soc. S. Aust* **94**, 193–221.

DE VRIES, S.T., PRYER, L.L., AND FRY, N. 2008. Evolution of Neoarchaean and Proterozoic basins of Australia. *Precambrian Research* **166**, 39–53.

WADE, B.P., BAROVICH, K.M., HAND, M., SCRIMGEOUR, I.R., AND CLOSE, D.F. 2006. Evidence for early Mesoproterozoic arc magmatism in the Musgrave Block, central Australia: implications for Proterozoic crustal growth and tectonic reconstructions of Australia. *The Journal of Geology* **114**, 43–63.

WADE, B.P., PAYNE, J.L., HAND, M., AND BAROVICH, K.M. 2007. Petrogenesis of ca 1.50 Ga granitic gneiss of the Coompana Block: filling the 'magmatic gap' of Mesoproterozoic Australia. *Australian Journal of Earth Sciences* **54**, 1089–1102.

WADE, C.E., MCAVANEY, S.O., AND GORDON, G.A. 2014. The Beda Basalt : new geochemistry , isotopic data and its definition. 24–41.

WALLACE, M.L., JOWITT, S.M., AND SALEEM, A. 2015. Geochemistry and petrogenesis of mafic–ultramafic suites of the Irindina Province, Northern Territory, Australia: Implications for the Neoproterozoic to Devonian evolution of central Australia. *Lithos* **234-235**, 61–78.

WANG, X.-C., LI, X.-H., LI, Z.-X., LIU, Y., AND YANG, Y.-H. 2010. The Willouran basic province of South Australia: Its relation to the Guibei large igneous province in South China and the breakup of Rodinia. *Lithos* **119**, 569–584.

WINDRIM, D.P., MCCULLOCH, M.T., CHAPPELL, B.W., AND CAMERON, W.E. 1984. Nd isotopic systematics and chemistry of Central Australian sapphirine granulites: an example of rare earth element mobility. *Earth and Planetary Science Letters* **70**, 27–39.

WINGATE, M.T.., CAMPBELL, I.H., COMPSTON, W., AND GIBSON, G.M. 1998a. Ion microprobe U–Pb ages for Neoproterozoic basaltic magmatism in south-central Australia and implications for the breakup of Rodinia. *Precambrian Research* **87**, 135–159.

WINGATE, M.T.., CAMPBELL, I.H., COMPSTON, W., AND GIBSON, G.M. 1998b. Ion microprobe U–Pb ages for Neoproterozoic basaltic magmatism in south-central Australia and implications for the breakup of Rodinia. *Precambrian Research* **87**, 135–159.

WOODHEAD, J., AND HERGT, J. 2005. A preliminary appraisal of seven natural zircon reference materials for in situ Hf isotope determination. *Geostandards and Geoanalytical …*.

ZHAO, J., AND MCCULLOCH, M.T. 1993. Sm-Nd mineral isochron ages of Late Proterozoic dyke swarms in Australia: evidence for two distinctive events of mafic magmatism and crustal extension. *Chemical Geology* **109**, 341–354.

ZHAO, J., MCCULLOCH, M.T., AND KORSCH, R.J. 1994. Characterisation of a plume-related ~ 800 Ma magmatic event and its implications for basin formation in central-southern Australia. *Earth and Planetary Science Letters* **121**, 349–367.

APPENDIX A: U-Pb geochronology and Lu-Hf isotopic analysis of detrital zircons from sedimentary units overlying mafic magmatism in the Coompana Province

At the initial stages of this study, we also proposed to complete U-Pb zircon geochronology and Lu-Hf isotopic analysis on samples taken from the sedimentary units which stratigraphically basalt in drillhole CD1. This frame of this work was later expanded to included Lu-Hf isotopic analysis on detrital zircons from various sedimentary units across the Coompana Province. This work was completed over the course of the year. However, in order to produce a concise report which was directly relevant to the Western Craton margins project of the Geological Survey of South Australia, it was left out of the thesis. A brief report on initial results from this work are provided below.

Analytical methods

LA-ICP-MS U-Pb geochronology

Two samples from the sedimentary units overlying the basalt interval in drill hole CD1 used for Sm-Nd geochronology were selected for U-Pb geochronology of detrital zircons. Samples were sent to Geotrack International in Melbourne, Australia for zircon mineral separation. Zircon separates from each sample were handpicked and mounted in epoxy resin disks. Care was taken to not overly bias the zircons by randomly selecting zircon grains of all shapes, sizes, and colours. The epoxy resin disks where then polished flat to expose zircons grains, carbon coated, and imaged using standard backscattered electron and cathodoluminescence imaging techniques on a Phillips XL20 SEM with attached Gatan CL at Adelaide Microscopy. Zircon grains were imaged using a 15.0 working distance and accelerating voltage of 12.0kV.

U-Pb analyses of zircon grains were conducted on a New Wave 213 nm Nd-YAG laser coupled with the Agilent 7500cs inductively coupled plasma–mass spectrometer (ICP-MS) at Adelaide Microscopy. The analytical methods follow those of Plavsa et al. (2014). To avoid biasing the results, all zircon grains in any particular row on a grain mount were analysed. A 30 µm spot size was used, producing typical pit depths of 30–50 µm. Isotopes measured include ^{204}Pb, ^{206}Pb, ^{207}Pb, ^{208}Pb, ^{232}Th and ^{238}U with 10, 15, 30, 10, 10 and 15 ms respective dwell times. Isotopic ratios were monitored and corrected for drift and within-run U-Pb fractionation by repeat analyses of the GEMOC GJ-1 zircon standard ^{207}Pb/^{206}Pb = 607.7 ± 4.3 Ma, 206Pb/238 U = 600.7 ± 1.1 Ma, and 207 Pb/235 U = 602.0 ± 1.0 Ma; Jackson et al., 2004). Instrument drift was also corrected for by standard bracketing every 15 or 20 unknown analyses

and applying a linear correction. Raw data was processed using the software GLITTER (Achterbergh et al., 2001), which calculates $^{207}Pb/^{206}Pb$, $^{206}Pb/^{238}U$, $^{207}Pb/^{235}U$ and $^{208}Pb/^{232}Th$ ages, where ^{235}U is determined assuming $^{238}U = {}^{238}U/137.88$. The reduced data was then exported into Microsoft Excel™ where conventional Concordia and weighted average plots were generated using Isoplot (Ludwig, 2003). For this study $^{207}Pb/^{206}Pb$ ages are used as the samples data are mostly older than ca. 1000 Ma.

Lu-Hf Isotopic Analysis

Hafnium isotopic compositions of zircons were obtained from grains dated using U-Pb LA-ICPMS and on grains dated by Secondary Ion Mass Spectrometry provided by Dr. Geoff Fraser from Geoscience Australia. Analyses were carried at a joint University of Adelaide and Commonwealth Scientific and Industry Research Organisation (CSIRO) facility in Adelaide using a Thermo-Electron Neptune MC-ICP-MS coupled to a New Wave UP-193 Excimer laser. Analyses follow the method detailed in Payne et al. (2013) and were carried out on the same spots or age domains for age determinations of the concordant grains. Most analyses were conducted using a beam diameter of 50 μm, a 5 Hz repetition rate, and an intensity of approximately 6 J/cm^2. Typical ablation times were 60–225 s involving a maximum of 15 measurement cycles, resulting in pits 40 - 50 μm deep. All analyses were carried out in static mode. Data reduction was undertaken using *HfTRAX* (Payne et al., 2013).

Data is normalised to $^{179}Hf/^{177}Hf=0.7325$ (Patchett et al., 1982) using an exponential correction for mass bias. Yb mass bias is directly measured and used to correct Yb and Lu interferences on ^{176}Hf. Lu is assumed to have the same mass bias as Yb (Payne et al., 2013). An outlier rejection threshold of 3σ was used. During this study, instrument performance and stability was monitored by analysis of Instrument performance and stability was monitored by analysis of Plesovice ($^{176}Hf/^{177}Hf = 0.282482 \pm 0.000013$ (Sláma et al., 2008)) and Mudtank zircon ($^{176}Hf/^{177}Hf = 0.282507 \pm 0.000006$ (Woodhead and Hergt, 2005)) standards.

Results

LA-ICP-MS U-Pb Geochronology

LA-ICP-MS U-Pb geochronology was completed on samples from the two sedimentary units that overly the basalt dated using Sm-Nd isotope geochronology intersected by drill hole CD1. One hundred and forty four analysis were completed on detrital zircons from the Permian Tillite sample (2129324) that directly overlies the basalt in CD1, and 265 analyses were completed on detrital zircons from a sandstone units stratigraphically overlying the Permian Tillite. For detrital zircon studies, analyses with well-defined age peaks which are within 10% concordant are considered for interpretations of maximum and minimum deposition ages (Plavsa et al., 2014). Analyses which are less than 10% discordant are shown in probability density plots (Figure__).

From the 144 analyses completed on zircons from sample 2129324, 68 analyses were less than 10% discordant. The concordant analyses show a range of $^{207}Pb/^{206}Pb$ ages between ca. 1770 Ma and 1056 Ma. Two distinct age groups occur between ca. 1620 – ca.1680 Ma and ca. 1140 – ca. 1260 Ma, with respective peaks at ca. 1580 Ma and ca. 1160 Ma.. The youngest, less than 10% discordant zircon was 916 ± 83 Ma. Eighty-two of the analyses of zircons from sample 2129325 were less than 10% discordant. These show a range of $^{207}Pb/^{206}Pb$ ages between ca. 1100 Ma and ca. 1700 Ma (Figure__). Two distinct age groups can be identified between ca. 1700 Ma – ca. 1520 Ma and ca. 1300 Ma – ca. 1060 Ma, with respective peaks at ca. 1580 Ma and ca. 1180 Ma. These age ranges are similar to sample 2129324.

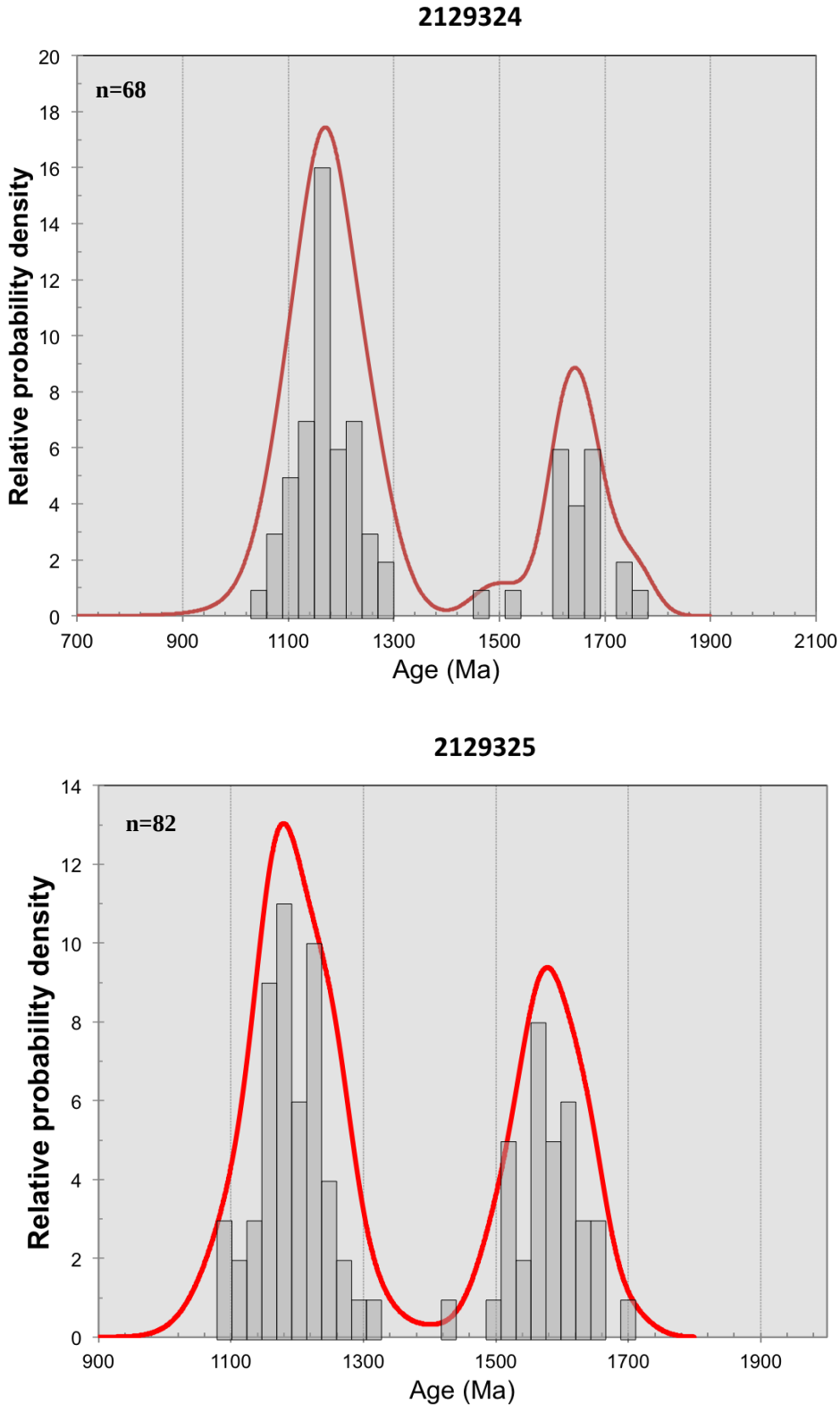

Figure 18: Probability density distribution plots of the sedimentary samples 2129324 and 2129325 that overlie mafic magmatism in the Coompana Block. A discordance cut-off of 10% was used for this study.

Lu-Hf Isotopic Analysis

Hafnium isotopic analyses were completed on detrital zircon grains that were less than 10% discordant from the sedimentary samples overlying mafic magmatism in drill hole CD1 (2129324 and 2129325) and on sedimentary samples taken from drill holes Apollo 1 (2231441), Guinewarra Bore, and Mallabie 1 (2179751 and 2179753) dated using U-Pb SHRIMP analysis by Dr. Geoff Fraser from GA. Analyses were completed on zircons within each of the dominant age populations in each sample. Data are plotted on epsilon Hf (εHf) versus age plots below. The Hf model ages used for this study assume derivation of magma from average continental crust, which was originally derived from the depleted mantle.

Samples 2129324 and 2129325 show ranges of restricted T^{C}_{DM} values between 1.67 – 2.73 Ga and 1.56 – 2.54 Ga respectively. Sample 2129324 yielded a restricted εHf(*T*) range between -12.77 and + 8.62. Within this sample, the age peak identified between ca. 1140 – ca. 1260 Ma yielded εHf(*T*) values between -12.77 and +1.75, and the age peak between ca. 1580 Ma and ca. 1160 Ma yielded a range between -0.93 and +8.62. εHf(*T*) values for sample 2129325 range between -3.07 and +12.59. Within this sample, εHf(*T*) values in the age peak identified at ca. 1300 Ma – ca. 1060 Ma range between -3.07 and + 3.33, and εHf(*T*) values in age peak at ca. 1700 Ma – ca. 1520 Ma range between +2.57 and +12.59.

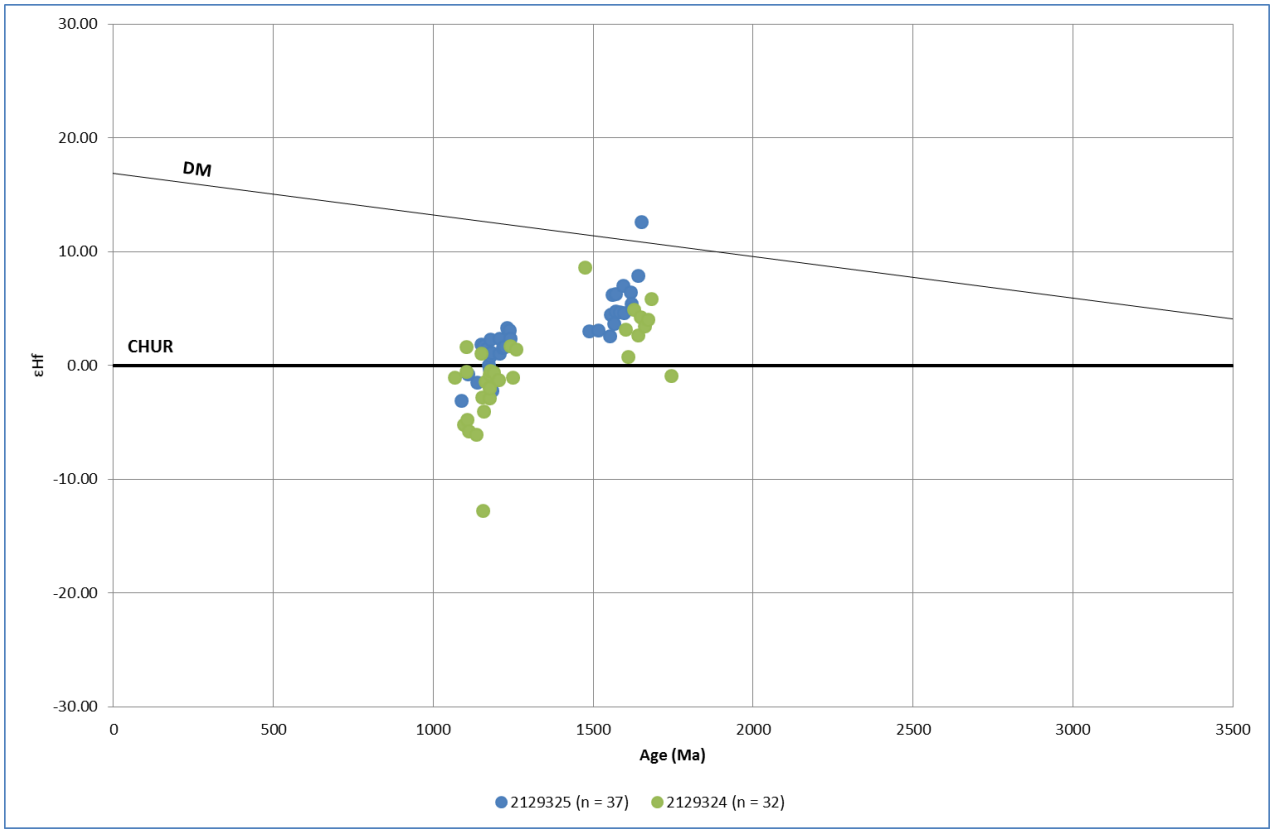

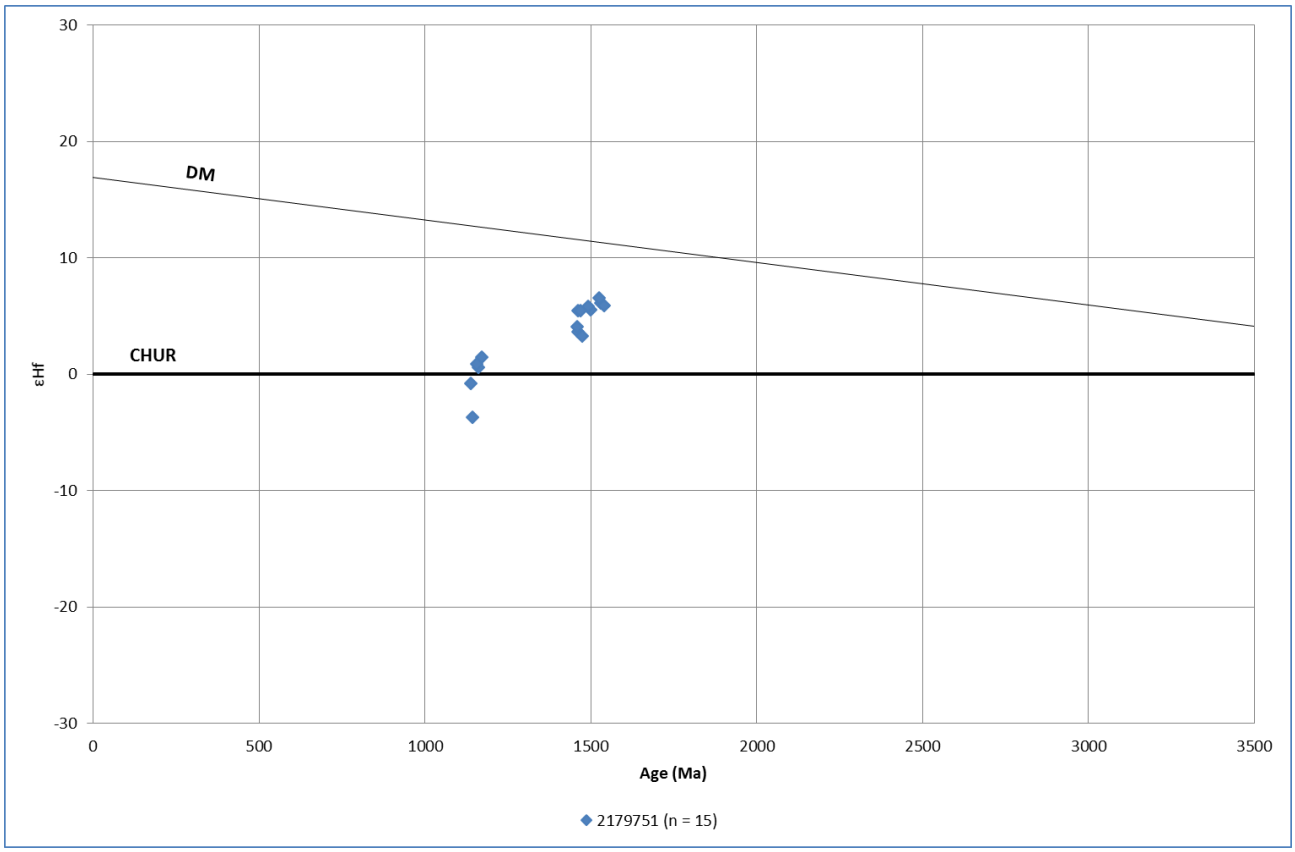
30
20
10
0
-10
-20
-30
0
500
1000
1500
2000
2500
3000
3500
DM
CHUR
εHf
Age (Ma)
2179751 (n = 15)

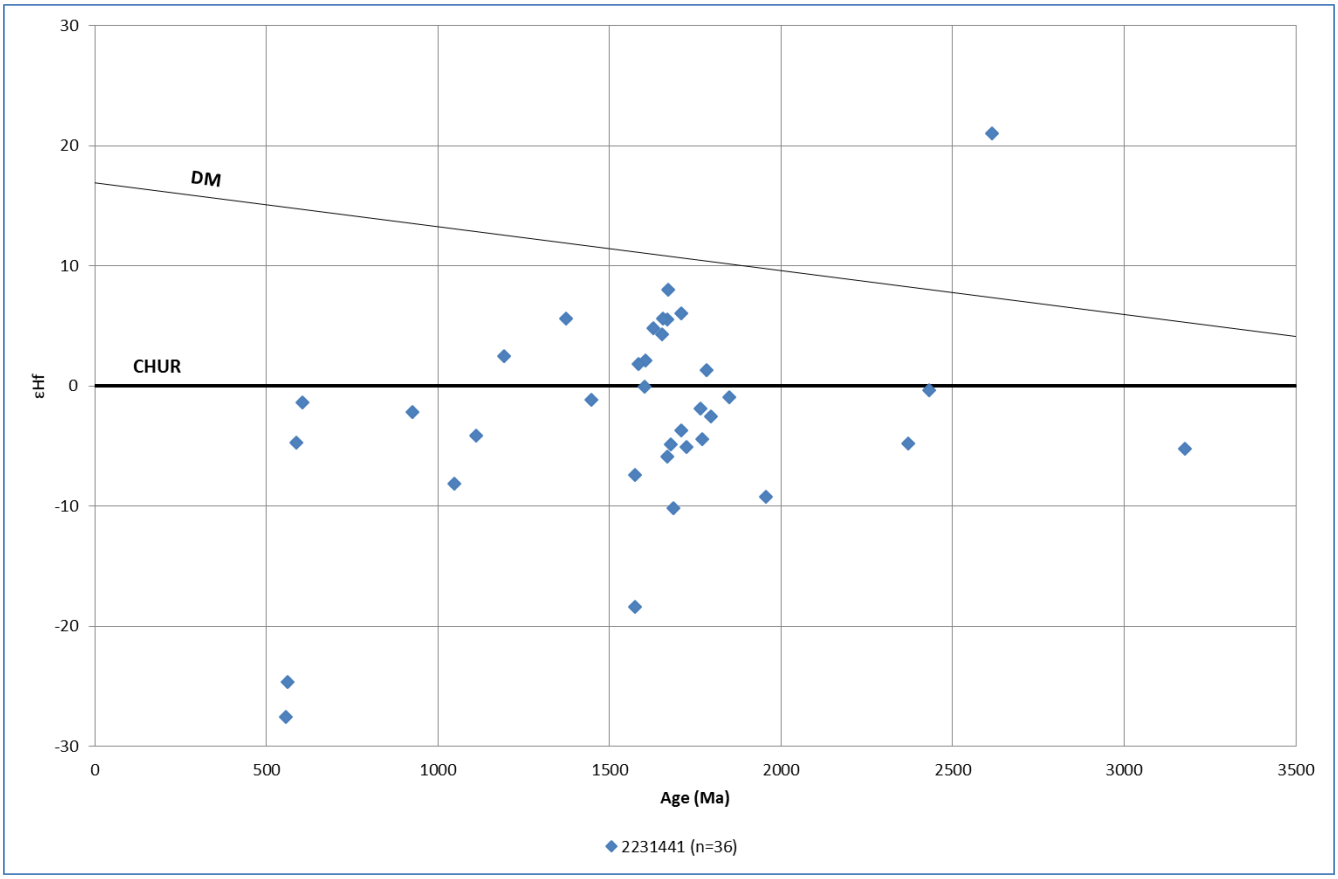
30
20
10
0
-10
-20
-30
0
500
1000
1500
2000
2500
3000
3500
DM
CHUR
εHf
Age (Ma)
2231441 (n=36)

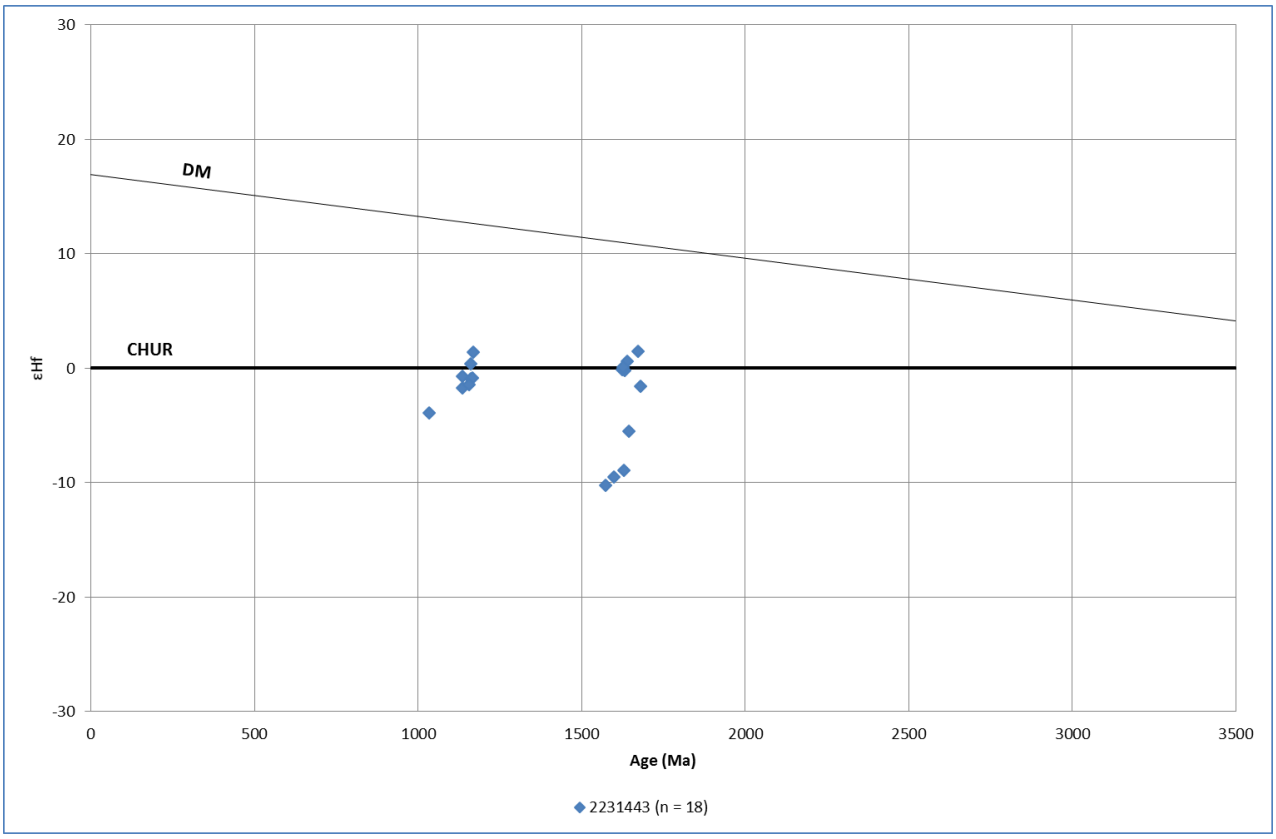

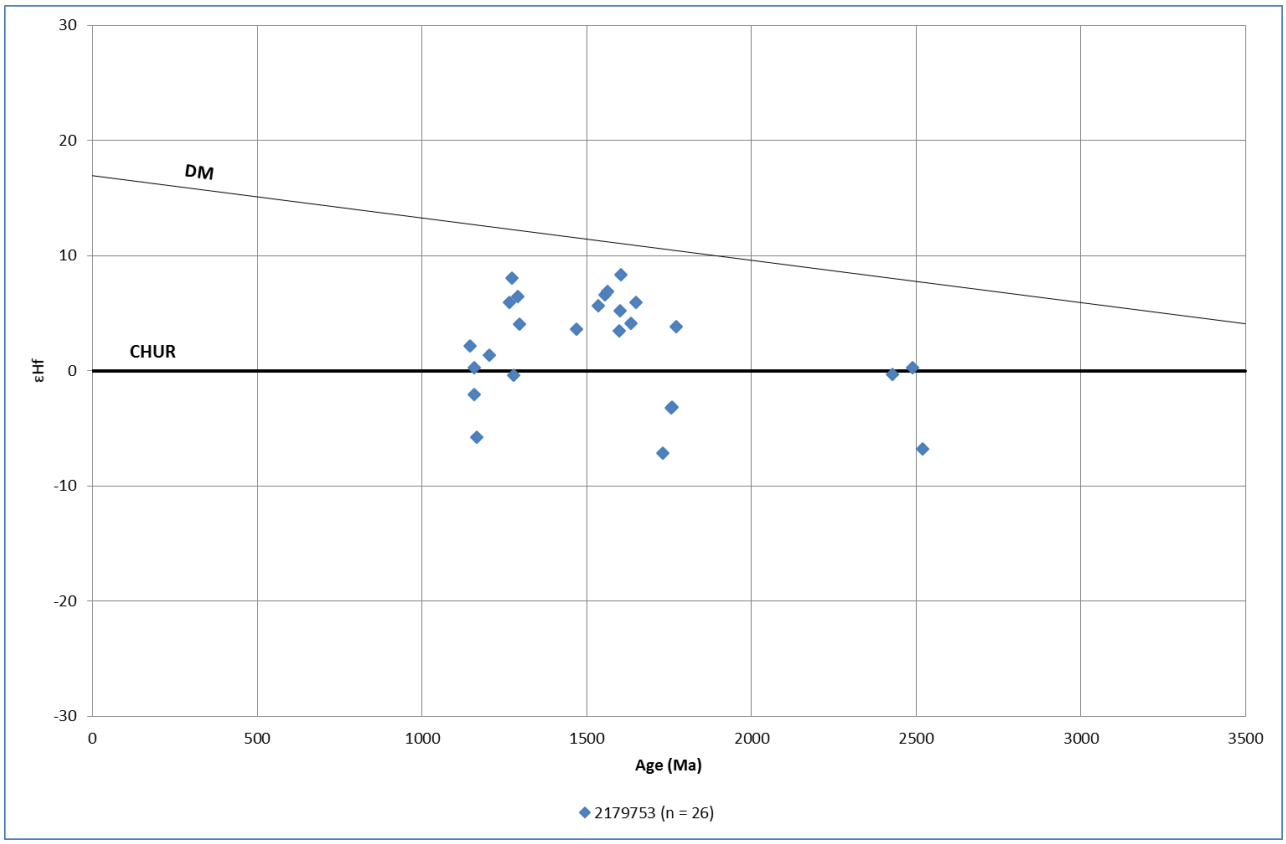

Figure 18: Epsilon Hf (εHf) plotted against corresponding spot ages (in Ma).

APPENDIX B: Whole rock geochemistry

	CD1									
Major elements (wt %)	**2129327**	**2129328**	**2129329**	**2129330**	**2129331**	**2129332**	**2129333**	**2078887**	**2078888**	**2078889**
SiO2	49.7	49.7	49.5	48	47.7	49.6	47.7	48.6	48.6	48.1
Al2O3	15.9	15.65	15.3	14.85	15.6	14.9	14.95	14.8	16.15	15.2
Fe2O3	11.05	11.65	11.65	11.55	10.95	11.95	11.8	11.9	11.5	12.25
CaO	8.18	9.48	9	8.89	9.01	5.93	6.46	3.12	8.77	7.32
MgO	8.01	7.75	8.12	7.74	7.65	7.99	7.8	9.4	7.46	7.4
Na2O	2.29	2.06	2.17	2.01	2	3.26	3.05	3.2	2.05	2.61
K2O	0.9	0.52	0.55	0.86	0.81	1.68	1.7	0.68	0.86	1.16
Cr2O3	0.01	0.01	0.01	0.01	0.01	0.01	0.01	0.02	0.02	0.01
TiO2	0.94	1.01	0.98	0.99	0.93	1.14	1.11	0.99	0.92	1.06
MnO	0.16	0.17	0.18	0.17	0.18	0.18	0.17	0.14	0.18	0.17
P2O5	0.17	0.18	0.18	0.17	0.16	0.19	0.19	0.15	0.17	0.18
SrO	0.03	0.03	0.03	0.02	0.02	0.03	0.03	0.01	0.02	0.03
BaO	0.04	0.03	0.03	0.03	0.04	0.06	0.05	0.01	0.04	0.04
LOI	2.73	2.36	2.43	2.17	2.48	2.7	3.07	4.58	2.73	2.63
Total	100.11	100.6	100.13	97.46	97.54	99.62	98.09	97.6	99.47	98.16
Trace (ppm)										
Ba	359	258	256	293	327	502	461	125	367	365
Cr	110	110	110	110	110	90	100	160	140	130
Cs	1.15	0.69	0.4	0.36	0.43	3.74	4.97	0.25	0.49	3.05
Ga	16	16.7	16.3	15.7	16	16.4	16	15.9	17.4	18.5
Nb	4.1	4.2	4.3	4	3.8	5.1	4.8	5.2	4.5	5.3
Rb	18	9.1	7.2	11.1	10.9	40.3	42.9	10.1	12.9	25.3
Sr	212	194	194.5	186	194	268	271	118.5	216	285
Th	1.15	0.9	0.92	0.95	0.88	1.05	1.04	1.19	1.06	1.08
Tl	<0.5	<0.5	<0.5	<0.5	<0.5	<0.5	<0.5	<0.5	<0.5	<0.5
U	0.15	0.14	0.12	0.12	0.11	0.14	0.16	0.11	0.1	0.14
V	242	243	244	242	243	266	246	262	261	268
W	<1	<1	<1	<1	<1	1	<1	<1	<1	<1
Y	24.7	26.5	25.5	26.6	25.9	28.8	27.7	26.5	25.8	27.3
Zr	101	112	106	110	105	121	114	124	114	123
As	0.4	0.2	0.2	0.2	0.2	0.3	0.5	0.3	<0.1	0.2
Bi	0.01	0.01	0.01	0.01	0.01	0.02	0.01	0.01	0.01	0.04
Sb	<0.05	<0.05	<0.05	<0.05	<0.05	<0.05	<0.05	<0.05	<0.05	<0.05
Se	0.7	0.8	0.8	0.7	0.7	0.9	0.9	0.7	0.6	0.6
Te	0.01	0.01	<0.01	<0.01	0.01	0.01	<0.01	0.01	0.01	0.01
Ag	<0.5	<0.5	<0.5	<0.5	<0.5	<0.5	<0.5	<0.5	<0.5	0.5
Cd	<0.5	<0.5	<0.5	<0.5	<0.5	<0.5	<0.5	<0.5	<0.5	<0.5
Co	47	50	49	50	47	52	49	52	64	51
Cu	131	132	120	113	108	150	159	77	133	148
Li	40	20	30	20	20	40	40	90	40	40
Mo	1	1	1	1	1	1	<1	1	<1	<1
Ni	184	181	184	175	179	165	165	170	241	170
Pb	3	6	6	6	4	7	6	5	9	10
Sc	29	28	27	28	28	32	30	34	26	28
Zn	90	96	97	96	89	105	98	101	136	104
In	0.026	0.021	0.025	0.023	0.019	0.028	0.029			
REE (ppm)										
Ce	30.4	32.1	32.2	32.3	31.7	36.3	34	33.8	33.5	35.8
Dy	4.38	4.73	4.76	4.68	4.39	4.94	4.85	4.73	4.53	4.63
Er	2.91	3.08	3.06	3.06	2.88	3.37	3.18	3.15	2.98	3.03
Eu	1.28	1.18	1.2	1.2	1.14	1.3	1.27	1.18	1.2	1.3
Gd	4.19	4.21	3.86	4.11	3.73	4.52	4.52	4.34	4.3	4.63
Ho	1.02	1.01	1	0.98	0.92	1.05	1.03	1.01	0.97	1.02
La	15.2	16	16.1	16	15	18.1	16.8	16.2	16.6	17.7
Lu	0.43	0.45	0.42	0.44	0.45	0.48	0.47	0.46	0.44	0.46
Nd	15.2	16.2	15.5	15.8	15	16.7	16.4	17	16.8	17.1
Pr	3.76	4.05	3.86	3.79	3.64	4.1	3.91	4.3	4.22	4.38
Sm	3.47	3.58	3.63	3.62	3.44	3.9	3.65	3.76	3.48	3.98
Tb	0.66	0.7	0.73	0.73	0.7	0.74	0.72	0.71	0.68	0.69
Tm	0.41	0.44	0.45	0.45	0.42	0.46	0.46	0.42	0.4	0.43
Yb	3	3.12	2.92	2.98	2.76	3.18	2.99	2.98	2.82	2.96
Hf	2.7	2.9	2.8	2.7	2.6	3	2.9	3.2	2.8	3.1

	BN2									
Major elements (wt %)	**2129334**	**2129335**	**2129336**	**2129337**	**2129338**	**2129339**	**2129340**	**2129341**	**2129342**	**2129343**
SiO2	54	57.6	55	54.2	56.3	53.5	55.6	54.8	53.4	52.8
Al2O3	11.35	12.1	10.9	11.5	11.4	11.1	11.25	11.45	11.25	11.1
Fe2O3	17	15.4	16.15	16	15.3	15.85	15.2	15.95	16.1	16.2
CaO	5.06	4.96	5.02	5.44	5.35	5.06	5.25	4.91	5.16	5.25
MgO	1.45	1.42	1.44	1.72	1.49	1.51	2.09	1.53	1.56	1.53
Na2O	3.25	5.07	3.84	3.43	5.08	3.29	3.3	4.12	3.38	3.18
K2O	2.97	1.96	2.45	2.68	1.38	2.82	2.77	2.34	2.77	2.69
Cr2O3	<0.01	<0.01	<0.01	<0.01	<0.01	<0.01	<0.01	<0.01	<0.01	<0.01
TiO2	1.65	1.57	1.64	1.65	1.65	1.65	1.65	1.69	1.65	1.64
MnO	0.28	0.33	0.27	0.27	0.28	0.27	0.27	0.29	0.28	0.27
P2O5	0.51	0.47	0.48	0.45	0.45	0.45	0.46	0.45	0.45	0.43
SrO	0.02	0.02	0.02	0.02	0.02	0.02	0.02	0.02	0.02	0.02
BaO	0.15	0.1	0.11	0.13	0.06	0.16	0.1	0.12	0.12	0.11
LOI	0.94	0.97	0.64	0.95	0.76	0.67	0.86	0.58	0.84	1.02
Total	98.63	101.97	97.96	98.44	99.52	96.35	98.82	98.25	96.98	96.24
Trace (ppm)										
Ba	1245	824	991	1100	529	1375	898	1020	1045	998
Cr	<10	<10	10	<10	<10	10	<10	<10	<10	<10
Cs	0.92	4.38	1.8	1.54	3.7	1.1	1.75	1.01	1.52	1.52
Ga	23.1	18.4	20.8	22.7	20.5	20.6	20.5	21.3	22.1	21.3
Nb	13.1	12.2	12.6	12.5	12.4	12.6	12.6	12.1	12.3	12.1
Rb	94.8	55.7	77.6	89.4	42.8	91.1	92.4	68.7	91.2	86.4
Sr	153.5	128	143	187	120	157.5	175	133.5	166.5	167.5
Th	10.4	9.45	9.44	9.85	9.55	9.51	9.74	9.59	9.9	9.25
Tl	<0.5	<0.5	<0.5	<0.5	<0.5	<0.5	<0.5	<0.5	<0.5	<0.5
U	1.54	1.44	1.5	1.5	1.46	1.48	1.53	1.46	1.44	1.46
V	31	40	40	51	46	46	50	51	52	52
W	1	2	1	<1	1	<1	<1	<1	9	<1
Y	77	73.8	75.3	71.7	69.5	72.7	69.1	72.8	69.6	69.5
Zr	304	287	295	287	278	293	289	283	278	274
As	0.6	0.6	0.5	0.6	0.4	0.7	0.5	0.5	0.6	0.5
Bi	0.08	0.13	0.12	0.08	0.12	0.11	0.1	0.07	0.27	0.09
Sb	0.06	<0.05	<0.05	<0.05	<0.05	0.05	<0.05	<0.05	<0.05	<0.05
Se	2	2.1	2	1.9	1.8	2	2	1.8	2	2.1
Te	<0.01	<0.01	<0.01	<0.01	<0.01	<0.01	<0.01	<0.01	<0.01	<0.01
Ag	<0.5	<0.5	<0.5	<0.5	<0.5	<0.5	<0.5	<0.5	<0.5	<0.5
Cd	<0.5	<0.5	<0.5	<0.5	<0.5	<0.5	<0.5	<0.5	<0.5	<0.5
Co	30	24	29	30	27	30	29	29	30	31
Cu	249	275	273	303	299	258	264	273	310	295
Li	10	10	10	10	10	10	20	10	20	20
Mo	1	1	1	1	2	1	1	1	2	1
Ni	1	7	<1	5	<1	2	1	2	<1	2
Pb	19	44	16	25	12	10	21	5	38	16
Sc	33	31	34	35	33	35	34	34	34	34
Zn	183	160	164	179	142	175	168	251	189	181
In	0.059	0.044	0.043	0.038	0.032	0.048	0.053	0.042	0.035	0.047
REE (ppm)										
Ce	117	110	116.5	109	109.5	106	107	113.5	103.5	112
Dy	12.8	12.25	12.3	12.2	11.8	11.75	12	12.4	11.8	12.05
Er	8.71	8	7.9	8.18	8.16	7.7	7.96	7.84	7.8	7.62
Eu	2.83	3.03	2.85	2.62	2.87	2.59	2.43	2.76	2.53	2.78
Gd	12.05	10.7	11.2	11.2	10.75	10.7	10.75	11.1	10.6	10.3
Ho	2.77	2.67	2.67	2.64	2.54	2.56	2.56	2.61	2.59	2.55
La	59.1	55.6	58.3	53.7	57.2	48.6	53.7	56.1	50.9	57.8
Lu	1.26	1.19	1.17	1.23	1.17	1.17	1.2	1.14	1.15	1.15
Nd	49.8	45.5	46.1	46.3	45.3	44.3	44.1	45.8	44.4	44
Pr	12.9	11.95	11.75	12.2	11.9	11.15	11.3	11.9	11.05	11.6
Sm	10.55	9.84	9.87	9.68	9.63	9.75	9.29	9.81	9.3	9.27
Tb	1.96	1.83	1.86	1.82	1.8	1.76	1.79	1.85	1.75	1.74
Tm	1.27	1.2	1.2	1.23	1.16	1.17	1.19	1.22	1.16	1.14
Yb	8.45	7.78	7.93	8.06	7.63	7.62	8.08	7.67	7.68	7.58
Hf	8.2	7.5	7.8	7.7	7.7	8	8	7.8	7.9	7.6

		BN2			Mallabie 1	BN1	KN1
Major elements (wt %)	**2129344**	**2078884**	**2078885**	**2078886**	**2078890**	**2078892**	**2078893**
SiO2	54.1	53.4	54.6	55	45.3	54	51.8
Al2O3	11.1	11.75	11.85	11.8	12.7	11.25	16.25
Fe2O3	16.3	16.3	16.5	16.45	11.35	17.45	10.45
CaO	5.47	4.77	5.01	5.27	4.86	5.43	5.09
MgO	1.65	1.58	1.51	1.61	9.07	1.57	6.57
Na2O	2.98	3.22	3.65	3.7	0.37	3.2	1.33
K2O	2.74	3.25	2.7	2.51	5.71	2.73	2.25
Cr2O3	<0.01	<0.01	<0.01	<0.01	0.01	<0.01	0.02
TiO2	1.69	1.65	1.62	1.7	0.8	1.78	0.22
MnO	0.27	0.28	0.27	0.27	0.11	0.28	0.11
P2O5	0.42	0.47	0.43	0.45	0.14	0.45	0.05
SrO	0.02	0.02	0.02	0.03	0.01	0.02	0.02
BaO	0.14	0.16	0.12	0.1	0.11	0.11	0.02
LOI	1.15	1.13	0.91	0.98	8.14	1.02	4.2
Total	98.03	97.98	99.19	99.87	98.68	99.29	98.38
Trace (ppm)							
Ba	1225	1485	1155	869	975	1040	191.5
Cr	<10	20	30	30	80	30	200
Cs	0.96	1.07	1.84	1.52	6.2	2.81	3.21
Ga	21.1	24.3	23.8	24.5	15	23.7	13.2
Nb	12.3	14.6	13.6	13.3	3.5	14	1.3
Rb	84.6	114.5	96.1	85.3	73.1	97.3	39.2
Sr	118	173	171.5	221	70.9	181	184
Th	9.6	10.35	9.66	9.37	0.91	9.8	1.64
Tl	<0.5	<0.5	<0.5	<0.5	<0.5	<0.5	<0.5
U	1.47	1.65	1.51	1.5	0.51	1.51	0.58
V	58	41	55	63	139	56	91
W	<1	<1	1	<1	<1	1	4
Y	67.8	74.1	71.7	70.3	25.1	74.1	6.9
Zr	278	340	320	314	87	334	52
As	0.5	0.6	0.4	0.4	1.6	0.3	1.1
Bi	0.14	0.21	0.12	0.21	0.21	0.03	0.09
Sb	<0.05	0.06	<0.05	0.06	0.2	0.34	0.09
Se	1.9	1.8	1.6	1.7	1.1	0.4	<0.2
Te	<0.01	<0.01	0.01	0.01	0.03	<0.01	0.04
Ag	<0.5	<0.5	<0.5	<0.5	<0.5	<0.5	<0.5
Cd	<0.5	<0.5	<0.5	<0.5	<0.5	0.6	<0.5
Co	31	32	32	33	40	30	40
Cu	289	315	299	294	42	295	20
Li	20	20	20	30	50	20	40
Mo	1	1	1	1	<1	2	1
Ni	<1	<1	<1	<1	118	<1	257
Pb	13	35	10	36	8	25	9
Sc	35	39	37	39	30	39	23
Zn	169	244	180	204	44	194	60
In	0.052						
REE (ppm)							
Ce	110.5	115	112.5	107.5	25.6	113.5	10
Dy	11.8	12.5	11.95	12.25	4.03	12.35	1.2
Er	7.75	8.19	7.9	7.72	2.61	8.09	0.75
Eu	2.57	2.96	2.94	2.71	1.03	2.93	0.44
Gd	10.4	12.1	11.45	11.4	3.7	12.05	1.15
Ho	2.51	2.81	2.59	2.64	0.91	2.71	0.28
La	56.2	57.8	55.5	52.6	11.8	56	5.1
Lu	1.14	1.22	1.19	1.19	0.39	1.24	0.09
Nd	44.4	53	50.5	48.3	13.4	50.1	4.6
Pr	11.4	13.9	13.4	13	3.3	13.45	1.19
Sm	9.11	10.85	10.6	10.15	3.13	10.9	1.07
Tb	1.75	1.93	1.83	1.85	0.62	1.81	0.17
Tm	1.17	1.2	1.14	1.14	0.36	1.23	0.08
Yb	7.53	7.91	7.84	7.41	2.61	8.01	0.74
Hf	7.8	8.9	8.3	8	2.1	8.8	1.3

APPENDIX C: Plagioclase and clinopyroxene mineral chemistry

						2129327						
Spot	**9327_1**	**9327_14**	**9327_15**	**9327_2**	**9327_3**	**9327_4**	**9327_1**	**9327_11**	**9327_12**	**9327_13**	**9327_8**	**9327_9**
Mineral	**CPX**	**CPX**	**CPX**	**CPX**	**CPX**	**CPX**	**Plag**	**Plag**	**Plag**	**Plag**	**Plag**	**Plag**
Major elements (wt.%)												
SiO2	49.417	49.7579	49.8569	49.3275	49.3642	5.869	49.2461	56.423	49.758	51.2819	48.2984	49.31
ZrO2			0.1927		0.57322	0.19928	0.4334	0.25749		0.9857		
TiO2	0.647889	0.689716	0.657286	0.671662	0.77283	0.648894	0.41191	0.11152	0.48329	0.42783	0.42577	0.5531
ZnO		0.418		0.33172			0.23269					
Al2O3	2.58486	2.18948	2.9378	2.63458	2.92198	2.74314	28.5237	23.794	27.7859	26.7428	28.8357	28.5565
V2O3	0.124268	0.931	0.59281	0.678	0.85575	0.898	0.3377					
Cr2O3	0.214664	0.9479	0.3112	0.27976	0.254845	0.78781	0.3443			0.23755		
FeO	9.77285	11.2915	8.6947	1.133	9.53482	1.1585	1.16177	0.842965	2.9918	0.81578	0.875919	0.84689
MnO	0.24821	0.326483	0.248995	0.29377	0.27479	0.241657	0.5992	0.667	0.19493			
MgO	16.414	16.1531	15.829	15.7763	15.63	15.5739	0.223285	0.263612	1.5234	0.169827	0.25322	0.132529
CaO	17.4947	17.1146	18.5642	18.1233	18.584	17.3257	13.2737	7.451	12.9181	9.86854	13.5774	13.247
BaO		0.1333		0.17617			0.31126	0.7782		0.33197		
Na2O	0.268693	0.2398	0.311775	0.237426	0.291333	0.439997	3.68846	7.246	3.7619	3.92163	3.37686	3.75763
K2O			0.2823			0.6848	0.144797	0.5997	0.13635	2.46571	0.194459	0.97143
P2O5		0.116						0.29946				
Cl		0.5522	0.8778	0.12335			0.19442	0.2664	0.9254	0.12312		0.2685
F		0.32		0.21656				0.2465	0.63627			
O		-0.1395	-0.199	-0.1191	0.4	0.8	-0.438	-0.8653	-0.25627	-0.277		-0.6
TOTAL	97.1682	97.9729	97.4829	97.5716	97.6721	97.452	96.4589	96.2575	97.2466	95.4597	95.466	95.9488
ppm												
Mg	92745.53	9196.5	41369.7	87245.48	7647.78	48256.18	1344.99	4912.29	5961.8	1827.39	16997.19	2979.11
Al	16754.54	124.91	54912.11	1366.1	38155.19	71948.71	96475.19	21443.98	127426.28	223252.53	18579.25	185498.58
Si	248386.89	25115.53	184164.23	237127.41	253372	243998.27	153133.34	361752.44	221949.48	382468.84	292598.94	32851.25
Ca	129527.4	132678.53	8549.1	13282.3	123826.95	91818.34	5351.41	92325.79	753.55	122318.22	94374.13	94867.27
Fe	2411.5	28131.18	152.4	23845.67	19399.2	14381.57	7452.14	22776.54	3495.61	2921.55	7866.8	316.9
REE (ppm)												
La	1.917	1.846	2.87	2.12	1.788	1.87	0.491	2.2	1.453	1.9	1.9	1.95
Ce	5.96	6.73	7.28	7.1	5.83	4.68	1.28	4.75	2.51	2.95	1.48	3.15
Pr	1.157	1.335	1.151	1.248	0.957	0.757	0.112	0.595	0.3	0.276	0.172	0.332
Nd	6.85	8.51	5.45	7.57	5.53	3.68	0.42	2.23	1.5	1.25	0.63	0.91
Sm	2.6	3.38	1.7	2.61	2.2	1.26	<.116	0.62	0.286	<.29	<.25	<.23
Eu	0.785	0.899	0.647	0.7	0.74	0.646	0.231	1.8	0.762	0.72	0.367	0.798
Gd	3.21	3.98	1.71	3.65	2.9	1.58	0.13	0.78	0.166	<.27	<.2	<.2
Tb	0.61	0.875	0.33	0.594	0.54	0.286	0.244	0.92	0.47	<.43	<.26	<.34
Dy	4.44	5.88	2.16	4.7	3.63	2.28	<.66	0.78	0.22	<.179	<.14	<.135
Ho	0.972	1.312	0.513	0.897	0.837	0.482	<.193	0.18	0.32	<.42	<.34	<.32
Er	2.73	3.74	1.4	2.5	2.19	1.41	0.6	0.45	0.97	<.116	<.98	<.17
Tm	0.41	0.556	0.194	0.429	0.317	0.212	<.166	0.71	0.3	<.42	<.31	<.3
Yb	2.95	3.53	1.39	2.77	2.18	1.37	<.78	0.34	0.189	<.183	<.15	<.162
Lu	0.367	0.551	0.22	0.385	0.31	0.239	<.126	0.71	<.22	<.35	<.28	<.29

						2129329						
Spot	**9239_1**	**9239_18**	**9239_19**	**9239_2**	**9239_23**	**9239_4**	**9239_5**	**9239_7**	**9239_8**	**9239_13**	**9239_14**	**9239_15**
Mineral	**CPX**	**CPX**	**CPX**	**CPX**	**CPX**	**CPX**	**CPX**	**CPX**	**CPX**	**Plag**	**Plag**	**Plag**
Major elements (wt.%)												
SiO2	49.626	49.1241	5.438	49.585	49.8487	48.953	47.246	49.3739	49.361	5.2937	51.371	47.554
ZrO2	0.53353		0.19	0.17137		0.19939	0.535	0.169		0.29978	0.4622	
TiO2	0.59149	0.597992	0.446243	0.565515	0.63132	0.698322	0.572854	0.5612	0.576549	0.4443	0.87844	0.27724
ZnO		0.13163	0.19472				0.64438		0.43926	0.2452		
Al2O3	2.3453	3.9815	2.51526	1.98515	2.95558	3.16522	4.164	2.47645	2.42152	26.213	25.9552	28.991
V2O3	0.71892	0.84147	0.2951	0.81233	0.1233	0.97584	0.9585	0.54369	0.85983		0.9172	
Cr2O3	0.11617	0.15835	0.121481	0.445	0.23946	0.299924	0.2228	0.85211	0.174917		0.6352	
FeO	9.92883	8.97289	9.66272	11.2197	8.72285	8.7248	11.7625	9.13314	9.14932	1.23389	1.17318	1.47484
MnO	0.234957	0.223272	0.276273	0.39458	0.258833	0.23751	0.287726	0.217	0.22426	0.26239	0.15346	
MgO	16.5721	15.8948	16.1998	14.9589	16.1752	15.5239	16.2479	15.6972	16.456	0.314964	0.223446	0.786599
CaO	17.3656	18.1287	16.7796	17.8888	18.3463	18.6134	14.5427	18.1127	17.8534	11.9651	11.859	13.337
BaO				0.1611			0.1343	0.8945	0.3583		0.43367	0.18634
Na2O	0.263998	0.359619	0.34522	0.244782	0.298743	0.353866	0.25424	0.31113	0.22956	4.3244	4.6442	3.13765
K2O	0.1444		0.5434	0.1865		0.1412	0.32822	0.6263	0.4448	0.14823	0.162139	0.129
P2O5		0.3719						0.1323				
Cl		0.1116	0.1298	0.7895	0.7499	0.1198	0.14446	0.1692	0.9347	0.687	0.9746	0.2974
F		0.1867	0.27463	0.13713			0.9135	0.32651		0.12264	0.1894	
O	0.8	-0.37	-0.1448	-0.756	-0.169	-0.27	-0.71	-0.1617	-0.211	-0.532	-0.299	-0.68
TOTAL	97.1517	96.6678	96.4725	97.132	97.5544	96.6817	95.1774	96.697	96.5583	94.64	94.7624	94.538
ppm												
Mg	63735.18	95586.92	88211.58	8885.64	84361	91867.95	75237.8	9164.63	8667.2	34117.61	3667.24	8414.15
Al	7825.9	451.97	12219.33	12393.64	14387.7	15726.13	12469.39	28277.43	1176.29	142727.19	149528.67	165715.41
Si	14947.94	26785.53	28497.53	2166.86	199716.8	221976.56	186157.3	23343.3	2747.95	28274.16	238586.67	252835.47
Ca	8549	129565.99	119923.97	127851.42	131121.19	1333.14	13936.81	129451.63	127598.43	85514.68	79231.3	95274.64
Fe	2258.22	31923.88	29412.16	28977.13	25739.63	2688.19	2858.41	2939.55	26441.85	1662.1	255.11	7498.44
REE (ppm)												
La	1.51	2.32	1.6	1.68	1.67	1.46	1.5	1.78	1.78	1.34	1.45	1.99
Ce	4.76	6.55	5.43	5.97	5.67	5.59	5.39	5.93	6.12	2.5	3.7	3.97
Pr	0.85	1.15	0.95	1.23	1.4	1.5	1.2	1.13	1.7	0.315	0.354	0.448
Nd	5.8	6.4	5.84	7.48	6.5	6.9	6.2	6.84	6.15	1.24	1.51	2
Sm	1.75	1.85	2.9	2.7	2.4	2.39	2.17	2.73	2.87	0.218	0.41	0.37
Eu	0.543	0.81	0.669	0.9	0.696	0.76	0.738	0.8	0.74	0.46	0.578	0.669
Gd	2.47	2.64	3.11	3.76	3.18	3.49	3.11	3.66	3.16	0.242	0.223	0.52
Tb	0.412	0.465	0.523	0.684	0.56	0.615	0.575	0.635	0.615	0.5	0.41	0.79
Dy	3.11	3.65	3.93	4.82	3.58	4.46	3.96	4.17	4.24	0.3	0.46	0.411
Ho	0.735	0.79	0.84	1.1	0.83	0.93	0.93	0.98	0.91	0.73	0.87	0.89
Er	2.21	2.47	2.43	2.92	2.33	2.67	2.8	2.72	2.54	0.134	0.197	0.253
Tm	0.296	0.357	0.364	0.432	0.36	0.49	0.45	0.361	0.373	<.145	0.53	0.33
Yb	2.7	2.51	2.44	2.96	2.28	2.59	2.75	2.62	2.43	<.74	0.264	0.182
Lu	0.292	0.369	0.35	0.48	0.328	0.382	0.411	0.375	0.378	0.213	0.43	0.37

			2129329			
Spot	**9239_16**	**9239_17**	**9239_2**	**9239_22**	**9239_25**	**9239_9**
Mineral	**Plag**	**Plag**	**Plag**	**Plag**	**Plag**	**Plag**
Major elements (wt.%)						
SiO2	45.4322	48.867	47.161	31.9377	86.5417	52.495
ZrO2			0.13823		0.12395	0.194
TiO2	0.82114	0.2822	0.39379	0.4111	0.119791	0.63822
ZnO						
Al2O3	26.476	28.2323	22.9217	17.3349	3.12562	26.388
V2O3	0.988	0.29256	0.11325	0.13219		
Cr2O3			0.17196		0.3187	
FeO	4.5875	1.17917	4.88871	18.7137	1.42284	1.2373
MnO	0.4745		0.7844	0.255343	0.41122	0.23851
MgO	3.1319	0.337286	5.4939	16.5995	1.389	0.311813
CaO	11.6316	13.3439	7.7134	1.55691	0.53939	1.9469
BaO		0.22				0.11432
Na2O	2.73641	3.49179	3.65831	0.63432	0.566993	4.7864
K2O	0.8738	0.93792	0.153496	0.1835	0.732916	0.15253
P2O5			0.6556	0.363	0.13198	
Cl	0.6235	0.2488	0.2481	0.17258	0.16841	0.9182
F			0.78897	0.72567		
O	-0.14	-0.56	-0.3882	-0.3446	-0.38	-0.27
TOTAL	94.695	95.648	92.1544	87.2851	94.4411	95.966
ppm						
Mg	21768.7	12862.21	11469.37	2392.27	1572.72	28821.25
Al	146812.36	161325.5	8658.3	93685.21	7785.92	144848.13
Si	219789.5	238943.17	13644.88	22136.84	15175.54	23914.83
Ca	83131.16	95368.98	5541.55	11127.25	3855.3	78237.6
Fe	1498.4	9522.33	6924.25	123.96	1112.79	1819.39
REE (ppm)						
La	1.17	1.59	0.597	0.524	0.374	1.22
Ce	2.12	2.8	1.17	0.96	0.724	2.63
Pr	0.241	0.328	0.132	0.134	0.74	0.313
Nd	0.96	1.1	0.47	0.379	0.24	1.34
Sm	0.271	0.34	0.135	0.129	<.64	0.285
Eu	0.355	0.461	0.218	0.66	0.155	0.457
Gd	0.211	0.138	0.162	0.98	0.82	0.226
Tb	0.28	0.34	0.28	0.162	<.84	0.81
Dy	0.237	0.96	0.118	0.137	0.48	0.327
Ho	0.57	0.51	0.46	0.33	<.8	0.48
Er	0.117	0.66	0.82	0.68	0.52	0.233
Tm	0.241	<.121	0.16	0.173	<.78	0.235
Yb	0.63	0.69	0.12	0.73	<.33	0.16
Lu	0.26	<.149	0.155	<.77	<.83	0.32

								2129330						
Spot	**9330_13**	**9330_14**	**9330_15**	**9330_18**	**9330_3**	**9330_4**	**9330_5**	**9330_6**	**9330_11**	**9330_12**	**9330_16**	**9330_17**	**9330_2**	**9330_7**
Mineral	**CPX**	**CPX**	**CPX**	**CPX**	**CPX**	**CPX**	**CPX**	**CPX**	**Plag**	**Plag**	**Plag**	**Plag**	**Plag**	**Plag**
Major elements (wt.%)														
SiO2	48.911	49.731	49.889	48.7333	48.9628	48.647	48.578	48.9258	34.5991	52.7655	46.4643	5.2847	85.942	44.29
ZrO2								0.38494	0.77	0.4933		0.27171		0.57197
TiO2	0.285321	0.663615	0.62855	0.712817	0.734147	0.84817	0.914234	0.797411	0.5649	0.15866	0.378	0.6368	0.24912	0.2633
ZnO					0.14138		0.5446	0.116		0.4447	0.1382		0.5529	
Al2O3	2.5153	2.5846	2.18768	2.81463	3.42382	2.94557	3.8394	2.94135	19.3751	21.646	25.7276	26.4317	2.15991	24.4234
V2O3	0.34115	0.5333	0.89938	0.114211	0.96893	0.17616	0.13565	0.74129		0.8768			0.436	0.4746
Cr2O3	0.11793	0.6335	0.5693	0.1877	0.167761	0.18642	0.213119	0.183966	0.3379		0.8845	0.3582		
FeO	11.13	1.711	1.618	1.8496	1.4612	1.5582	9.6599	1.5783	16.1189	4.8654	3.3551	1.21399	1.96335	9.8441
MnO	0.463557	0.255884	0.318633	0.24765	0.287232	0.283473	0.244147	0.25377	0.191811	0.35756	0.59948	0.21556	0.13247	0.89857
MgO	14.3362	16.67	15.3519	15.4252	14.6118	15.8	14.435	15.241	13.6471	4.26964	2.89184	0.567962	2.52214	5.285
CaO	16.421	17.1724	17.6393	17.12	17.851	17.5331	19.2862	17.9133	2.8394	4.18891	8.99885	12.593	1.27665	8.12745
BaO		0.4359		0.4645		0.1512	0.6254	0.27264			0.284	0.8976		
Na2O	0.37976	0.372277	0.334698	0.337431	0.716336	0.316339	0.297421	0.37315	1.36981	6.4642	2.67119	4.2433	0.451122	2.82797
K2O	0.52641	0.256	0.4457	0.699	0.12897	0.5916		0.7565	0.75865	0.59836	1.98671	0.187532	0.25828	0.145642
P2O5									0.6947				0.16754	0.15191
Cl	0.13911	0.9474	0.361	0.8629	0.29772	0.9221	0.5147	0.11766	0.15146	0.28796	0.12574		0.246	0.18438
F	0.19139	0.7345	0.2898	0.3384			0.13454	0.22743	0.45854	0.1637	0.2471			
O	-0.499	-0.523	-0.949	-0.1474	-0.672	-0.28	-0.683	-0.1224	-0.2273	-0.719	-0.1146	-0.1	-0.541	-0.416
TOTAL	93.6336	97.595	96.387	96.4618	96.5971	96.4857	96.2784	97.3484	88.2725	94.229	92.2576	95.744	94.424	94.3914
ppm														
Mg	9666.82	96281.88	13973.73	84366.18	19581.41	94551.8	1772.83	9716.32	8675.28	13467.2	13298.9	86483.6	122.47	138.93
Al	1258.32	212.49	13388.12	14297.44	47994.71	23229.41	13848.85	1376.4	3764.95	5729.26	111666.95	168185.95	15278.47	89329.4
Si	213712.8	234643.98	238517.14	197692.16	283641.9	22994.2	24285.89	225769.17	65129.99	11148.88	196855.8	355367.5	27855.69	19194.9
Ca	114653.5	122731.3	12668.24	121572.6	12217.38	12539.23	137838.66	12826.52	239.79	29938.18	64314.87	86187.94	9124.23	5886.96
Fe	25769.77	26542.92	2953.28	24771.73	31645.13	23589.3	25776.71	25715.73	4471.39	595.52	8222.27	37897.63	47.86	3395.8
REE (ppm)														
La	1.41	1.88	1.67	2.15	2.3	1.79	2.64	1.93	0.39	0.668	1.62	2.2	0.168	1.8
Ce	5.25	6.62	5.97	7.15	6.65	6.28	8.47	6.75	0.538	1.11	2.93	3.69	0.262	3.3
Pr	0.981	1.28	1.2	1.38	1.17	1.19	1.49	1.42	0.656	0.133	0.36	0.455	0.279	0.353
Nd	6.66	6.89	7	7.5	6.59	6.82	9.32	7.77	0.22	0.491	1.11	1.77	0.114	1.21
Sm	2.25	2.67	2.83	2.73	2.3	2.61	2.96	2.66	0.52	0.89	0.211	0.264	0.217	0.271
Eu	0.683	0.79	0.788	0.815	0.823	0.818	0.838	0.846	0.121	0.152	0.519	0.471	0.377	0.619
Gd	3.3	3.66	3.73	4.9	3.13	3.14	4.13	3.86	0.51	0.84	0.2	0.42	<.12	0.238
Tb	0.598	0.699	0.695	0.689	0.615	0.66	0.77	0.742	0.95	0.179	0.42	0.42	<.165	0.214
Dy	4.32	4.72	4.97	4.74	4.5	4.29	5.25	4.74	0.43	0.74	0.24	0.43	0.119	0.249
Ho	0.975	1.1	1.13	1.8	0.874	0.98	1.12	1.5	0.99	0.155	0.418	0.66	0.27	0.362
Er	2.8	3.18	3.11	3.17	2.79	2.91	3.35	3.23	0.35	0.46	0.91	0.247	<.56	0.99
Tm	0.44	0.46	0.433	0.423	0.389	0.42	0.447	0.474	<.37	0.86	<.12	0.3	<.139	0.228
Yb	2.86	2.82	3.12	2.88	2.6	2.67	3.1	3.21	0.26	0.56	0.16	0.233	<.7	0.1
Lu	0.48	0.415	0.469	0.447	0.414	0.386	0.462	0.461	0.43	<.63	0.265	0.47	0.152	0.121

						2129331						
Spot	**9331_1**	**9331_11**	**9331_12**	**9331_13**	**9331_14**	**9331_15**	**9331_9**	**9331_1**	**9331_4**	**9331_5**	**9331_6**	**9331_7**
Mineral	**CPX**	**CPX**	**CPX**	**CPX**	**CPX**	**CPX**	**CPX**	**Plag**	**Plag**	**Plag**	**Plag**	**Plag**
Major elements (wt.%)												
SiO2	49.997	49.9847	49.8469	5.192	48.442	49.292	5.531	5.4264	51.377	48.4478	49.5426	49.847
ZrO2		0.29311	0.38328	0.3464					0.65273		0.452	0.48641
TiO2	0.637294	0.535679	0.751856	0.599879	0.25388	0.71897	0.65373	0.57584	0.5647	0.42111	0.469	0.6798
ZnO		0.1642					0.1892		0.37454		0.1322	0.5766
Al2O3	2.2437	2.42732	3.441	2.62927	8.53264	4.18529	2.46346	28.4198	26.5545	29.59	28.3286	28.6579
V2O3	0.5286	0.87973	0.11555	0.76355	0.9752	0.68849	0.89112					0.22281
Cr2O3	0.27353	0.16322	0.369786	0.28517		0.5553	0.161464		0.581			
FeO	11.384	9.27169	8.87367	9.96581	1.56	1.5449	1.34	1.1853	0.94627	1.58425	0.724128	1.9161
MnO	0.272474	0.23976	0.255475	0.27794	0.33843	0.296425	0.2682			0.46146	0.11	
MgO	15.5758	16.2237	15.7574	16.7814	12.5268	14.5871	15.9647	0.5156	0.7296	0.912158	0.2516	0.178659
CaO	17.3645	18.3312	19.212	16.7762	13.7777	16.53	17.439	12.595	1.5389	5.66495	12.8999	12.773
BaO		0.3697	0.18253			0.8875	0.31696	0.251	0.17926	0.39353		0.244
Na2O	0.33517	0.233555	0.222161	0.278946	1.42844	0.652519	0.233717	3.68574	4.36364	2.393	3.7486	3.97328
K2O	0.528	0.3583		0.818	0.92531	0.173		0.856913	0.655963	5.8263	0.161156	0.14673
P2O5												
Cl	0.838	0.5238	0.11132	0.16699	0.14745	0.3115		0.598	0.1864	0.11973	0.1986	0.15443
F		0.49375	0.7889		0.112851			0.42584				
O	-0.181	-0.2197	-0.583	-0.377	-0.586	-0.71	0.8	-0.1929	-0.42	-0.27	-0.45	-0.348
TOTAL	97.782	97.5784	98.3136	97.8239	95.52	96.8684	97.717	97.893	95.2787	93.673	95.6293	96.8879
ppm												
Mg	91549.2	98514.48	99156.97	91585.23	73281.59	88286.69	92547.13	14756.95	418.31	4619.65	1783.6	11621.4
Al	16296.6	1557.86	15138.45	1571.65	13492.76	11166.44	13733.75	13914.7	125489.68	6392.5	14464.58	156116.2
Si	217274.75	224883.5	225872.2	2851.56	176912.33	26769.94	213575.83	28675.61	186787.28	1663.95	29594.66	25187.95
Ca	12414.25	13113.26	135944.7	119899.67	98469.35	11814.7	124636.69	86189.36	75321.62	4487.45	92195.71	91288.75
Fe	25261.43	25983.61	25314.61	25259.42	2369.3	2698.76	2559.9	7848.4	3134.33	2698.16	1788.32	7518.42
REE (ppm)												
La	1.9	1.62	1.39	1.64	3.87	1.46	1.85	1.3	1.6	1.74	1.6	1.29
Ce	7.3	6.11	5.24	5.65	8.61	5.52	6.27	1.83	1.9	3.79	1.82	2.35
Pr	1.25	1.14	0.98	1.1	1.19	1.5	1.17	0.23	0.211	0.451	0.193	0.263
Nd	7.35	6.9	6.64	6.5	6.31	6.35	7.42	0.76	0.84	2	0.61	1
Sm	2.8	2.52	2.27	2.34	1.92	2.43	2.63	0.149	0.124	0.421	0.136	0.251
Eu	0.793	0.795	0.695	0.73	0.594	0.751	0.757	0.423	0.45	0.276	0.374	0.498
Gd	3.76	3.41	3.33	3.23	2.59	3.38	3.66	0.198	0.111	0.482	0.17	0.183
Tb	0.694	0.651	0.588	0.68	0.483	0.655	0.639	0.218	0.182	0.68	<.127	0.48
Dy	4.73	4.61	4.37	4.28	3.58	4.37	4.49	0.19	0.52	0.389	0.16	0.24
Ho	1.3	1	0.921	0.93	0.852	0.99	1.5	0.36	0.297	0.81	0.23	0.69
Er	3.23	2.92	2.73	2.86	2.77	2.85	2.81	0.12	<.35	0.229	<.51	0.228
Tm	0.457	0.443	0.419	0.4	0.435	0.411	0.423	<.128	0.121	0.414	<.144	0.35
Yb	3.18	2.82	2.57	2.83	3.14	2.76	2.68	0.71	0.68	0.243	<.52	0.187
Lu	0.456	0.419	0.384	0.414	0.459	0.422	0.47	<.153	0.18	0.295	<.19	0.42

						2129333						
Spot	**9333_11**	**9333_12**	**9333_13**	**9333_14**	**9333_15**	**9333_16**	**9333_17**	**9333_1**	**9333_5**	**9333_6**	**9333_8**	**9333_9**
Mineral	**CPX**	**CPX**	**CPX**	**CPX**	**CPX**	**CPX**	**CPX**	**Plag**	**Plag**	**Plag**	**Plag**	**Plag**
Major elements (wt.%)												
SiO2	49.734	49.6312	48.9448	49.729	49.161	5.2139	49.8542	53.7356	63.427	49.4354	63.548	59.5984
ZrO2	0.4239	0.31524	0.39847	0.68723	0.59465	0.47483		0.61873	0.17257			
TiO2	0.72693	0.686389	0.74285	0.81713	0.87383	0.467172	0.766	0.7444	0.16842	0.4677	0.58	0.277
ZnO	0.3699	0.2264		0.3513		0.58655				0.4962		
Al2O3	2.72859	2.58613	2.63263	2.379	2.82416	1.5392	2.55333	24.6229	2.5421	28.3844	17.564	19.838
V2O3	0.831	0.11693	0.121149	0.1812	0.9241	0.38588	0.46921	0.14467	0.11987		0.19864	0.418
Cr2O3	0.299179	0.97581	0.25785	0.45462	0.212482	0.131337	0.2253					
FeO	9.63238	1.6449	11.831	11.3913	11.177	11.626	12.3657	0.817699	0.52328	0.589581		0.927466
MnO	0.25588	0.296218	0.291647	0.37986	0.291984	0.33311	0.288761	0.17996	0.11613			
MgO	15.6433	14.8734	14.5192	14.7749	14.614	16.568	16.99	0.261673	0.17939	0.25342	0.7879	2.96
CaO	18.7728	18.3885	18.4214	17.9157	17.8294	15.4889	15.564	9.85817	2.7189	13.4735	0.136471	2.72423
BaO			0.1457	0.14626				0.1977		0.9329	0.41785	0.4425
Na2O	0.31875	0.378922	0.342451	0.318271	0.363215	0.3612	0.244872	5.7855	9.89567	3.4426	0.499733	5.53527
K2O		0.1697	0.8643	0.322	0.23473	0.11284		0.18811	0.23416	0.248693	15.543	4.3928
P2O5											0.9782	
Cl	0.255		0.439	0.191	0.6442	0.7588	0.214	0.1243	0.1425	0.1684	0.5541	0.1754
F			0.23891	0.5869		0.15					0.847	0.98698
O	-0.6	0.4	-0.114	-0.676	-0.145	-0.234	-0.45	-0.28	-0.235	-0.242	-0.464	-0.4541
TOTAL	98.2291	97.7536	97.4372	97.9191	97.395	96.8248	97.8919	95.3775	97.612	95.8944	96.867	95.1337
ppm												
Mg	88749.41	88384.95	88255.69	81676.52	8443.12	76313.91	6927.2	2117.97	125.52	45934.89	376.98	6882.5
Al	12743.8	12559.36	13972.42	13992.1	12849.98	1152.7	963.48	129975.36	1444.97	45856.89	1882.41	1477.22
Si	24883.2	229333.33	236359.5	227563.33	231697.19	214881.2	172273.31	515748	12211.25	57725.56	931.13	74765.38
Ca	134169.38	131422.78	131657.92	12843.69	127426.89	11699.31	8549	7456.43	1931.43	96295.23	975.36	1947.1
Fe	2757.43	33284.51	29749.1	2916.35	3248.48	3163.94	3134.5	27.28	1395.7	4554.6	21.6	1216.69
REE (ppm)												
La	1.75	2.6	1.88	2.59	2.17	2.9	1.26	2.98	1.34	6.36	0.485	0.772
Ce	5.99	7.11	6.47	7.8	7.53	6.41	4.27	4.68	2.46	9.88	0.797	1.25
Pr	1.1	1.27	1.23	1.38	1.37	1.13	0.83	0.641	0.313	1.25	0.99	0.157
Nd	6.18	7.83	7.31	8.8	8.14	6.69	5	2.48	1.26	4.83	0.359	0.695
Sm	2.48	2.73	2.71	2.87	2.71	2.47	1.76	0.38	0.221	0.85	0.66	0.133
Eu	0.668	0.9	0.82	0.83	0.93	0.72	0.547	0.251	0.56	0.196	0.47	0.66
Gd	3.36	4.21	4.6	3.75	4.7	3.58	2.75	0.42	0.221	0.92	0.97	0.19
Tb	0.579	0.727	0.676	0.68	0.749	0.641	0.513	0.85	0.278	0.122	0.126	0.254
Dy	4.25	5.44	4.56	4.34	5.36	4.13	3.54	0.339	0.213	0.82	0.67	0.189
Ho	0.9	1.16	1.5	0.94	1.12	0.94	0.86	0.84	0.41	0.177	0.157	0.417
Er	2.55	3.16	3.1	2.88	3.36	2.57	2.37	0.282	0.122	0.57	0.397	0.144
Tm	0.388	0.466	0.412	0.388	0.43	0.399	0.364	0.42	0.22	0.64	0.81	0.175
Yb	2.55	3.16	3.6	2.85	3.4	2.61	2.42	0.283	0.156	0.48	0.7	0.121
Lu	0.361	0.483	0.43	0.447	0.43	0.372	0.399	0.51	0.239	0.72	0.82	0.174

APPENDIX D: Extended analytical methods

Mineral separation of plagioclase and clinopyroxene

Following grain liberation with a selFrag Lab machine, clinopyroxene and plagioclase were then separated from the basalt samples from drill hole CD1 at the University of Adelaide. The disaggregated samples were first sieved using a 90-micron mesh. Strongly magnetic grains such as magnetite were removed by passing a hand magnet over the sieved portions. The non-magnetic portion from the hand magnet was then run through a Frantz magnetic separator™ set to 1.4A to remove plagioclase. Conventional electromagnetic separation typically involves beginning the separation process with a lower magnetic amplitude and increasing this over time. However, for this study it was decided to begin with a higher magnetic amplitude to reduce the number of steps involved in the separation process and thereby reduce possible contamination. Different end-members of clinopyroxene were observed in the basalt samples during petrographic analysis. These included more Fe-rich, altered end members (possible hedenbergite), and also augite. The more Fe-rich end members have higher magnetic susceptibilities than augite. Zhao and McCulloch (1993) noted that clinopyroxene with lower magnetic susceptibility is likely to have lower total REE abundances and higher Sm/Nd ratios. Furthermore, alteration comprising chlorite and hematite was observed throughout the samples. The magnetic susceptibilities of chlorite, hematite, and the more Fe-rich clinopyroxenes overlap, whereas augite has a lower magnetic susceptibility than these minerals. Therefore, for this study it was decided to only separate augite. The magnetic portion at 1.4A was re-passed through the Frantz at 1.0A. The non-magnetic portion at 1.0A was then re-passed through the Frantz at 0.4A and 0.3A to remove chlorite, oxides, and Fe-rich end-members of clinopyroxene. The final clinopyroxene portion from the frantz contained approximately 80% clinopyroxene and 20% impurities such as residual plagioclase. This portion was passed through Methlyene Iodide with a specific gravity of 3.19 to remove residual plagioclase and other impurities. Remaining impurities in both the plagioclase and clinopyroxene portions were then handpicked under an optical microscope where necessary. The resulting separates of plagioclase and clinopyroxene were more than 99% pure.

Whole-rock geochemical analysis

Details of sample preparation and analysis procedures can be found in ALS Minerals (2009) and ALS Geochemistry (2015). Samples were crushed to produce a powder containing grains 6 mm or finer. A sample of approximately 0.200 g was added to a lithium metaborate or lithium tetraborate flux (0.90 g), mixed, and then fused in a furnance at 1000°C. The resulting melt was then cooled and dissolved in 100 mL of nitric acid / 2% hydrochloric solution. Major oxides were analysed by inductively coupled plasma atomic emission spectroscopy (ICP-AES), while REE and trace elements were analysed by inductively coupled plasma mass spectroscopy (ICP-MS). Samples analysed for base metals were dissolved in a four acid digestion and subsequently fused in a furnace. The resulting solution was then analysed by ICP-AES. Total carbon was measured through combustion in a LECO furnace.

In-situ Electron Probe Micro Analysis of clinopyroxene and plagioclase

Polished thin sections were analysed via. Electron probe microanalysis (EPMA) on a Cameca SXFive electron microprobe to determine major element compositions of plagioclase and clinopyroxene in the basalt samples selected for Sm-Nd geochronology. Mineral compositions were measured with a focused electron beam at an accelerating voltage of 15 kV and a beam current of 20 nA. Elements were standardised with a mixture of Astimex, Taylor, and P&H natural mineral standards. Peak counting and background times were 15 and 10 seconds respectively, with data reduction performed in the Probe for EPMA software™.

In-situ LA-ICP-MS trace element analysis of clinopyroxene and plagioclase

Trace element analysis of plagioclase and clinopyroxene grains analysed by EPMA were undertaken via Laser Ablation Inductively Coupled Plasma Mass Spectrometry (LA-ICP-MS) using an ESI NWR-213 laser attached to an Agilent 7500cs ICP-MS at Adelaide Microscopy. Ablation was conducted in a helium atmosphere after which argon gas added immediately to the cell to aid transport of material. A spot size of 30 micron was chosen, with a laser frequency of 5 Hz resulting in an average fluence of 5 J/cm^2. A single analytical spot consisted of a 30s gas blank followed by 30s of data acquisition with the laser firing. External calibration was performed with reference to the NIST612 standard. Data reduction was completed using GLITTER software (Achterbergh et al., 2001) with ^{43}Ca employed for internal calibration using concentrations from EPMA analysis.